

ANALYSIS OF THE PARALLEL RESONANT CONVERTER USING A FREQUENCY DOMAIN MODEL

A Thesis Submitted
in Partial Fulfilment of the Requirements
for the Degree of

MASTER OF TECHNOLOGY

by
SUJOY DEB

to the

DEPARTMENT OF ELECTRICAL ENGINEERING
INDIAN INSTITUTE OF TECHNOLOGY KANPUR
MAY, 1986

157 86

U. I. AANFUR
CENTRAL LIBRARY

U. I. A 92045

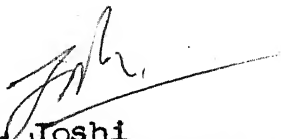
EE-1986-M-DEB-ANA

To

MY PARENTS

CERTIFICATE


This is to certify that the thesis entitled 'ANALYSIS OF THE PARALLEL RESONANT CONVERTER USING A FREQUENCY DOMAIN MODEL' by Mr. Sujoy Deb has been carried out under our supervision and that this has not been submitted elsewhere for a degree.



A. Joshi

Assistant Professor

Dept. of Electrical Engineering
Indian Institute of Technology
Kanpur



S. R. Doradla

Professor

Dept. of Electrical Engineering
Indian Institute of Technology
Kanpur

ACKNOWLEDGEMENTS

I take this opportunity to express my deep sense of gratitude and sincere thanks to my thesis supervisors, Dr. S. R. Doradla and Dr. A. Joshi. I am deeply grateful to them for suggesting this topic and for their invaluable guidance and constant encouragement throughout the course of this work.

A special note of thanks is due to my friends Soumyesh, Sidhu, Utpal, Chandrashekhar, Ujjwal, Tarun, Maji and many others who have all contributed towards making my stay at I.I.T. Kanpur a truly pleasant and memorable one. I am thankful to them for their everlasting moral support and encouragement.

Last but not the least, I would like to thank Mr. R.N. Srivastava for his excellent typing.

- Sujoy Deb

CONTENTS

CHAPTER	Page
LIST OF FIGURES	vi
NOMENCLATURE	x
ABSTRACT	xii
1 INTRODUCTION	1
1.1 Description of Operation of Resonant Converters	2
1.2 Trends in Analysis of Resonant Converters	8
1.3 Objectives and Scope of the Present Work	10
1.4 Organisation of the Thesis	11
2 A FREQUENCY DOMAIN MODEL FOR THE PARALLEL RESONANT CONVERTER	13
2.1 Introduction	13
2.2 Development of the Model Assuming Infinite Q of the Resonant Circuit	14
2.3 Detailed Analysis of the Parallel Resonant Converter Using the Infinite Q Model	15
2.4 Conclusions	32
3 MODIFICATION OF THE BASIC FREQUENCY DOMAIN MODEL ALLOWING FOR A FINITE RESISTANCE IN THE INDUCTOR COIL	36
3.1 Introduction	36
3.2 Detailed Analysis of the Parallel Resonant Converter Using the Modified Model	38
3.3 Comparison of the Results Obtained from the Simpler Model, the Modified Model and Experimental Results Reported in Literature	56
3.4 Conclusions	58
4 SOME IMPORTANT PERFORMANCE CHARACTERISTICS	60
4.1 Introduction	60
4.2 Variation of Phase Difference ϕ	62
4.3 Variation of Maximum Possible Value of $I_{O_{pu}} X_{L1_{pu}}$, $(I_{O_{pu}} X_{L1_{pu}})_{max}$ with Frequency	68
4.4 Boundary of Multiple Conduction Mode	71
4.5 Variation of Per Unit Peak Capacitor Voltage $V_{C_{peak_{pu}}}$	75
4.6 Variation of Per Unit Output Voltage $V_{O_{pu}}$	78

4.7	Variation of Per Unit Turn-Off Time $t_{q_{pu}}$	81
4.8	Conclusions	84
5	VARIATION OF POWER AND EFFICIENCY FOR DIFFERENT CONTROL SCHEMES	86
5.1	Introduction	86
5.2	Control Schemes for the Parallel Resonant Converter	87
5.3	Expressions for Output Power, Input Power, Circuit Losses and Efficiency	88
5.4	Variation of Output Power, Input Power, Circuit Losses and Efficiency	92
5.5	Comparison of f-Control and ϕ -Control	121
5.6	Conclusions	122
6	A DESIGN EXAMPLE	123
6.1	Introduction	123
6.2	Input and Output Parameters	123
6.3	Selection of Component Values	124
6.4	Determination of Component Ratings	127
6.5	Comments on the Design Procedure	134
7	CONCLUSIONS	137
7.1	Summary of Work Done and Important Conclusions Reached	137
7.2	Advantages and Limitations of the Proposed Model	139
7.3	Suggestions for Future Work	141
	REFERENCES	143

LIST OF FIGURES

Number	Title	Page
1.1(a)	Series resonant converter	3
1.1(b)	Parallel resonant converter	4
1.2	Inductor current and the capacitor voltage waveforms for the resonant converter	6
2.1(a)	A simple equivalent circuit for the parallel resonant converter with an inductor filter at the output	16
2.1(b)	Voltage and current waveforms for the equivalent circuit of Figure 2.1(a)	17
2.2(a)	Circuit waveforms for the equivalent circuit of Figure 2.1(a) assuming only sinusoidal sources	27
2.2(b)	Phasor diagram for the equivalent circuit of Figure 2.1(a) assuming only sinusoidal sources	28
2.3	Flow chart for determination of the value of ϕ for the infinite-Q model	31
2.4	Inductor current and capacitor voltage waveforms obtained from the model of Figure 2.1(a) for $L = 73 \mu\text{H}$, $C = 5 \mu\text{F}$, $Q = 7.3$ and $V_s = 120 \text{ V}$	33
3.1	A modified frequency domain model for the parallel resonant converter	37
3.2	Phasor diagram for the equivalent circuit of Figure 3.1 assuming only sinusoidal sources	44
3.3	Flow chart for determination of the value of ϕ for the modified model	48
3.4	Inductor current and the capacitor voltage waveforms obtained from the model of Figure 3.1 for $L = 73 \mu\text{H}$, $C = 5 \mu\text{F}$, $Q = 7.3$ and $V_s = 120 \text{ V}$	50
3.5	Inductor current and capacitor voltage waveforms in the multiple continuous conduction mode ($L = 73 \mu\text{H}$, $C = 5 \mu\text{F}$, $Q = 7.3$ and $V_s = 120 \text{ V}$)	54
3.6	Inductor current waveform in the multiple continuous conduction mode	55

3.7	Experimental waveforms for the inductor current and the capacitor voltage for $L = 73 \mu\text{H}$, $C = 5 \mu\text{F}$, $Q = 7.3$ and $V_s = 120 \text{ V}$ (Reproduced from [11])	57
4.1(a)	Variation of ϕ with $I_{o_{pu}} X_{L1_{pu}}$ for $0.5 < \omega_{pu} < 1.0$	64
4.1(b)	Variation of ϕ with $I_{o_{pu}} X_{L1_{pu}}$ for $0.5 < \omega_{pu} < 1.0$ (Expanded version of Figure 4.1(a))	65
4.1(c)	Variation of ϕ with $I_{o_{pu}} X_{L1_{pu}}$ for $\omega_{pu} \leq 0.5$ and $\omega_{pu} \geq 1.0$	66
4.1(d)	Variation of ϕ with $I_{o_{pu}} X_{L1_{pu}}$ for $\omega_{pu} \leq 0.5$ and $\omega_{pu} \geq 1.0$ (expanded version of Figure 4.1(c))	67
4.2	Variation of ϕ with $I_{o_{pu}} X_{L1_{pu}}$ at $\omega_{pu} = 0.65$ with Q as a parameter	69
4.3	Variation of $(I_{o_{pu}} X_{L1_{pu}})_{\text{max}}$ with ω_{pu} taking Q as a parameter	70
4.4	Boundary of multiple conduction mode	73
4.5	Variation of per unit peak capacitor voltage $V_{C_{\text{peak}_{pu}}}$ with $I_{o_{pu}} X_{L1_{pu}}$	76
4.6(a)	Variation of per unit dc output voltage $V_{o_{pu}}$ with $I_{o_{pu}} X_{L1_{pu}}$	79
4.6(b)	Variation of per unit dc output voltage $V_{o_{pu}}$ with $I_{o_{pu}} X_{L1_{pu}}$ (expanded version of Figure 4.6(a))	80
4.7	Variation of per unit turn-off time $t_{q_{pu}}$ with $I_{o_{pu}} X_{L1_{pu}}$ at different frequencies	82
5.1(a)	Variation of $P_{o_{pu}} X_{L1_{pu}}$ with $I_{o_{pu}} X_{L1_{pu}}$ for f -control	95

5.1(b)	Variation of $P_{o\text{pu}} X_{L1\text{pu}}$ with $I_{o\text{pu}} X_{L1\text{pu}}$ for f-control (expanded version of Figure 5.1(a))	96
5.2(a)	Variation of $P_{i\text{pu}} X_{L1\text{pu}}$ with $I_{o\text{pu}} X_{L1\text{pu}}$ for f-control	97
5.2(b)	Variation of $P_{i\text{pu}} X_{L1\text{pu}}$ with $I_{o\text{pu}} X_{L1\text{pu}}$ for f-control (expanded version of Figure 5.2(a))	98
5.3(a)	Variation of $P_{l\text{pu}} X_{L1\text{pu}}$ with $I_{o\text{pu}} X_{L1\text{pu}}$ for f-control	99
5.3(b)	Variation of $P_{l\text{pu}} X_{L1\text{pu}}$ with $I_{o\text{pu}} X_{L1\text{pu}}$ for f-control (expanded version of Figure 5.3(a))	100
5.4(a)	Variation of efficiency η with $I_{o\text{pu}} X_{L1\text{pu}}$ for f-control	101
5.4(b)	Variation of efficiency η with $I_{o\text{pu}} X_{L1\text{pu}}$ for f-control (expanded version of Figure 5.4(a))	102
5.5(a)	Variation of $P_{o\text{pu}} X_{L1\text{pu}}$ with $I_{o\text{pu}} X_{L1\text{pu}}$ for \emptyset -control	103
5.5(b)	Variation of $P_{o\text{pu}} X_{L1\text{pu}}$ with $I_{o\text{pu}} X_{L1\text{pu}}$ for \emptyset -control (expanded version of Figure 5.5(a))	104
5.6(a)	Variation of $P_{i\text{pu}} X_{L1\text{pu}}$ with $I_{o\text{pu}} X_{L1\text{pu}}$ for \emptyset -control	105
5.6(b)	Variation of $P_{i\text{pu}} X_{L1\text{pu}}$ with $I_{o\text{pu}} X_{L1\text{pu}}$ for \emptyset -control (expanded version of Figure 5.6(a))	106
5.7(a)	Variation of $P_{l\text{pu}} X_{L1\text{pu}}$ with $I_{o\text{pu}} X_{L1\text{pu}}$ for \emptyset -control	107
5.7(b)	Variation of $P_{l\text{pu}} X_{L1\text{pu}}$ with $I_{o\text{pu}} X_{L1\text{pu}}$ for \emptyset -control (expanded version of Figure 5.7(a))	108
5.8(a)	Variation of efficiency η with $I_{o\text{pu}} X_{L1\text{pu}}$ for \emptyset -control	109

5.8(b)	Variation of efficiency η with $I_{o_{pu}} X_{L1_{pu}}$ for \emptyset -control (expanded version of Figure 5.8(a))	110
5.9	Variation of per unit output power $P_{o_{pu}}$ with $I_{o_{pu}}$ for f-control for a given set of circuit parameters	111
5.10	Variation of per unit input power $P_{i_{pu}}$ with $I_{o_{pu}}$ for f-control for a given set of circuit parameters	112
5.11	Variation of per unit power loss $P_{l_{pu}}$ with $I_{o_{pu}}$ for f-control for a given set of circuit parameters	113
5.12	Variation of efficiency η with $I_{o_{pu}}$ for f-control for a given set of circuit parameters	114
5.13	Variation of per unit output power $P_{o_{pu}}$ with $I_{o_{pu}}$ for \emptyset -control for a given set of circuit parameters	115
5.14	Variation of per unit input power $P_{i_{pu}}$ with $I_{o_{pu}}$ for \emptyset -control for a given set of circuit parameters	116
5.15	Variation of per unit power loss $P_{l_{pu}}$ with $I_{o_{pu}}$ for \emptyset -control for a given set of circuit parameters	117
5.16	Variation of efficiency η with $I_{o_{pu}}$ for \emptyset -control for a given set of circuit parameters	118
6.1	Inductor current and capacitor voltage waveforms expected for the designed converter at the rated output voltage and the maximum specified load current	128

NOMENCLATURE

C	Resonant capacitor
C_f	Output filter capacitor
C_{i1}, C_{i2}	Input capacitors which serve as voltage dividers
D_1, D_2	Feedback diodes connected across the power switches S_1 and S_2 respectively
f	Frequency of operation of the converter
f_o	Resonant frequency of the LC circuit
$I_{D_{av}}$	Average current rating of the feedback diodes D_1 and D_2
$I_{D_{rms}}$	rms current rating of the feedback diodes D_1 and D_2
i_L	Current through the resonant inductor L
i_o	Square wave current source in parallel across the resonant capacitor in the equivalent circuit
I_o	Output load current
$I_{S_{av}}$	Average current rating of the power switches S_1 and S_2
$I_{S_{rms}}$	rms current rating of the power switches S_1 and S_2
L	Resonant inductor
L_f	Output filter inductor
P_i	Input power delivered by the input voltage source
P_l	Power loss due to the resistance of the inductor coil
P_o	Output power delivered to the load by the converter
Q	Quality factor of the LC resonant circuit $(= \frac{\omega_o L}{R})$
Q_n	Quality factor of the inductor coil at frequency $n\omega$ $(= \frac{n\omega L}{R})$
R	Resistance of the resonant inductor coil
R_L	Output load resistance

S_1, S_2	Power switches (thyristors, power transistors, FETs or GTOs)
T	Time period of the converter
t_q	Turn off time available to the power switches S_1 and S_2
v_C	Voltage across the resonant capacitor C
$v_{C_{peak}}$	Peak value of the capacitor voltage v_C
v_{C_1}	Component of the capacitor voltage v_C due to voltage source v_1 only
v_{C_2}	Component of the capacitor voltage v_C due to current source i_o only
v_1	Square wave voltage source in series with the LC resonant circuit in the equivalent circuit
V_{in}	Input dc voltage
V_o	Output dc voltage
V_s	DC voltage across each input capacitor
X_{Cn}	Impedance of the capacitor at frequency $n\omega$ ($= \frac{1}{n\omega C}$)
X_{Ln}	Impedance of the inductor L at frequency $n\omega$ neglecting the resistance of the coil ($= n\omega L$)
Z_{Ln}	Magnitude of the impedance of inductor L at frequency $n\omega$ taking into account the resistance of the coil ($= \{R^2 + (X_{Ln})^2\}^{1/2}$)
Z_n	Magnitude of the impedance of LC resonant circuit at frequency $n\omega$ ($= \{R^2 + (X_{Ln} - X_{Cn})^2\}^{1/2}$)
η	Efficiency of the converter
\emptyset	Phase difference between the voltage source v_1 and the current source i_o of the equivalent circuit
ω	Angular frequency of operation of the converter
ω_o	Angular resonant frequency of the LC circuit
Subscripts	
base	Denotes base quantities
pu	Denotes per unit quantities
n	Refers to quantities at the n^{th} harmonics.

ABSTRACT

The resonant converters are generally analysed using a time domain approach. In this thesis the steady state analysis of a parallel resonant converter is presented using a frequency domain model. For a parallel resonant converter with an inductor filter at the output, the output current may be considered to be ripple free dc. With this assumption the parallel resonant converter can be modelled as a high-Q series LC circuit fed by a square wave voltage source in series and a square wave current source in parallel with the resonant capacitor.

Generalised expressions for circuit currents and voltages have been determined using the model. Waveforms of inductor current and capacitor voltage have been obtained and these have been compared with published experimental results. A multiple continuous conduction mode in which each power switch conducts twice in each half cycle has been identified.

The variations of output voltage, peak capacitor voltage and turn off time have been studied. Relationships among several other important quantities have also been determined. The variations of output power, input power, circuit loss and converter efficiency have been studied for two of the common control schemes, namely, the open-loop frequency control and the closed-loop phase control.

Lastly an example of the design of a parallel resonant converter to meet a given set of specifications has been given making use of the relations derived in the earlier chapters.

CHAPTER 1

INTRODUCTION

High frequency resonant converters are becoming increasingly popular in recent times. They have found wide application in the aerospace systems and in the industry. Some typical areas of application include regulated power supplies and battery chargers. These converters use a high frequency LC resonant circuit and employ natural commutation of the power switches. As a consequence they have several desirable properties. Some of these are discussed briefly.

(1) Since natural commutation is employed, no additional commutation circuitry is required. This reduces complexity of the circuit. Moreover, because of high frequency operation the reactive components and the coupling transformers are small. As a result there is considerable saving in space and weight. These features make the converter particularly suitable for aerospace applications.

(2) Switching losses are much less compared to those of conventional switching converters. This ensures higher efficiency.

(3) The voltages and currents in the circuit are inherently sinusoidal. The intermediate ac voltage, as a result, has low harmonic content. This makes the filtering easier.

(4) The output dc voltage can be either higher or lower than the input dc voltage. So the converter has both step-up and step-down capability.

1.1 DESCRIPTION OF OPERATION OF RESONANT CONVERTERS

The resonant converter essentially consists of a high frequency LC series resonant circuit. The LC circuit is driven by the square wave output of a variable frequency inverter. The alternating resonant currents and voltages across the resonant components can be varied by changing the frequency of the input square wave from the inverter.

Steigerwald [1] has given several possible configurations of resonant converters. Figures 1.1(a) and 1.1(b) show the circuit configurations of the series and the parallel resonant converter respectively. Half-bridge versions have been shown, although full bridge versions can also be used. In the series resonant converter the inductor current is rectified and filtered, usually through a transformer coupling, to obtain an isolated and adjustable dc output voltage. For the parallel resonant converter, however, it is the capacitor voltage that is rectified and filtered to produce the dc output voltage. The input capacitors C_{i1} and C_{i2} (Figure 1.1) in both the cases are much larger than the resonant capacitor C and simply serve as voltage dividers. S_1 and S_2 are power switches which may be thyristors, power transistors, VMOS FETs or GTOs. D_1 and D_2 are the feedback diodes.

The basic principle of operation of the resonant converter is outlined briefly here. The following discussion applies to both the series resonant converter and the parallel resonant converter. When S_1 is turned on a resonant current pulse passes through S_1 , L , C and the power supply. When this

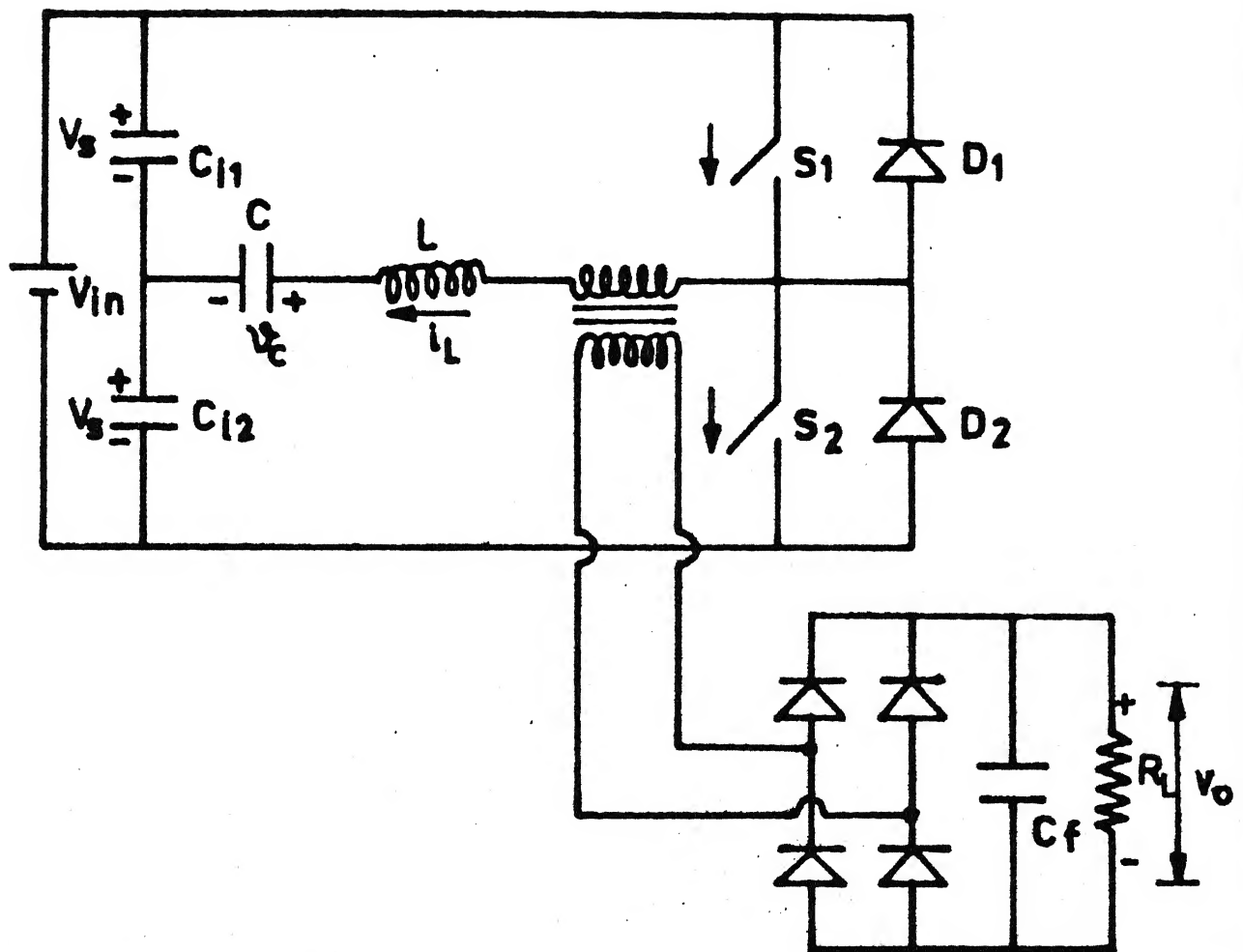


FIG. 1.1(a). Series resonant converter

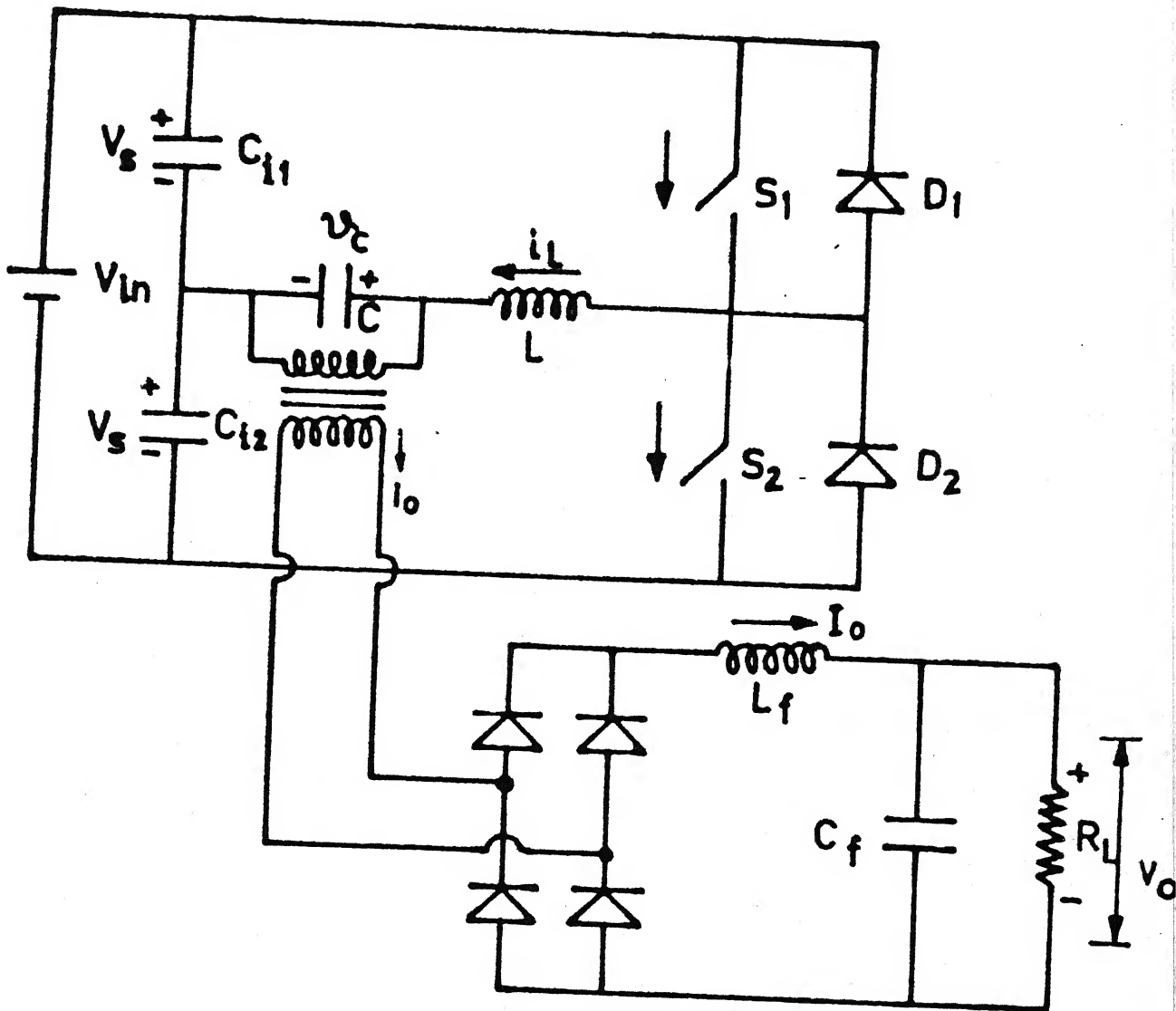


FIG.1.1 (b). Parallel resonant converter

current reverses the power switch S_1 is automatically turned off and the current flows through the feedback diode D_1 . The diode D_1 is reverse-biased by a voltage of magnitude V_{in} when S_2 is turned on. D_1 is therefore commutated and conduction passes to S_2 . This pattern continues during the next half-cycle, with the conduction passing from S_2 to D_2 when the resonant current reverses again. When S_1 is turned on again, D_2 is reverse-biased and is turned off and S_1 starts conducting once more, thus completing one full cycle of converter operation (Figure 1.2(a)). This mode of operation corresponds to the frequency range $0.5 < \frac{f}{f_0} < 1$, where f and f_0 are the switching frequency of the converter and the resonant frequency of the LC circuit respectively. This is the normal continuous conduction mode and is the preferred mode of operation, since it takes advantage of the natural commutation of the power switches.

It should be noted that even in the region $0.5 < \frac{f}{f_0} < 1$ conduction can be discontinuous for large values of R_L . In this mode the output bridge becomes reverse-biased as soon as S_1 conducts, since the voltage at the output side of the bridge becomes greater than the voltage at the input side. Consequently following the conduction of S_1 , diode D_1 does not conduct and instead a discontinuous interval exists (Figure 1.2(b)). For the series resonant converter the boundary between continuous and discontinuous conduction regions for $0.5 < \frac{f}{f_0} < 1$ have been determined in [2].

$$Q' < \left(\frac{f}{f_0}\right) \frac{4}{\pi} : \text{discontinuous conduction}$$

$$Q' > \left(\frac{f}{f_0}\right) \frac{4}{\pi} : \text{continuous conduction}$$

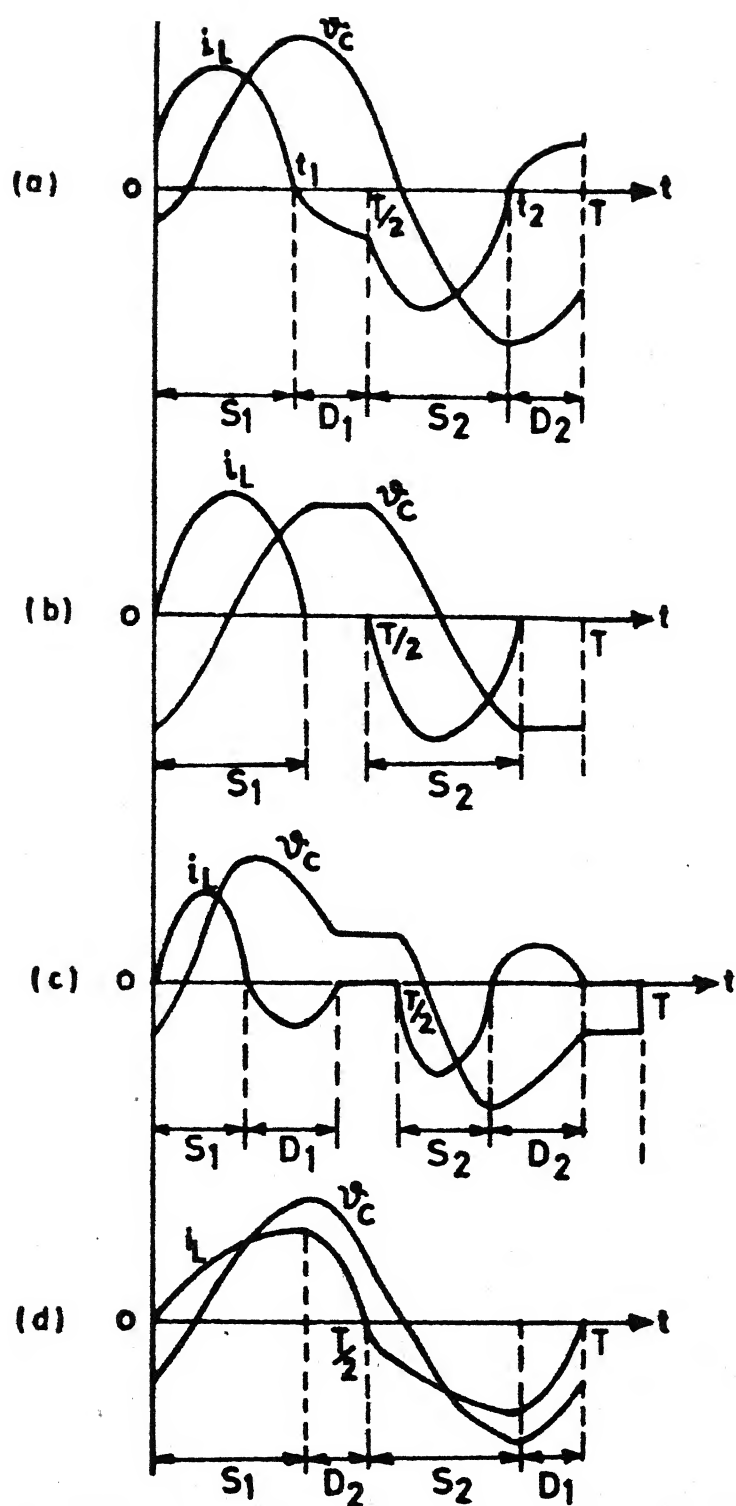


Figure 1.2. Inductor current and capacitor voltage waveforms for the resonant converter

(a) $0.5 < \frac{f}{f_o} < 1$ (continuous conduction)

(b) $0.5 < \frac{f}{f_o} < 1$ (discontinuous conduction)

(c) $\frac{f}{f_o} < 0.5$ (discontinuous conduction)

(d) $f > f_o$ (operation above resonance)

where $Q' = \frac{\omega_o L}{R_L}$ and R_L is the load resistance.

Figure 1.2(c) illustrates the case when $\frac{f}{f_o} < 0.5$. The conduction is discontinuous. S_1 conducts, followed by D_1 . This is followed by a discontinuous interval which ends when S_2 is turned on to produce another half-cycle.

Operation of the resonant converter above resonance ($f > f_o$) is also possible (Figure 1.2(d)). In this case, however, the power switches S_1 and S_2 must be such that they can be turned off by gate control. The diode D_1 conducts first, followed by S_1 which is turned off preferably by gate control. The current then transfers to D_2 and the pattern repeats. The power switches are turned on at zero current crossings. Although natural commutation is not taken advantage of this mode has several advantages ([1], [3]). The higher frequency of operation results in a smaller size of the transformer and the filter. No discontinuous conduction is possible in this mode, and therefore there is no upper limit on the value of R_L . As soon as a power device is switched on, it takes over from the corresponding feedback diode after the resonant current goes to zero. During the conduction interval of the power device the feedback diode remains reverse-biased by the forward voltage drop of the power device. Consequently feedback diodes with medium recovery speed may be used. So a Darlington power transistor or a power FET with its inherent slow parasitic capacitance may be used as a composite power switch.

It may be noted that the series resonant converter essentially appears as a high frequency current source to the

load R_L . Consequently for operations marked by rapid fluctuations of load regulation of the output voltage becomes difficult. However, the parallel resonant converter appears as a high frequency voltage source to the load. Consequently for rapidly varying loads, such converters are more suitable.

Instead of the conventional voltage-input version, it is possible to have resonant converters where the input is a constant current. This, however, requires a switching arrangement which is capable of blocking reverse voltage instead of passing reverse current. This can be achieved using the GTO as the switching device. Steigerwald [1] has discussed the current-input type resonant converters.

It may be mentioned that the resonant converters can be used with active loads, since regeneration is inherently possible in these types of converters.

1.2 TRENDS IN ANALYSIS OF RESONANT CONVERTERS

In view of the increasing importance and application of the resonant converters, several efforts have been made in recent times in modelling and analysis of the resonant converters. Some of the major efforts in this direction are outlined briefly.

One of the earliest contributions in this area came from Schwarz [4]. The operation of the series resonant converter has been discussed and the manifold advantages of resonant converters have been pointed out in [4]. A steady state analysis has been carried out.

Vorperian and Cuk [2] have carried out a detailed dc analysis of the series resonant converter. The ratio of the output voltage to input voltage has been determined explicitly as a function of the switching frequency f and the load R_L . The different continuous and discontinuous modes have been identified for the most general case and boundaries between these modes have been determined. The dc analysis has been carried out for each such mode. In a subsequent publication [3] the same authors have considered the effects of small signal perturbations in the switching frequency and the input voltage on the small signal response of the resonant converters.

King and Stuart have determined steady state models for both the half-bridge [5] and the full-bridge [6] series resonant converter and have obtained normalized parametric curves for various currents and voltages taking the conduction angle of the feedback diode as a parameter. A dynamic model [7] based on a large signal approach has been developed by the same authors. The simulation of the transient states using a desktop calculator is possible using this model. Based on this work a small-signal model for the series resonant converter has been derived [8]. This model which is valid for low frequency control signals is based on the modulation of the diode conduction angle for control. The model is expected to be useful for the design of feedback loops.

A method of analysis recently put forward by Oruganti and Lee [9] uses the state-space techniques to analyse the transient and the steady state behaviour. The inductor current

and the capacitor voltage are taken as the two state variables. The resonant tank energy at any point on the state-plane can then be directly observed. A comparative assessment of different control schemes is possible using this technique [10].

Ranganathan, Ziogas and Stefanovic [11] and Steigerwald [1] have discussed the operation and control of the parallel resonant converter. The operation of the converter has been analysed and design curves have been given.

The series resonant converter has been simulated using the J3SCR model for SCRs by Avant and Lee [12]. Using this model possible fault transients in the series resonant converter have been simulated.

1.3 OBJECTIVES AND SCOPE OF THE PRESENT WORK

All methods of analysis of the resonant converters have till now used a time domain approach. This essentially involves solution of differential equations by numerical integration. The steady state analysis using differential equations requires considerable computational effort. The analysis of the resonant converters can also be done with the help of the standard programs for circuit simulation such as SPICE, SUPER-SCEPTRE etc. Such techniques, however, are inefficient in terms of computer time required. The purpose of the present work is to develop a technique for analysis of the resonant converters from the frequency domain standpoint. This considerably facilitates steady state analysis. The various circuit variables can then be determined using simple methods of circuit analysis.

Although there has been several efforts at modelling and analysis of the series resonant converter, the parallel resonant converter has not been analysed in sufficient detail to date. Hence it was decided to concentrate on the parallel resonant converter for this work.

The literature survey that was carried out revealed that till now the variation of power and efficiency in the resonant converters has not been studied in sufficient detail. Consequently it was decided to investigate this aspect of the parallel resonant converter also in detail.

1.4 ORGANISATION OF THE THESIS

The basic frequency domain model for the parallel resonant converter has been developed in Chapter 2. Assuming the quality factor Q of the resonant circuit to be infinite, expressions for the circuit currents and voltages have been determined in absolute as well as normalised forms. An algorithm for determining the phase difference ϕ between the voltage and the current sources of the model has been developed. Variations of the inductor current and the capacitor voltage with time have also been plotted.

In Chapter 3 the proposed model has been further refined by assuming a finite value of circuit resistance. The analysis proceeds in the same manner as in Chapter 2. A multiple conduction mode in which each power switch conducts twice in each half cycle has been identified. The behaviour of the converter in this mode has been discussed in detail. Waveforms

of the inductor current and the capacitor voltage obtained using the model have been compared with experimental results reported in literature.

Relationships among several important quantities have been obtained in Chapter 4. These relationships have been expressed graphically. The quantities whose variations have been studied include phase difference ϕ , peak capacitor voltage, average output voltage and turn off time available to the power switches. The boundary of the multiple conduction mode discussed in Chapter 3 has been obtained at different frequencies.

The variations of output power, input power, circuit losses and converter efficiency have been obtained in Chapter 5. These variations have been studied for two of the most popular control schemes: the open-loop frequency control and the closed-loop phase control. The performances of these two control schemes have been compared in the light of the results obtained in this chapter and in Chapter 4.

Using the results and the relationships obtained in Chapters 4 and 5, the procedure for designing a parallel resonant converter has been discussed in Chapter 6 with the help of an example. The modifications necessary in the design procedure to meet varying requirements have also been suggested.

The thesis concludes with Chapter 7 where a summary of the work done has been given together with some of the important conclusions reached. The advantages as well as the limitations of the proposed model have been pointed out. Some of the areas in which future work should concentrate have also been identified.

CHAPTER 2

A FREQUENCY DOMAIN MODEL FOR THE
PARALLEL RESONANT CONVERTER

2.1 INTRODUCTION

As pointed out in Chapter 1, all the methods employed till now for the analysis of the resonant converters have used a time domain approach. However, the resonant converters can be analysed from a frequency domain standpoint as well. A frequency domain model for the parallel resonant converter (Figure 1.1(b)) has been developed in this chapter.

The frequency domain model has been described in Section 2.2. The parallel resonant converter has been modelled as a series resonant L-C circuit fed by a square wave voltage source and a square wave current source in parallel with the resonant capacitor. Using this model a detailed analysis of the parallel resonant converter has been carried out in Section 2.3. Analytical expressions and waveforms for inductor current and capacitor voltage have been given.

In developing the model the resistance of the resonant L-C circuit has been neglected — i.e. the circuit Q has been assumed to be infinite. An improved model with finite Q has been developed later in Chapter 3. Furthermore, it has been assumed that the frequency of operation lies in the range $\frac{f_0}{2} < f < f_0$ which is the usual preferred mode of operation.

2.2 DEVELOPMENT OF THE MODEL ASSUMING INFINITE Q OF THE RESONANT CIRCUIT

The current and voltage waveforms for a resonant converter operating in the usual continuous conduction mode (with $\frac{f_o}{2} < f < f_o$) has been shown in Figure 1.2(a). During the half-cycle when the switch S_1 or the feedback diode D_1 conducts, the voltage across the input capacitor C_{11} is impressed across the L-C series circuit. During the next half-cycle, S_1 and D_1 are off and either the switch S_2 or the diode D_2 conducts and the voltage across C_{12} appears across the L-C circuit. Consequently, the input to the L-C circuit is a square wave voltage source of amplitude V_s . The frequency of this source is the same as the frequency at which the switches S_1 and S_2 are operated.

The output current I_o for a parallel resonant converter with a given load can be assumed to be a constant because of the presence of the inductor filter L_f at the output. Owing to the presence of the rectifier bridge the direction of the current at the input side of the transformer reverses every time the resonant capacitor voltage reverses. As a result the output current i_o (Figure 1.1(b)) looking from the capacitor terminals appears to be a square wave of amplitude I_o , whose frequency is the same as the converter frequency. This feature has been brought out in [11].

With these observations the parallel resonant converter can now be modelled as a series L-C circuit fed by a square wave voltage source v_1 in series with the L-C circuit and a square wave current source i_o in parallel with the resonant

capacitor (Figure 2.1(a)). The two sources, however, will not be in phase. The phase difference between the two sources is denoted by ϕ . This phase difference arises because of the fact that whereas the instant at which the polarity of the voltage source v_i reverses is determined by external switching of the inverter devices, the reversal of polarity of the current source i_o takes place when the capacitor voltage reverses. The various circuit waveforms relevant to the model are shown in Figure 2.1(b).

2.3 DETAILED ANALYSIS OF THE PARALLEL RESONANT CONVERTER USING THE INFINITE Q MODEL

Using the frequency domain model of the parallel resonant converter described in Section 2.2 the various voltages and currents in the circuit can be determined very conveniently using simple methods of circuit analysis. For this purpose the phase difference ϕ must be calculated for a given input voltage and a desired output current. In Section 2.3.1 generalized expressions for the inductor current and the capacitor voltage have been derived. These expressions have been given in a normalized form in Section 2.3.2. The technique used for the determination of ϕ have been described in Section 2.3.3. The time variations of inductor current and capacitor voltage have been given in Section 2.3.4.

2.3.1 Expressions for Inductor Current i_L and Capacitor Voltage v_C

The expressions for inductor current i_L and capacitor voltage v_C are determined by adding the harmonic components

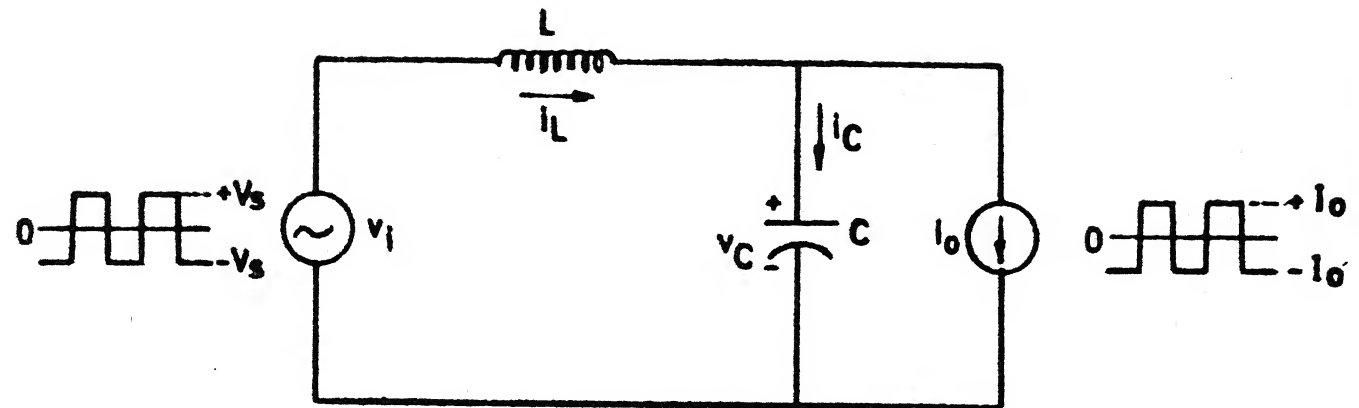


FIG. 2.1(a). A simple equivalent circuit for the parallel resonant converter with an inductor filter at the output

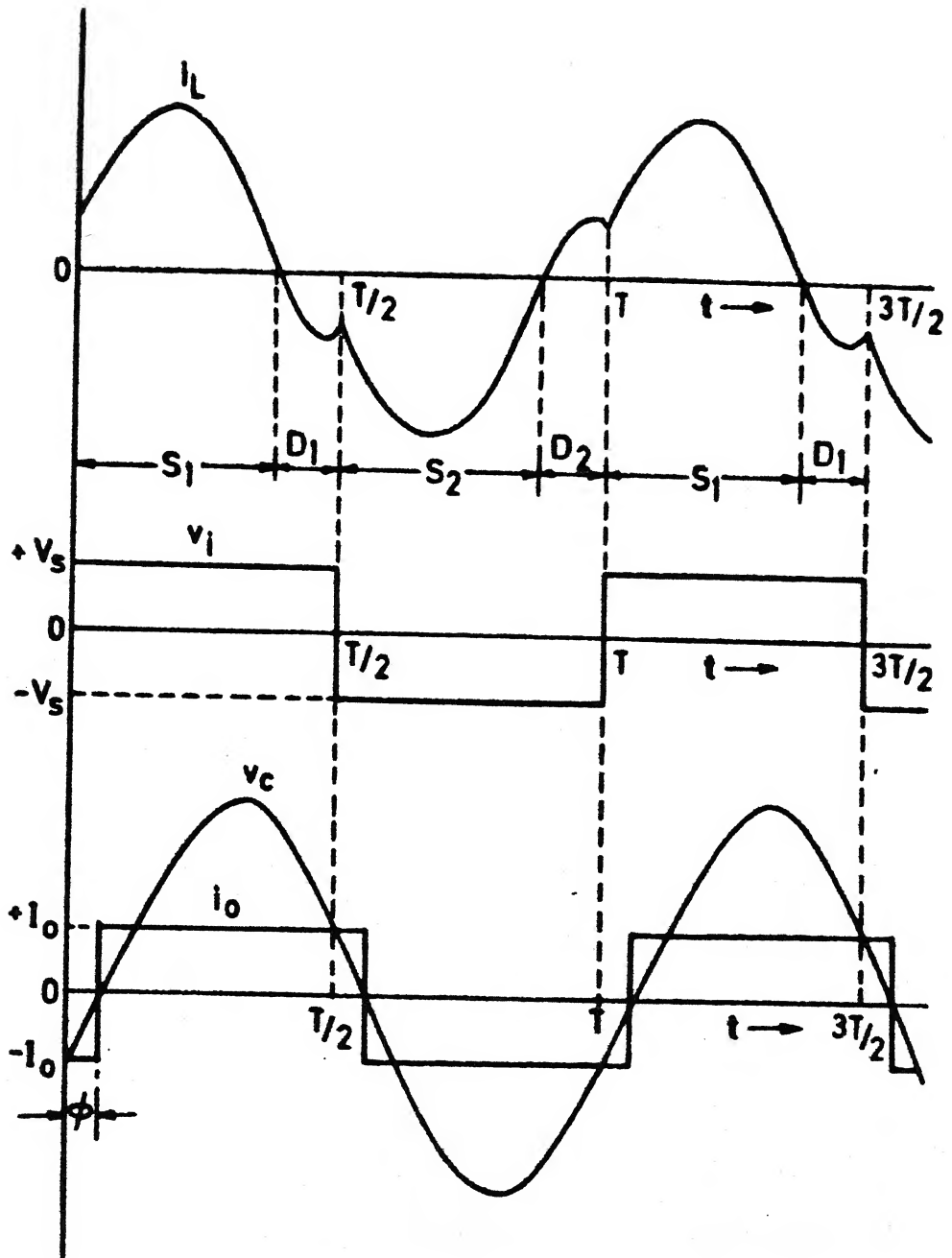


FIG. 2.1 (b). Voltage and current waveforms for the equivalent circuit of fig. 2.1 (a)

due to the various harmonics of the two sources, taking into account the phase differences between the corresponding harmonic components of the two sources. It should be noted that in all the summations used throughout n takes only odd integer values.

From the equivalent circuit of Figure 2.1(a) applying the principle of superposition, the expression for I_{Ln} , the n^{th} harmonic component of the inductor current, in phasor notation is given by

$$I_{Ln} = I_{Ln_1} + I_{Ln_2}$$

where I_{Ln_1} represents the n^{th} harmonic of the inductor current due to the voltage source v_1 only with the current source i_0 open circuited and I_{Ln_2} represents the n^{th} harmonic component of the inductor current due to i_0 only with v_1 short circuited.

The Fourier series expansion for a square wave of amplitude A is given by

$$f(t) = \sum_{n=1}^{\infty} \frac{4A}{n\pi} \sin n \omega t \quad (2.1)$$

where $n = 1, 3, 5, 7 \dots$

The phase difference between the fundamental components of two square waves separated by an angle ϕ is also ϕ . The phase difference between the n^{th} harmonic components is $n\phi$.

The time origin is chosen as shown in Figure 2.1(b), i.e. v_1 is taken as the reference. The expression for I_{Ln_1} may then be written as

$$I_{Ln_1} = \frac{1}{\sqrt{2}} \cdot \frac{4V_s}{n\pi} \angle 0 \cdot \frac{1}{jX_{Ln} - jX_{Cn}} \quad (2.2)$$

where $X_{Ln} = n\omega L$

$$X_{Cn} = \frac{1}{n\omega C} \quad (2.3)$$

$$n = 1, 3, 5, 7 \dots$$

The expression for I_{Ln_2} is given by

$$I_{Ln_2} = \frac{1}{\sqrt{2}} \cdot \frac{4I_o}{n\pi} \angle -n\phi \cdot \frac{-jX_{Cn}}{jX_{Ln} - jX_{Cn}} \quad (2.4)$$

From (2.2) and (2.4) the expression for I_{Ln} may be written as

$$\begin{aligned} I_{Ln} &= I_{Ln_1} + I_{Ln_2} \\ &= \frac{1.273}{n\sqrt{2}} V_s \angle 0 \cdot \frac{1}{(X_{Ln} - X_{Cn})} \angle -\frac{\pi}{2} \\ &\quad + \frac{1.273}{n\sqrt{2}} I_o \angle -n\phi \cdot \frac{X_{Cn}}{X_{Cn} - X_{Ln}} \end{aligned} \quad (2.5)$$

The corresponding expression in the time domain is

$$i_{Ln} = \frac{1.273 V_s}{n(X_{Ln} - X_{Cn})} \sin(n\omega t - \frac{\pi}{2}) + \frac{1.273 I_o X_{Cn}}{n(X_{Cn} - X_{Ln})} \sin(n\omega t - n\phi) \quad (2.6)$$

The time domain expression for i_L is

$$i_L = \sum_{n=1,3,5}^{\infty} i_{Ln} \quad (2.7)$$

where i_{Ln} is given by equation (2.6).

The expression for the capacitor voltage v_C can be derived in a similar manner. In phasor notation the n^{th} harmonic component of the capacitor voltage due to the voltage source v_i only is given by

$$V_{Cn_1} = \frac{1}{\sqrt{2}} \cdot \frac{4V_s}{n\pi} \angle 0 \cdot \frac{1}{jX_{Ln} - jX_{Cn}} \cdot -jX_{Cn} \quad (2.8)$$

where X_{Ln} and X_{Cn} are the same as defined in the expression (2.3)

The corresponding harmonic component of the capacitor voltage due to the current source i_o is

$$V_{Cn_2} = \frac{1}{\sqrt{2}} \cdot \frac{4(-I_o)}{n\pi} \angle -n\phi \cdot \frac{jX_{Ln}}{jX_{Ln} - jX_{Cn}} \cdot -jX_{Cn} \quad (2.9)$$

It should be noted that the negative sign is used before I_o because the polarity of the current source i_o is such that the component of the capacitor voltage due to i_o has a polarity which is opposite to that chosen for positive capacitor voltage.

From the expressions (2.8) and (2.9), the expression for V_{Cn} is given by

$$\begin{aligned} V_{Cn} &= V_{Cn_1} + V_{Cn_2} \\ &= \frac{1.273}{n\sqrt{2}} V_s \angle 0 \cdot \frac{1}{X_{Cn} - X_{Ln}} \cdot X_{Cn} - \\ &\quad \frac{1.273}{n\sqrt{2}} I_o \angle -n\phi \cdot \frac{X_{Ln}}{X_{Ln} - X_{Cn}} \cdot X_{Cn} \angle -\frac{\pi}{2} \end{aligned} \quad (2.10)$$

Equation (2.10) may be written in the time domain as

$$v_{Cn} = \frac{1.273 V_s X_{Cn}}{n(X_{Cn} - X_{Ln})} \sin n\omega t - \frac{1.273 I_o X_{Ln} X_{Cn}}{n(X_{Ln} - X_{Cn})} \sin(n\omega t - n\phi - \frac{\pi}{2}) \quad (2.11)$$

The resultant time domain expression for v_C , therefore, is

$$v_C = \sum_{n=1,3,5}^{\infty} v_{Cn} \quad (2.12)$$

where v_{Cn} is given by equation (2.11).

Referring to Figure 1.2(a) all other circuit currents and voltages may be determined from the state variables i_L and v_C by the following equations

$$i_C = i_L - i_o \quad (2.13)$$

$$v_L = L \frac{di_L}{dt} = v_i - v_C \quad (2.14)$$

$$i_{S_1} = i_L, \quad 0 \leq t \leq t_1 \quad (2.15)$$

$$i_{D_1} = i_L, \quad t_1 \leq t \leq T/2 \quad (2.16)$$

$$i_{S_2} = i_L, \quad T/2 \leq t \leq t_2 \quad (2.17)$$

$$i_{D_2} = i_L, \quad t_2 \leq t \leq T \quad (2.18)$$

2.3.2 Normalisation of Expressions

All expressions and relationships should be normalised in terms of per unit values for the convenience of the circuit designer. The various base and per unit quantities used for normalising different expressions henceforth are defined below.

$$\text{Base voltage } V_{\text{base}} = V_s \quad (2.19a)$$

$$\text{Base current } I_{\text{base}} = I_{o_{\text{max}}}, \text{ maximum possible value of output current } I_o \quad (2.19b)$$

$$\text{Base radian frequency } \omega_{\text{base}} = \frac{1}{\sqrt{LC}}, \text{ resonant frequency of the circuit} \quad (2.19c)$$

$$\text{Base impedance } Z_{\text{base}} = \frac{V_{\text{base}}}{I_{\text{base}}} = \frac{V_s}{I_{o_{\text{max}}}} \quad (2.19d)$$

$$L_{\text{base}} = \frac{Z_{\text{base}}}{\omega_{\text{base}}} \quad (2.19e)$$

$$C_{\text{base}} = \frac{1}{\omega_{\text{base}} Z_{\text{base}}} \quad (2.19f)$$

$$\text{Base power } P_{\text{base}} = V_{\text{base}} \cdot I_{\text{base}} = V_s \cdot I_{o_{\text{max}}} \quad (2.19g)$$

$$T_{\text{base}} = \frac{2\pi}{\omega_o} \quad (2.19h)$$

$$v_{\text{pu}} = \frac{v}{V_{\text{base}}} \quad (2.19i)$$

$$i_{\text{pu}} = \frac{i}{I_{\text{base}}} \quad (2.19j)$$

$$\omega_{\text{pu}} = \frac{\omega}{\omega_{\text{base}}} \quad (2.19k)$$

$$R_{\text{pu}} = \frac{R}{Z_{\text{base}}} \quad (2.19l)$$

$$L_{\text{pu}} = \frac{L}{L_{\text{base}}}, \quad x_{L_{\text{pu}}} = \frac{x_L}{Z_{\text{base}}} \quad (2.19m)$$

$$C_{\text{pu}} = \frac{C}{C_{\text{base}}}, \quad x_{C_{\text{pu}}} = \frac{x_C}{Z_{\text{base}}} \quad (2.19n)$$

$$P_{\text{pu}} = \frac{P}{P_{\text{base}}} \quad (2.19o)$$

$$T_{\text{pu}} = \frac{T}{T_{\text{base}}} \quad (2.19p)$$

From the above relationships one can easily conclude that

$$x_{L_{\text{pu}}} = \omega_{\text{pu}} L_{\text{pu}} \quad (2.19q)$$

$$x_{C_{\text{pu}}} = \frac{1}{\omega_{\text{pu}} C_{\text{pu}}} \quad (2.19r)$$

where $X_{L_{pu}}$ and $X_{C_{pu}}$ represent per unit reactances at frequency ω_{pu} .

In terms of per unit quantities the expressions for i_L and v_C given by equations (2.7) and (2.12) may be normalised.

$$\begin{aligned}
 i_{L_{pu}} &= \frac{i_L}{I_{base}} = \frac{i_L}{I_{o_{max}}} \\
 &= \sum_{n=1,3,5}^{\infty} \frac{1.273 V_s}{n I_{o_{max}} X_{Cn} \left(\frac{X_{Ln}}{X_{Cn}} - 1 \right)} \sin(n\omega t - \frac{\pi}{2}) \\
 &\quad + \sum_{n=1,3,5}^{\infty} \frac{1.273 I_o X_{Cn}}{n I_{o_{max}} X_{Cn} \left(1 - \frac{X_{Ln}}{X_{Cn}} \right)} \sin(n\omega t - n\phi) \quad (2.20)
 \end{aligned}$$

This may be written as

$$\begin{aligned}
 i_{L_{pu}} &= - \sum_n \frac{1.273}{n X_{Cn_{pu}} (1 - \beta_n)} \sin(n\omega t - \frac{\pi}{2}) \\
 &\quad + \sum_n \frac{1.273 I_{o_{pu}}}{n (1 - \beta_n)} \sin(n\omega t - n\phi) \quad (2.21)
 \end{aligned}$$

$$\text{where } \beta_n = \frac{X_{Ln}}{X_{Cn}} = n^2 \omega_{pu}^2 \quad (2.22)$$

$$\text{and } X_{Cn_{pu}} = \frac{X_{Cn}}{Z_{base}} = \frac{X_{Cn}}{\frac{V_s}{I_{o_{max}}}} = \frac{I_{o_{max}} X_{Cn}}{V_s}$$

as defined by equation (2.19n).

It should be noted that since the frequency of operation lies in the range $0.5 f_o < f < f_o$, $X_{Ln} < X_{Cn}$ for the fundamental component ($n = 1$). Consequently the quantity $(1 - \beta_n)$ is positive for the fundamental component. For the higher

harmonics ($n = 3, 5, 7, \dots$), however, $X_{Ln} > X_{Cn}$ and so $(1 - \beta_n)$ is negative.

Similarly one may write from equation (2.12)

$$v_{C_{pu}} = \frac{v_C}{V_{base}} = \frac{v_C}{V_s} = \sum_{n=1,3,5}^{\infty} \frac{1.273 V_s X_{Cn}}{n V_s X_{Cn} (1 - \frac{X_{Ln}}{X_{Cn}})} \sin n\omega t$$

$$- \sum_{n=1,3,5}^{\infty} \frac{1.273 I_o X_{Ln} X_{Cn}}{n V_s X_{Cn} (\frac{X_{Ln}}{X_{Cn}} - 1)} \sin(n\omega t - n\phi - \frac{\pi}{2}) \quad (2.23)$$

which could be written as

$$v_{C_{pu}} = \sum_n \frac{1.273}{n(1 - \beta_n)} \sin n\omega t + \sum_n \frac{1.273 I_o X_{Ln_{pu}}}{n(1 - \beta_n)} \sin(n\omega t - n\phi - \frac{\pi}{2}) \quad (2.24)$$

using the relationships defined in equation (2.19).

The expressions for $i_{L_{pu}}$ and $v_{C_{pu}}$ given by equations (2.21) and (2.24) respectively can be written in a more elegant form shown below. From equation (2.21)

$$i_{L_{pu}} = - \sum_{n=1,3,5}^{\infty} \frac{4}{n\pi(1 - n^2\omega_{pu}^2)X_{Cn_{pu}}} [\sin(n\omega t - \frac{\pi}{2})$$

$$- I_o X_{Cn_{pu}} \sin(n\omega t - n\phi)] \quad (2.25)$$

$$= - \sum_{n=1,3,5}^{\infty} \frac{K_n}{nX_{Cn_{pu}}} [\sin(n\omega t - \frac{\pi}{2}) - I_o X_{Cn_{pu}} \sin(n\omega t - n\phi)] \quad (2.26)$$

$$\text{where } K_n = \frac{4}{\pi(1 - n^2\omega_{pu}^2)} = \frac{1.273}{(1 - n^2\omega_{pu}^2)} \quad (2.27)$$

Similarly from equation (2.24) one may write

$$v_{C_{pu}} = \sum_{n=1,3,5}^{\infty} \frac{K_n}{n} \left[\sin n\omega t + I_{o_{pu}} X_{Ln_{pu}} \sin(n\omega t - n\phi - \frac{\pi}{2}) \right] \quad (2.28)$$

If $v_{C_{1_{pu}}}$ and $v_{C_{2_{pu}}}$ are the per unit components of the capacitor voltage due to voltage source v_1 and the current source i_o respectively, from equation (2.28) one may write

$$v_{C_{1_{pu}}} = \sum_n \frac{K_n}{n} \sin n\omega t \quad (2.29)$$

$$\begin{aligned} v_{C_{2_{pu}}} &= \sum_n \frac{K_n}{n} I_{o_{pu}} X_{Ln_{pu}} \sin(n\omega t - n\phi - \frac{\pi}{2}) \\ &= \frac{I_{o_{pu}} X_{Ln_{pu}}}{n} \sum_n K_n \sin(n\omega t - n\phi - \frac{\pi}{2}) \end{aligned} \quad (2.30)$$

since $\frac{I_{o_{pu}} X_{Ln_{pu}}}{n}$ is independent of n .

2.3.3 Determination of Phase Difference ϕ

In order to analyze the parallel resonant converter using the techniques illustrated above, the phase difference ϕ between the voltage and the current sources of Figure 2.1 needs to be determined. For a given value of input voltage V_s and output current I_o , ϕ can be calculated using the techniques discussed in this section. An approximate value of ϕ is first determined using a simple analytical result. This approximate solution is used as the initial value for numerically solving a non-linear equation to determine the actual value of ϕ .

2.3.3.1 Determination of Approximate Value of ϕ : The approximate value of ϕ is determined by taking into consideration only the fundamental components of the voltage and the current

source. The circuit waveforms under this condition are shown in Figure 2.2(a). The capacitor voltage v_C must be in phase with the sinusoidal current source i_o . Substituting $\omega t = \emptyset$, $v_C = 0$ and $n = 1$ in equation (2.28) gives

$$K_1 [\sin \emptyset + I_{o_{pu}} X_{L1_{pu}} \sin(-\frac{\pi}{2})] = 0 \quad (2.31)$$

$$\text{where } X_{L1_{pu}} = \frac{\omega L}{Z_{base}} \text{ and } K_1 = \frac{4}{\pi(1 - \omega_{pu}^2)}$$

Rewriting equation (2.31)

$$\sin \emptyset - I_{o_{pu}} X_{L1_{pu}} = 0$$

$$\therefore \emptyset = \sin^{-1}(I_{o_{pu}} X_{L1_{pu}}) \quad (2.32)$$

Equation (2.32) gives the approximate value of \emptyset assuming sinusoidal sources.

The above relationship (2.32) may also be derived from the phasor diagram for the fundamental components. From equations (2.28), (2.29) and (2.30) considering only the fundamental component ($n = 1$), the capacitor voltage in terms of per unit quantities can be expressed in phasor rotation as follows

$$\begin{aligned} V_{C_{pu}} &= V_{C1_{pu}} + V_{C2_{pu}} \\ &= \frac{K_1}{\sqrt{2}} \angle 0 + \frac{K_1}{\sqrt{2}} (I_{o_{pu}} X_{L1_{pu}}) \angle -\emptyset - \frac{\pi}{2} \\ \therefore V_{C_{pu}} &= \frac{K_1}{\sqrt{2}} (1 \angle 0 + I_{o_{pu}} X_{L1_{pu}} \angle -\emptyset - \frac{\pi}{2}) \end{aligned} \quad (2.33)$$

The phasor diagram corresponding to equation (2.33) is shown in Figure 2.2(b). All the phasors have been scaled down in magnitude by the factor $\frac{\sqrt{2}}{K_1}$.

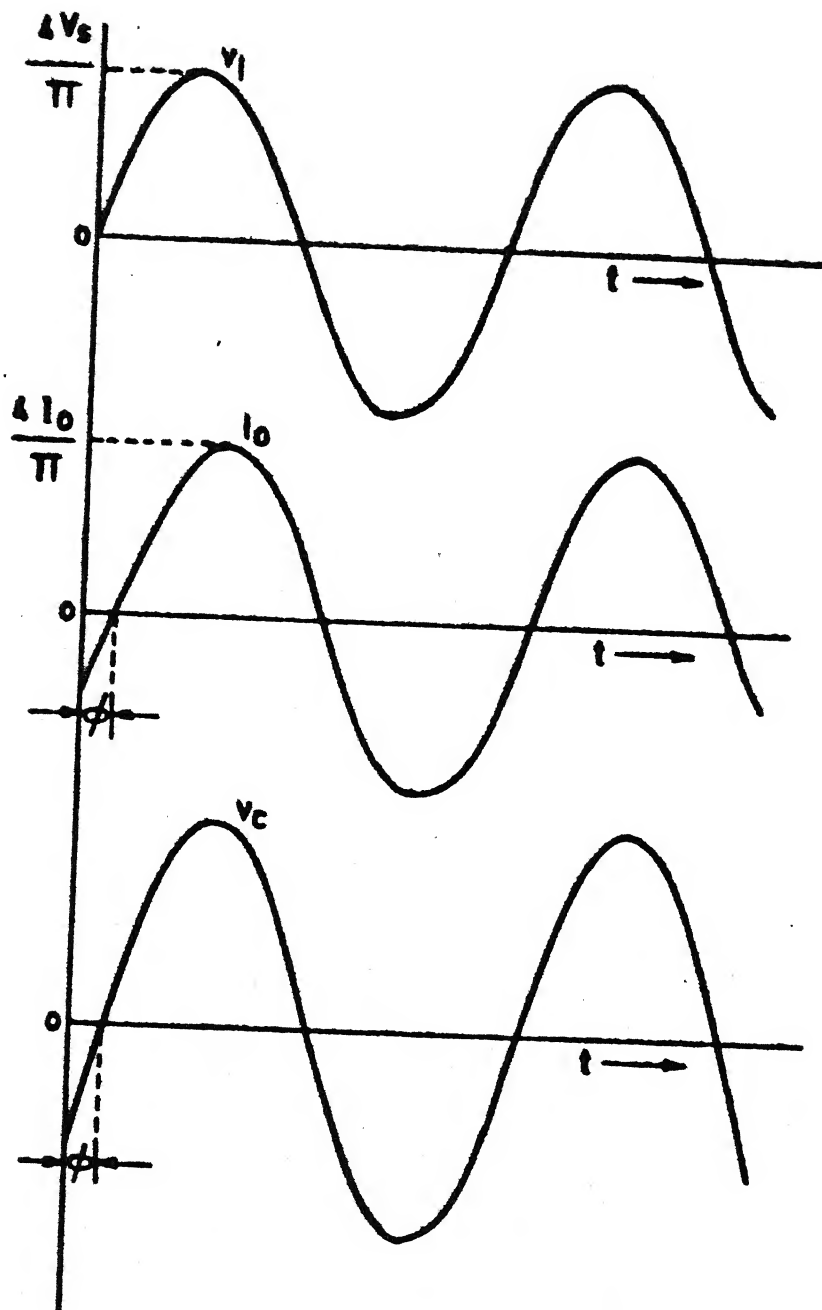


FIG. 2.2(a). Circuit waveforms for the equivalent circuit of fig. 2.1 (a) assuming only sinusoidal sources

From Figure 2.1(b) it follows that the resultant capacitor voltage $V_{C_{pu}}$ and the current source phasor $I_{o_{pu}}$ are in phase. So the phase difference between $V_{C_{pu}}$ and the voltage source phasor $V_{s_{pu}}$ is also \emptyset . The angle between the phasors $V_{C_{1_{pu}}}$ and $V_{C_{2_{pu}}}$ is $\frac{\pi}{2} + \emptyset$ and their resultant $V_{C_{pu}}$ makes an angle \emptyset with $V_{C_{1_{pu}}}$.

From the phasor diagram of Figure 2.2(b) one can write

$$\sin \emptyset = \frac{|V_{C_{2_{pu}}}|}{|V_{C_{1_{pu}}}|} \quad (2.34)$$

$$\text{i.e. } \emptyset = \sin^{-1} \frac{|V_{C_{2_{pu}}}|}{|V_{C_{1_{pu}}}|} \quad (2.35)$$

Substituting the values of $|V_{C_{1_{pu}}}|$ and $|V_{C_{2_{pu}}}|$ from equation (2.33) into (2.35) gives

$$\emptyset = \sin^{-1} |I_{o_{pu}} X_{L1_{pu}}| \quad (2.36)$$

2.3.3.2 Determination of the Actual Value of \emptyset : Both the sources in the equivalent circuit of Figure 2.1(a) are square wave sources and the effects of the source harmonics need to be taken into account in determining the actual value of \emptyset . From the waveforms of Figure 2.1(b) it is observed that the zero crossings of the resultant capacitor voltage v_C , obtained by adding all the harmonic components of v_C , must be the same as the zero crossings of the load current i_o , looking from the capacitor terminals (Figure 1.1(b)). This implies that substituting ωt equal to \emptyset in equations (2.12) or (2.28), the right

hand side must reduce to zero. This condition has been used to compute the value of ϕ by numerical techniques. Setting $\omega t = \phi$ and $v_C = 0$ in eqn. (2.28) results in the following non-linear equation in ϕ

$$\sum_{n=1,3,5}^{\infty} \frac{K_n}{n} \left[\sin n\phi + I_{o_{pu}} \frac{X_{Ln_{pu}}}{n} \sin\left(-\frac{\pi}{2}\right) \right] = 0$$

$$\text{or, } \sum_n \frac{K_n}{n} [\sin n\phi] = \frac{I_{o_{pu}} X_{Ln_{pu}}}{n} \sum_n K_n \quad (2.37)$$

since $\frac{I_{o_{pu}} X_{Ln_{pu}}}{n}$ is independent of n .

This equation has been solved by using the IMSL sub-routine ZFALSE. This routine finds the zero of a function over a specified interval. The approximate value of ϕ , ϕ_{approx} , as given by equation (2.32) has been used to narrow down the region $(\phi_{\text{approx}} - \delta)$ to $(\phi_{\text{approx}} + \delta)$ in which ϕ may possibly lie. δ is initially taken as 0.05. If the root does not lie in this interval, δ is incremented by 0.05 and the IMSL sub-routine ZFALSE is called again to solve the equation (2.37). This procedure is repeated till the root is obtained. This considerably lessens the amount of numerical computations required to solve the non-linear equation. A flow chart of the entire process of determination of ϕ has been given in Figure 2.3.

2.3.4 Time Domain Waveforms of Inductor Current i_L and Capacitor Voltage v_C

The variations of i_L and v_C with time have been plotted for two cycles of converter operation from $\omega t = 0$ to $\omega t = 4\pi$

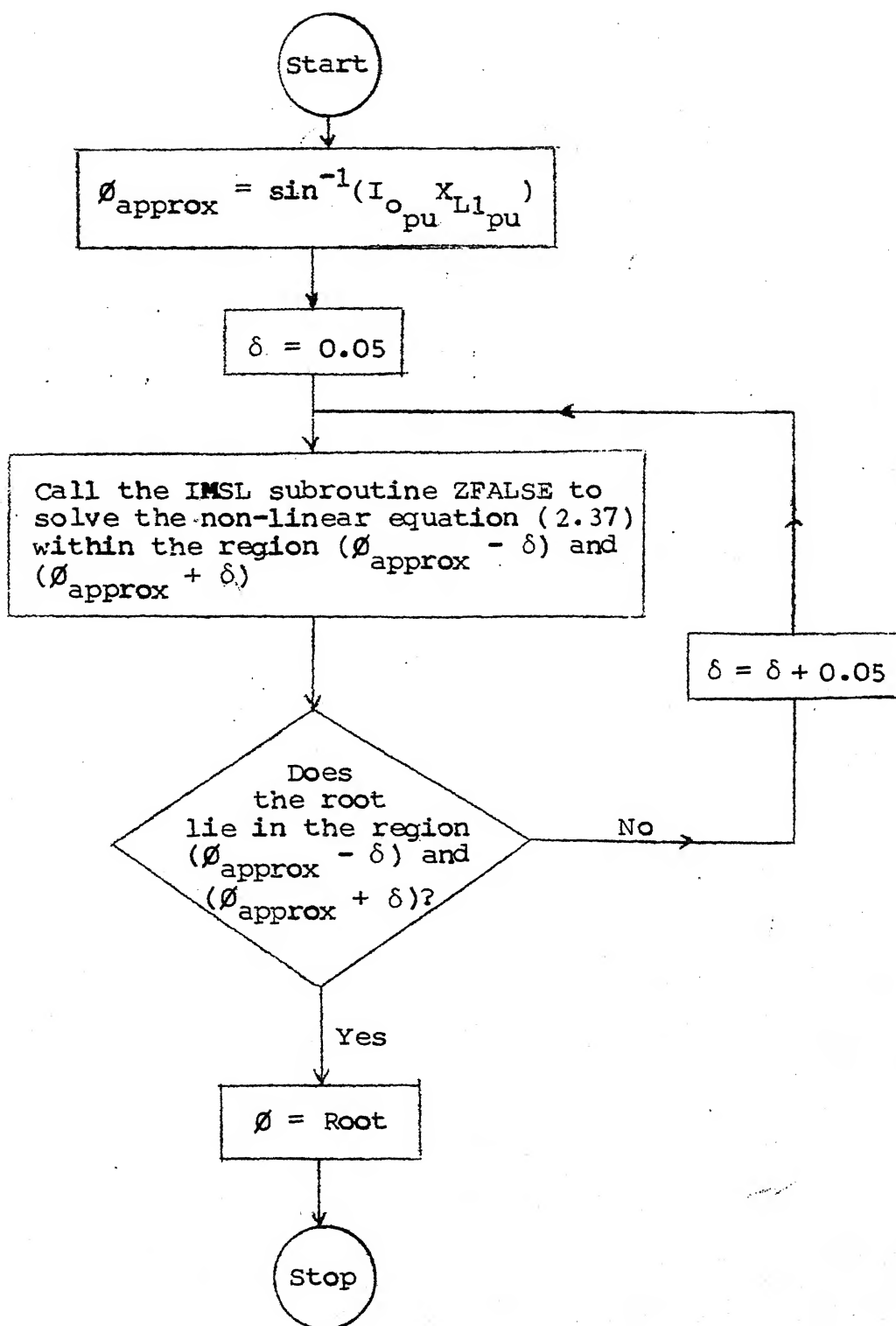


Fig. 2.3 Flow chart for determination of the value of \emptyset for the infinite-Q model.

for five different sets of frequency and output current I_o (Figures 2.4(a) through 2.4(e)). For each set of frequency and I_o , the corresponding value of ϕ has first been determined by the method described in Section 2.3.3. The values of i_L and v_C at various points have then been calculated with the help of the expressions (2.7) and (2.12). The circuit parameters considered in simulation study are:

$$L = 73 \mu\text{H} \qquad C = 5 \mu\text{F} \qquad V_s = 120 \text{ V}$$

The curves have been plotted using the GPGS (General Purpose Graphics System) subroutines in the DEC-10 computer system. To calculate i_L and v_C the effects of all source harmonics upto the 9th harmonic have been considered.

2.4 CONCLUSIONS

A novel frequency domain model for the parallel resonant converter with an inductor filter at the output has been proposed. It has been shown that the model can be used to analyze the parallel resonant converter in a very simple manner. The expression for the phase difference ϕ between the voltage and current source in this model has been found to be non-linear. An algorithm has been given to solve this equation. It has also been observed that the waveforms obtained using the frequency domain model match closely those expected from the analysis of the converter in the time domain.

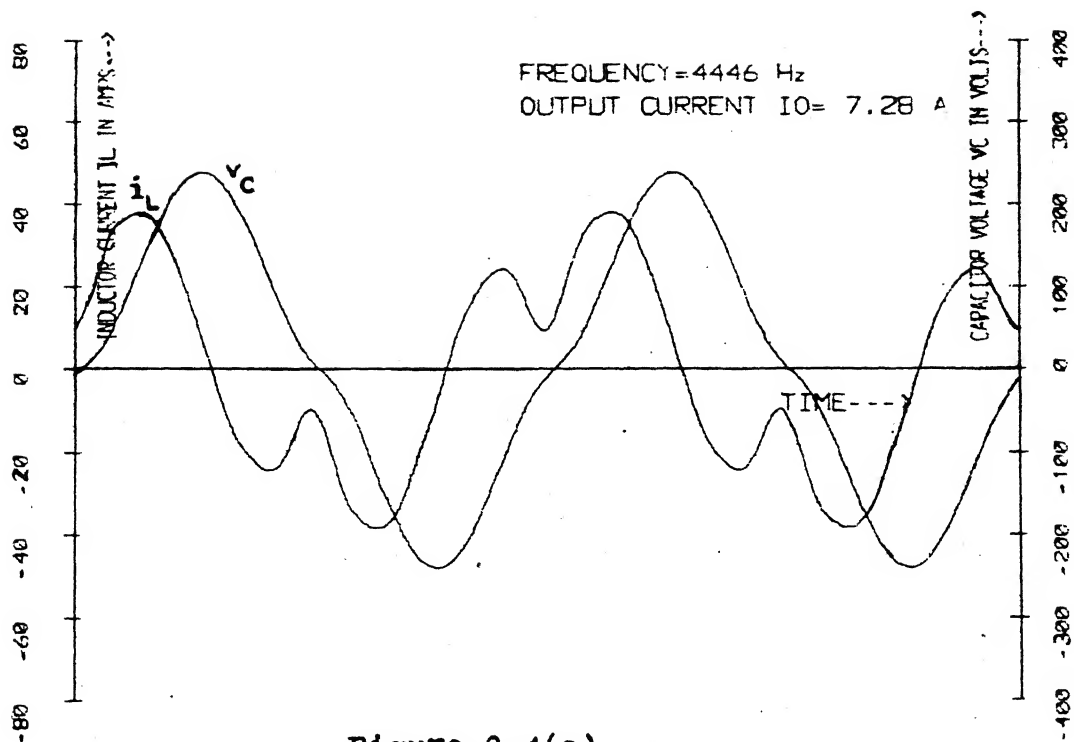


Figure 2.4(a)

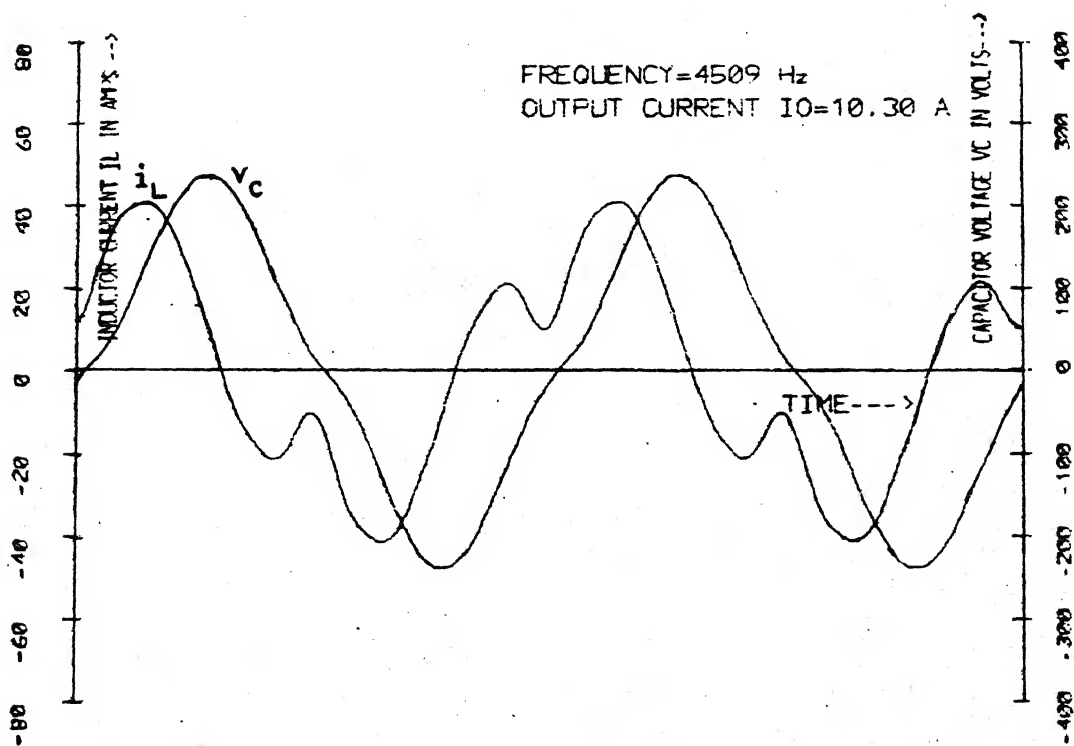


Figure 2.4(b)

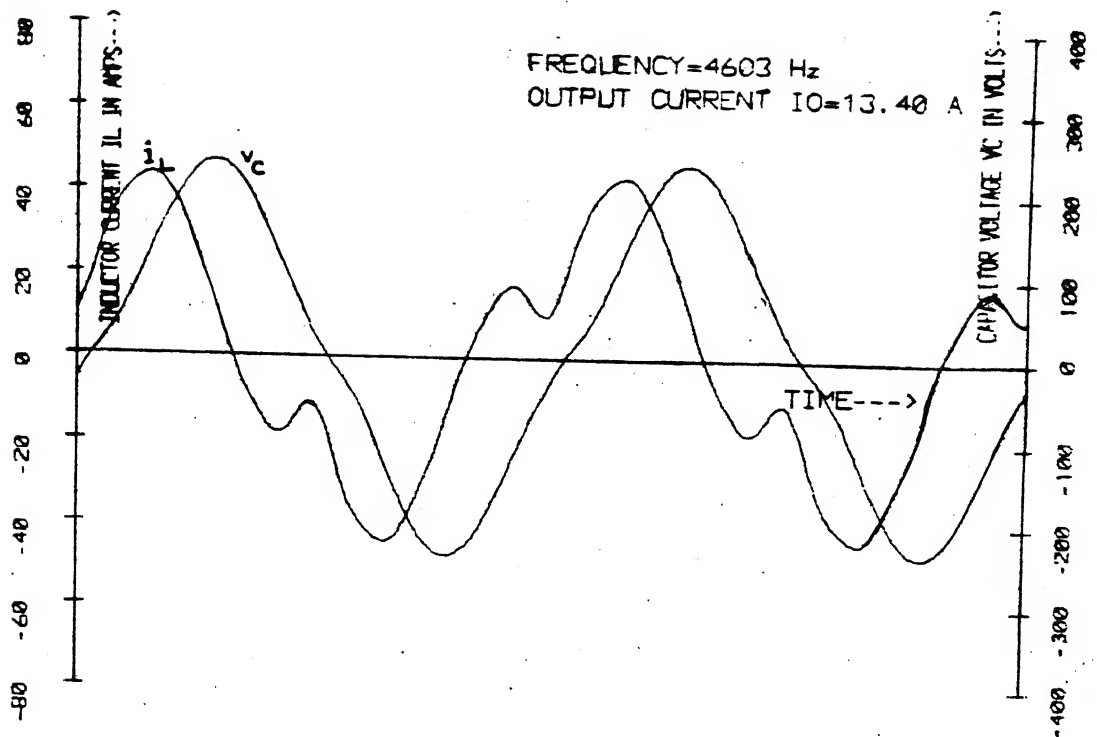


Figure 2.4(c)

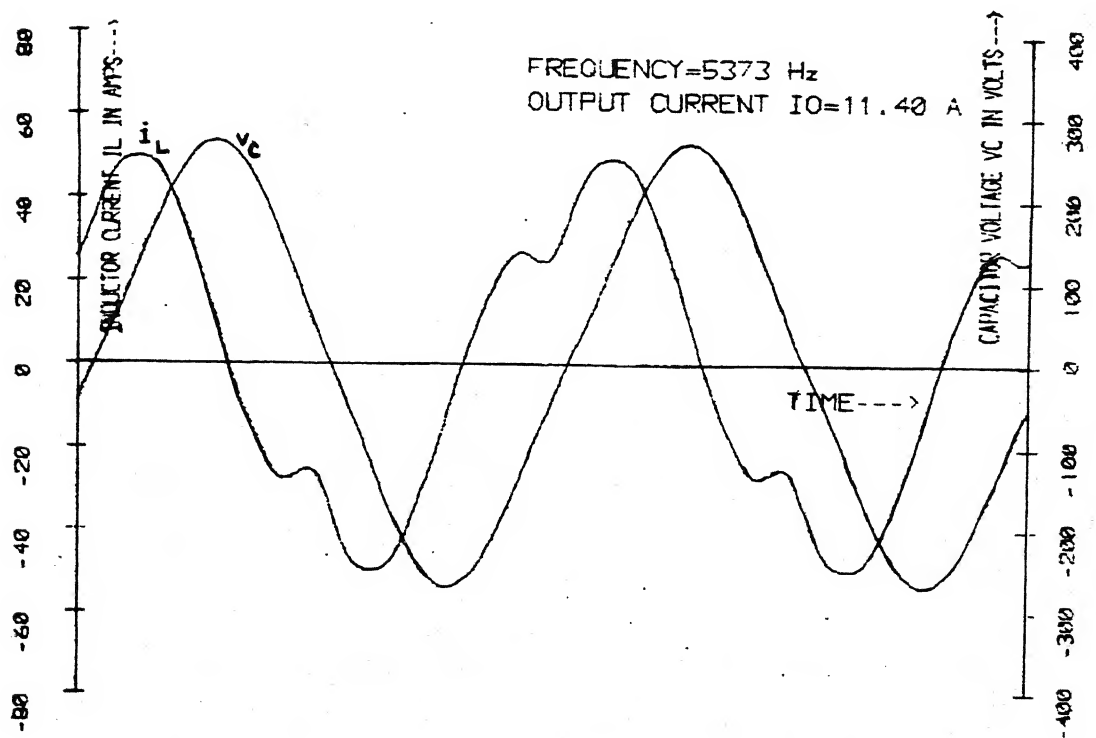


Figure 2.4(d)

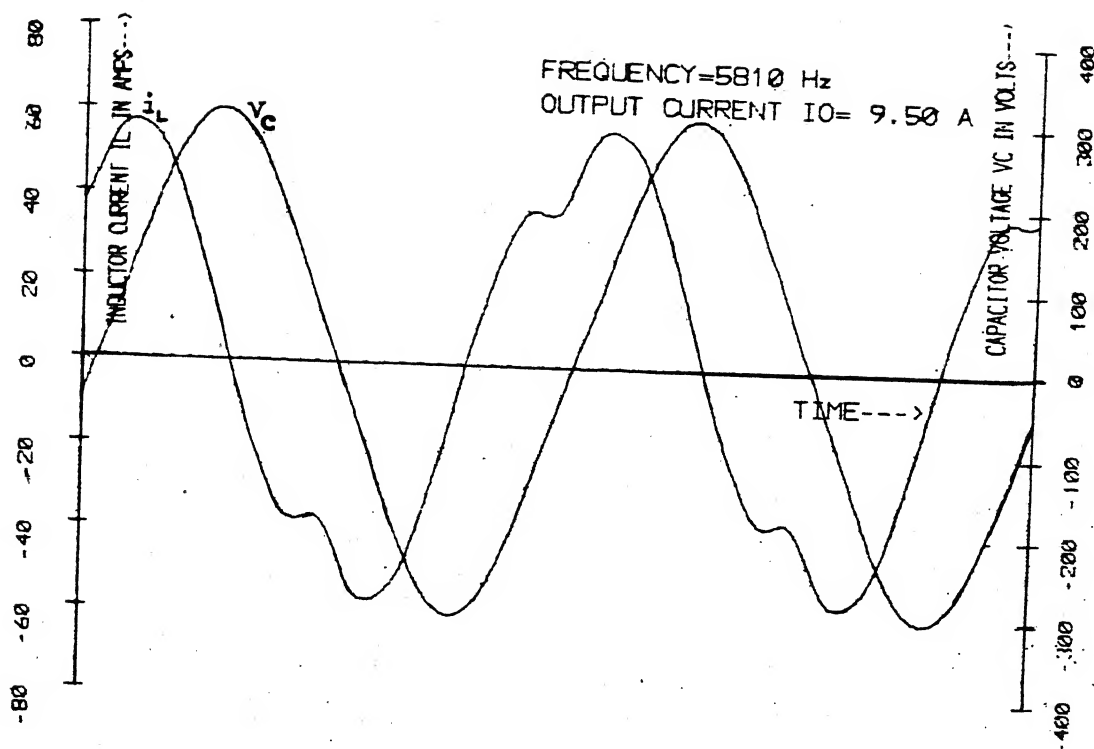


Figure 2.4(e)

Figure 2.4. Inductor current and capacitor voltage waveforms obtained from the model of Figure 2.1(a) for $L = 73 \mu\text{H}$, $C = 5 \mu\text{F}$ and $V_s = 120$ V.

CHAPTER 3

MODIFICATION OF THE BASIC FREQUENCY DOMAIN MODEL ALLOWING
FOR A FINITE RESISTANCE IN THE INDUCTOR COIL

3.1 INTRODUCTION

The frequency domain model of the parallel resonant converter described in Chapter 2 assumes infinite quality factor for the resonant circuit. In all practical circuits, however, the inductor coil has a finite resistance whose effect may not be neglected. The effect of this resistance on converter performance can be analysed using the modified model described in this chapter. The modified model is essentially the same as that of Figure 2.1(a) except that a small resistance R is assumed to be present in series with the ideal inductor L (Figure 3.1). The capacitor C as before is assumed to be ideal. Waveforms similar to those of Figure 2.1(b) apply equally for the circuit of Figure 3.1.

Using the modified model a detailed analysis of the parallel resonant converter similar to that of Section 2.3 has been carried out in Section 3.2. Time domain plots of inductor current and capacitor voltage have been obtained as in Chapter 2. Finally, the results obtained using the simpler model of Chapter 2 and the modified model described in this chapter have been compared in Section 3.3 with experimental results reported in literature [11].

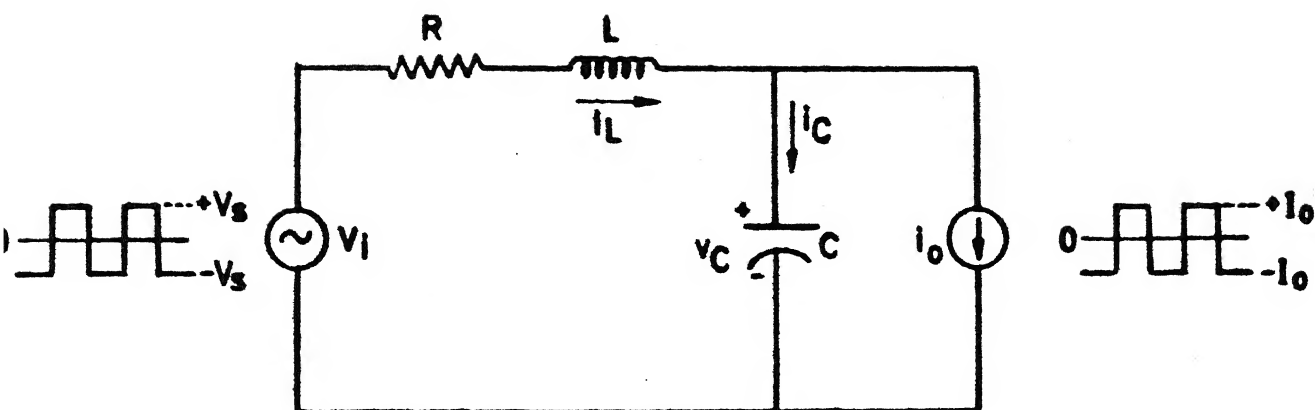


FIG. 3.1. A modified frequency domain model for the parallel resonant converter

3.2 DETAILED ANALYSIS OF THE PARALLEL RESONANT CONVERTER USING THE MODIFIED MODEL

The steps followed in this analysis are the same as those of Section 2.3 except that the resistance R has been taken into account in the derivation of all expressions.

3.2.1 Expressions for Inductor Current i_L and Capacitor Voltage v_C

Recalling the Fourier series expansion of a square wave (equation (2.1)) and the observation that the phase difference between the n^{th} harmonic components of the two square wave sources of Figure 3.1 is $n\phi$, the expression for the n^{th} harmonic component of the inductor current due to the voltage source v_1 only in phasor notation is

$$I_{Ln_1} = \frac{1}{\sqrt{2}} \cdot \frac{4V_s}{n\pi} \angle 0 \cdot \frac{1}{R + jX_{Ln} - jX_{Cn}} \quad (3.1)$$

where X_{Ln} , X_{Cn} and n are the same as defined by equation (2.3).

The corresponding expression for the n^{th} harmonic component of the inductor current due to the current source i_o only is

$$I_{Ln_2} = \frac{1}{\sqrt{2}} \cdot \frac{4I_o}{n\pi} \angle -n\phi \cdot \frac{-jX_{Cn}}{R + jX_{Ln} - jX_{Cn}} \quad (3.2)$$

Applying the principle of superposition, the expression for I_{Ln} , the n^{th} harmonic component of the inductor current is given by

$$I_{Ln} = I_{Ln_1} + I_{Ln_2} \quad (3.3)$$

i.e.

$$I_{Ln} = \frac{1.273}{n\sqrt{2}} V_s \angle 0 \cdot \frac{1}{Z_n} \angle -\theta_{Zn} + \frac{1.273}{n\sqrt{2}} I_o \angle -n\phi \cdot \frac{X_{Cn}}{Z_n} \angle -\frac{\pi}{2} - \theta_{Zn} \quad (3.4)$$

$$\text{where } Z_n = \{R^2 + (X_{Ln} - X_{Cn})^2\}^{1/2} \quad (3.5)$$

$$\text{and } \theta_{Zn} = \tan^{-1} \frac{X_{Ln} - X_{Cn}}{R} \quad (3.6)$$

The corresponding expression in the time domain is

$$i_{Ln} = \frac{1.273 V_s}{nZ_n} \sin(n\omega t - \theta_{Zn}) + \frac{1.273 I_o X_{Cn}}{nZ_n} \sin(n\omega t - n\phi - \frac{\pi}{2} - \theta_{Zn}) \quad (3.7)$$

Adding all the harmonic components, the time domain expression for i_L is

$$i_L = \sum_{n=1,3,5}^{\infty} i_{Ln} \quad (3.8)$$

where i_{Ln} is given by equation (3.7).

V_{Cn1} and V_{Cn2} , the components of the n^{th} harmonic of the capacitor voltage due to the voltage source v_i and the current source i_o respectively, are given by

$$V_{Cn1} = \frac{1}{\sqrt{2}} \cdot \frac{4V_s}{n\pi} \angle 0 \cdot \frac{1}{R + jX_{Ln} - jX_{Cn}} \cdot (-jX_{Cn}) \quad (3.9)$$

$$V_{Cn2} = \frac{1}{\sqrt{2}} \cdot \frac{4(-I_o)}{n\pi} \angle -n\phi \cdot \frac{R + jX_{Ln}}{R + jX_{Ln} - jX_{Cn}} \cdot (-jX_{Cn}) \quad (3.10)$$

As pointed out in Chapter 2, the negative sign is used before I_o because the polarity of the capacitor voltage due to the current source i_o is opposite to that chosen for the positive capacitor voltage.

The expression for the n^{th} harmonic component of the capacitor voltage V_{Cn} is

$$\begin{aligned}
v_{cn} &= v_{cn1} + v_{cn2} \\
&= \frac{1.273}{n\sqrt{2}} v_s \angle 0 \cdot \frac{1}{Z_n} \angle -\theta_{zn} \cdot x_{cn} \angle -\frac{\pi}{2} \\
&\quad - \frac{1.273}{n\sqrt{2}} I_o \angle -n\phi \cdot \frac{Z_{Ln}}{Z_n} \angle \theta_{Ln} - \theta_{zn} \cdot x_{cn} \angle -\frac{\pi}{2}
\end{aligned} \tag{3.11}$$

$$\text{where } Z_{Ln} = \{R^2 + (x_{Ln})^2\}^{1/2} \tag{3.12}$$

$$\theta_{Ln} = \tan^{-1} \frac{x_{Ln}}{R} = \tan^{-1} Q_n \tag{3.13}$$

(Q_n is the quality factor of the coil at frequency $n\omega$) and Z_n and θ_{zn} are as defined by expressions (3.5) and (3.6) respectively.

The corresponding time domain expression is

$$\begin{aligned}
v_{cn} &= \frac{1.273 v_s x_{cn}}{nZ_n} \sin(n\omega t - \frac{\pi}{2} - \theta_{zn}) \\
&\quad - \frac{1.273 I_o Z_{Ln} x_{cn}}{nZ_n} \sin(n\omega t - n\phi - \frac{\pi}{2} + \theta_{Ln} - \theta_{zn})
\end{aligned} \tag{3.14}$$

So the resultant time domain expression for v_C is

$$v_C = \sum_{n=1,3,5}^{\infty} v_{cn} \tag{3.15}$$

where v_{cn} is given by equation (3.14).

Using the normalisation technique of Section 2.3.2

i_L and v_C can be expressed in terms of per unit quantities as follows.

$$\begin{aligned}
i_{L_{pu}} &= \frac{i_L}{I_{base}} = \frac{i_L}{I_{o_{max}}} \\
&= \sum_{n=1,3,5}^{\infty} \frac{1.273}{n X_{Cn_{pu}} Z'_n} \sin(n\omega t - \theta_{Zn}) \\
&\quad + \sum_{n=1,3,5}^{\infty} \frac{1.273 I_{o_{pu}}}{n Z'_n} \sin(n\omega t - n\emptyset - \frac{\pi}{2} - \theta_{Zn}) \quad (3.16)
\end{aligned}$$

$$\begin{aligned}
v_{C_{pu}} &= \frac{v_C}{V_{base}} = \frac{v_C}{V_s} \\
&= \sum_{n=1,3,5}^{\infty} \frac{1.273}{n Z'_n} \sin(n\omega t - \frac{\pi}{2} - \theta_{Zn}) \\
&\quad - \sum_{n=1,3,5}^{\infty} \frac{1.273 I_{o_{pu}} X_{Ln_{pu}} Z'_{Ln}}{n Z'_n} \sin(n\omega t - n\emptyset \\
&\quad - \frac{\pi}{2} + \theta_{Ln} - \theta_{Zn}) \quad (3.17)
\end{aligned}$$

$$\text{where } Z'_n = \{\alpha_n^2 + (\beta_n - 1)^2\}^{1/2} \quad (3.18)$$

$$\text{and } Z'_{Ln} = (\gamma_n^2 + 1)^{1/2} \quad (3.19)$$

$$\text{with } \alpha_n = \frac{R}{X_{Cn}} \quad (3.20)$$

$$\beta_n = \frac{X_{Ln}}{X_{Cn}} = n^2 \omega_{pu}^2 \quad (3.21)$$

$$\text{and } \gamma_n = \frac{R}{X_{Ln}} = \frac{1}{Q_n} \quad (3.22)$$

All other circuit currents and voltages may be determined using equations (2.13) through (2.18) of Chapter 2.

The expressions for $i_{L_{pu}}$ and $v_{C_{pu}}$ could also be written as follows

$$i_{L_{pu}} = \sum_{n=1,3,5}^{\infty} \frac{A_n}{n X_{C_{pu}}} [\sin(n\omega t - \theta_{Zn}) + I_{O_{pu}} X_{C_{pu}} \sin(n\omega t - n\phi - \frac{\pi}{2} - \theta_{Zn})] \quad (3.23)$$

$$v_{C_{pu}} = \sum_{n=1,3,5}^{\infty} \frac{A_n}{n} [\sin(n\omega t - \frac{\pi}{2} - \theta_{Zn}) - I_{O_{pu}} X_{L_{pu}} Z'_{Ln} \sin(n\omega t - n\phi - \frac{\pi}{2} + \theta_{Ln} - \theta_{Zn})] \quad (3.24)$$

$$\text{where } A_n = \frac{4}{\pi Z'_n} = \frac{1.273}{Z'_n} = \frac{1.273}{\{\alpha_n^2 + (n^2 \omega_{pu}^2 - 1)^2\}^{1/2}} \quad (3.25)$$

It is easily observed that for $R = 0$, α_n is equal to zero and the expressions for inductor current and capacitor voltage (equations (3.23) and (3.24)) obtained using the modified model in this chapter reduce to the corresponding expressions (equations (2.26) and (2.28)) of Chapter 2.

$v_{C_{1pu}}$ and $v_{C_{2pu}}$, the per unit components of the capacitor voltage due to the voltage source v_1 and the current source i_o respectively are given by

$$v_{C_{1pu}} = \sum_n \frac{A_n}{n} \sin(n\omega t - \frac{\pi}{2} - \theta_{Zn}) \quad (3.26)$$

$$\begin{aligned} v_{C_{2pu}} &= - \sum_n \frac{A_n}{n} I_{O_{pu}} X_{L_{pu}} Z'_{Ln} \sin(n\omega t - n\phi - \frac{\pi}{2} + \theta_{Ln} - \theta_{Zn}) \\ &= - \frac{I_{O_{pu}} X_{L_{pu}}}{n} \sum_n A_n Z'_{Ln} \sin(n\omega t - n\phi - \frac{\pi}{2} + \theta_{Ln} - \theta_{Zn}) \end{aligned} \quad (3.27)$$

3.2.2 Determination of Phase Difference ϕ

As in Section 2.3.3 an approximate value of ϕ is first determined neglecting all harmonics except the fundamental. This value of ϕ has been used as the initial value for numerically solving a non-linear equation to determine a more accurate value of ϕ . For the modified frequency domain model, however, no simple mathematical formula, such as the one given by equation (2.32), may be derived from which an approximate value of ϕ can be obtained analytically to start with. However, a simple non-linear equation in ϕ has been obtained assuming only fundamental components. By solving this non-linear equation an approximate solution for ϕ has been obtained which can be used as the initial value.

3.2.2.1 Determination of Approximate Value of ϕ : To determine the approximate value of ϕ only the fundamental components of the voltage source v_i and the current source i_o of Figure 3.1 are considered. The circuit waveforms under such conditions are similar to those of Figure 2.2(a). The corresponding phasor diagram of Figure 2.2(b), however, has to be modified to include the effect of the resistance. The modified phasor diagram is shown in Figure 3.2.

$V_{C_{1pu}}$ and $V_{C_{2pu}}$ are the components of the per unit capacitor voltage $V_{C_{pu}}$ due to the voltage source v_o and the current source i_o respectively. Considering only the fundamental components ($n = 1$), the expression for $V_{C_{1pu}}$ and $V_{C_{2pu}}$ can be written from equations (3.26) and (3.27) respectively.

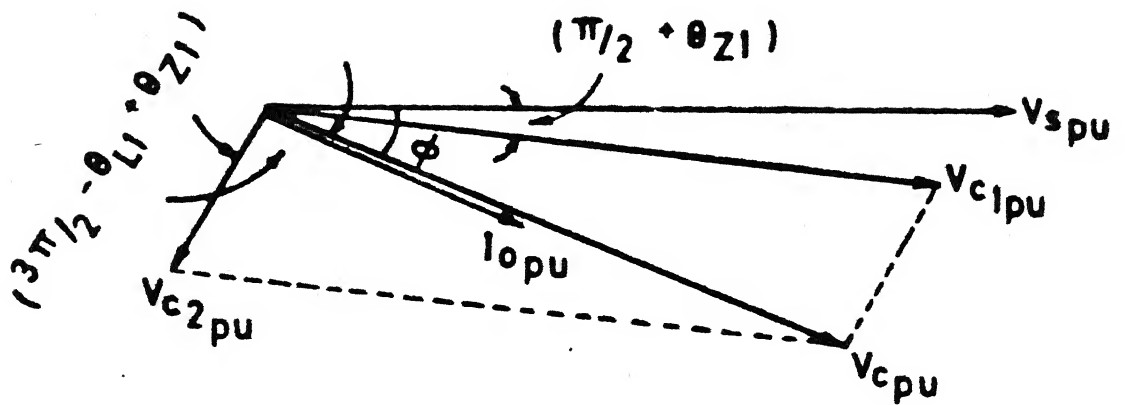


FIG. 3.2. Phasor diagram for the equivalent circuit of fig. 3.1 assuming only sinusoidal sources

$$V_{C_{1pu}} = \frac{A_1}{\sqrt{2}} \angle -\frac{\pi}{2} - \theta_{Z1} \quad (3.28)$$

$$V_{C_{2pu}} = - \frac{I_{o_{pu}} X_{L1_{pu}} A_1 Z'_{L1}}{\sqrt{2}} \angle -\emptyset - \frac{\pi}{2} + \theta_{L1} - \theta_{Z1}$$

$$\text{i.e. } V_{C_{2pu}} = \frac{I_{o_{pu}} X_{L1_{pu}} A_1 Z'_{L1}}{\sqrt{2}} \angle -\emptyset - \frac{3\pi}{2} + \theta_{L1} - \theta_{Z1} \quad (3.29)$$

$$\text{Here } A_1 = \frac{4}{\pi Z'_{L1}}, \quad Z'_{L1} = \left\{ \left(\frac{R}{X_{C1}} \right)^2 + \left(\frac{X_{L1}}{X_{C1}} - 1 \right)^2 \right\}^{1/2} \quad (3.30)$$

$$X_{L1} = \omega L, \quad X_{C1} = \frac{1}{\omega C} \quad (3.31)$$

$$Z'_{L1} = \left\{ \left(\frac{R}{X_{L1}} \right)^2 + 1 \right\}^{1/2} \quad (3.32)$$

$$\theta_{L1} = \tan^{-1} \frac{X_{L1}}{R} \quad (3.33)$$

$$\theta_{Z1} = \tan^{-1} \frac{X_{L1} - X_{C1}}{R} \quad (3.34)$$

It should be noted that since the fundamental frequency is below the resonant frequency, X_{L1} is less than X_{C1} and so θ_{Z1} is a negative acute angle. Consequently $(\frac{\pi}{2} + \theta_{Z1})$ is an acute angle and $(\frac{3\pi}{2} - \theta_{L1} + \theta_{Z1})$ is an obtuse angle.

Since the resultant capacitor voltage $V_{C_{pu}}$ and the current source phasor $I_{o_{pu}}$ are in phase, the phase difference between the phasors $V_{C_{pu}}$ and the voltage source phasor $V_{S_{pu}}$ is also \emptyset . The angle between the phasors $V_{C_{1pu}}$ and $V_{C_{2pu}}$ is $(\frac{3\pi}{2} - \theta_{L1} + \theta_{Z1}) + (\emptyset - \frac{\pi}{2} - \theta_{Z1})$, i.e. $(\pi + \emptyset - \theta_{L1})$ and their resultant $V_{C_{pu}}$ makes an angle $(\emptyset - \frac{\pi}{2} - \theta_{Z1})$ with V_{C_1} . This gives the relationship

$$\tan(\theta - \frac{\pi}{2} - \theta_{Z1}) = \frac{|V_{C_{2pu}}| \sin(\pi + \theta - \theta_{L1})}{|V_{C_{1pu}}| + |V_{C_{2pu}}| \cos(\pi + \theta - \theta_{L1})} \quad (3.35)$$

Equation (3.35) after simplification gives

$$\begin{aligned} |V_{C_{1pu}}| \cos(\theta_{Z1} - \theta) - |V_{C_{2pu}}| \cos(\theta_{Z1} - \theta) \cos(\theta - \theta_{L1}) \\ + |V_{C_{2pu}}| \sin(\theta_{Z1} - \theta) \sin(\theta - \theta_{L1}) = 0 \end{aligned} \quad (3.36)$$

Substituting the magnitudes of $V_{C_{1pu}}$ and $V_{C_{2pu}}$ from (3.28) and (3.29) into (3.36) and dividing both sides by $\frac{A_1}{\sqrt{2}}$ gives

$$\begin{aligned} \cos(\theta_{Z1} - \theta) - I_{Opu} X_{L1pu} Z'_{L1} \cos(\theta_{Z1} - \theta) \cos(\theta - \theta_{L1}) \\ + I_{Opu} X_{L1pu} Z'_{L1} \sin(\theta_{Z1} - \theta) \sin(\theta - \theta_{L1}) = 0 \end{aligned} \quad (3.37)$$

(3.37) is the resulting non-linear equation in θ the solution of which gives the approximate value of θ .

Equation (3.37) has been solved using the same technique described in Section 2.3.3.2 that has been used to solve equation (2.37). The value of θ as given by equation (2.32) has been taken as a rough estimate of θ . This approximate value of θ has been used as the initial value for solving equation (3.37) in the region $(\theta_{approx} - \delta)$ and $(\theta_{approx} + \delta)$. δ is assigned an initial value of 0.05 and is incremented in steps of 0.05 till a solution of (3.37) is obtained.

3.2.2.2 Determination of the Actual Value of θ : The actual value of θ has been determined using exactly the same method

described in Section 2.3.3.2. Setting $\omega t = \emptyset$ and $v_c = 0$ in equation (3.24) results in the following non-linear equation in \emptyset .

$$\sum_{n=1,3,5}^{\infty} \frac{A_n}{n} \left[\sin(n\emptyset - \frac{\pi}{2} - \theta_{Zn}) - I_{o_{pu}} X_{Ln_{pu}} Z'_{Ln} \sin(-\frac{\pi}{2} + \theta_{Ln} - \theta_{Zn}) \right] = 0$$

i.e.

$$\sum_n \frac{A_n}{n} \cos(\theta_{Zn} - n\emptyset) = \frac{I_{o_{pu}} X_{Ln_{pu}}}{n} \sum_n A_n Z'_{Ln} \cos(\theta_{Ln} - \theta_{Zn}) \quad (3.38)$$

This equation is solved using the IMSL subroutine ZFALSE. As before, the approximate value of \emptyset as given by the solution of the equation (3.37) has been used to narrow down the region $(\emptyset_{approx} - \delta)$ to $(\emptyset_{approx} + \delta)$ in which \emptyset may possibly lie. δ is initially assigned a value of 0.05 and is incremented in steps of 0.05 till the root is obtained. The entire process of determination of \emptyset has been outlined in the flow chart of Figure 3.3.

It may be pointed out here that while the determination of the value of \emptyset corresponding to a given value of I_o involves the solution of a complicated non-linear equation such as equation (3.38), it is much simpler to proceed in a reverse manner. In Section 4.2 it has been shown that for a given value of \emptyset the corresponding value of the quantity $I_{o_{pu}} X_{L1_{pu}}$ can very easily be calculated with the help of equation (4.10).

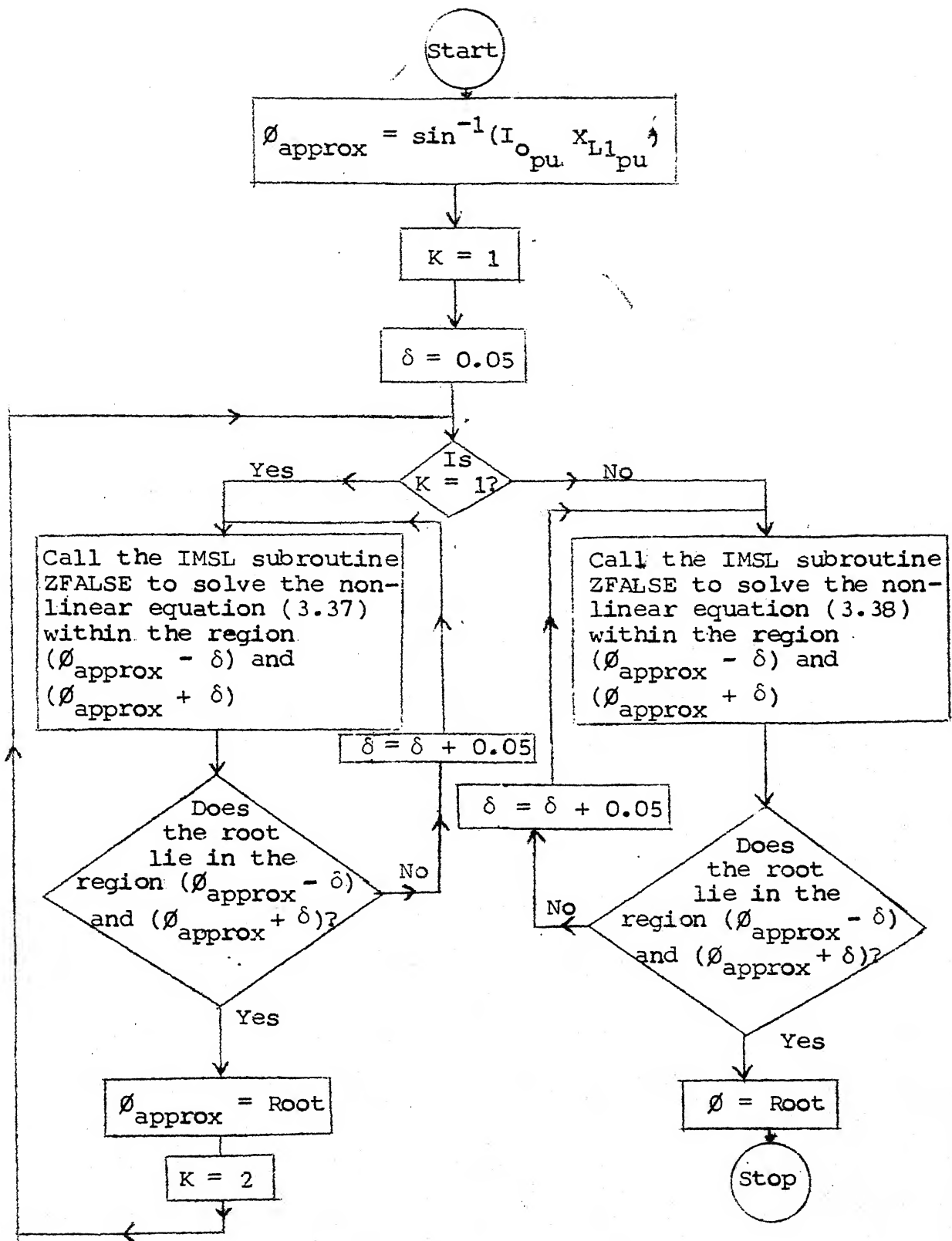


Fig. 3.3 Flow chart for determination of the value of ϕ for the modified model.

3.2.3 Time Domain Waveforms of Inductor Current i_L and Capacitor Voltage v_C

The variations of i_L and v_C with time have been plotted for two cycles of converter operation from $\omega t = 0$ to $\omega t = 4\pi$ for the same five sets of frequency and output current I_O as in Section 2.3.4. The plots have been obtained using the GPGS. These plots have been shown in Figure 3.4(a) through Figure 3.4(e). For each set of frequency and I_O , the corresponding value of ϕ has first been calculated using the algorithm described in Section 3.2.2. The values of i_L and v_C at various points have been then calculated using the expressions (3.8) and (3.15) respectively. The various circuit parameters chosen are the same as before except that instead of assuming an infinite Q , a circuit Q of 7.3 is assumed. The different circuit parameters are

$$L = 73 \mu\text{H} \quad C = 5 \mu\text{F} \quad Q = 7.3 \quad V_S = 120 \text{ V}$$

$$R = \frac{\omega_o L}{Q} = \frac{1}{Q} \left(\frac{L}{C} \right)^{1/2} = 0.5234 \Omega$$

In calculating i_L and v_C the effects of all source harmonics upto 9th were considered.

3.2.3.1 Multiple Continuous Conduction Mode in which Each

Power Switch Conducts Twice in Each Half Cycle: While plot-

ting the inductor current i_L it was observed that when the output current I_O is increased keeping the frequency fixed somewhere in the frequency range $0.5 < \frac{f}{f_o} < 1$, there is a tendency on the part of the converter to enter into a continuous conduction mode which is quite different from that of

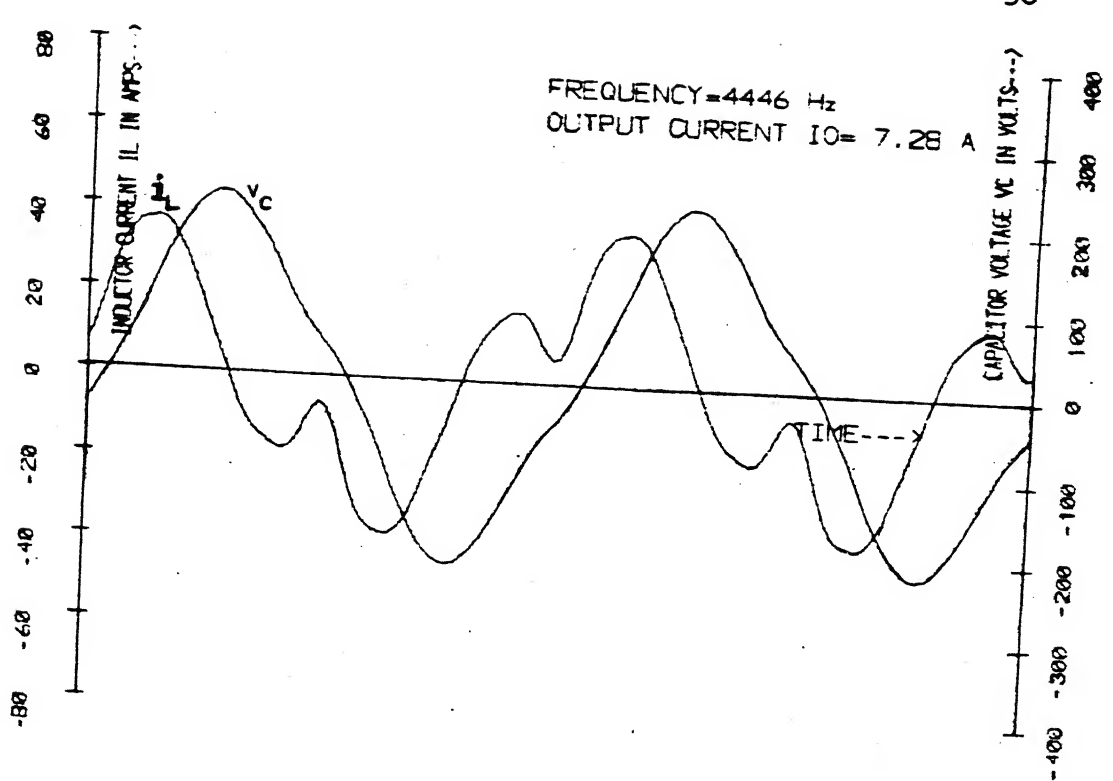


Figure 3.4(a)

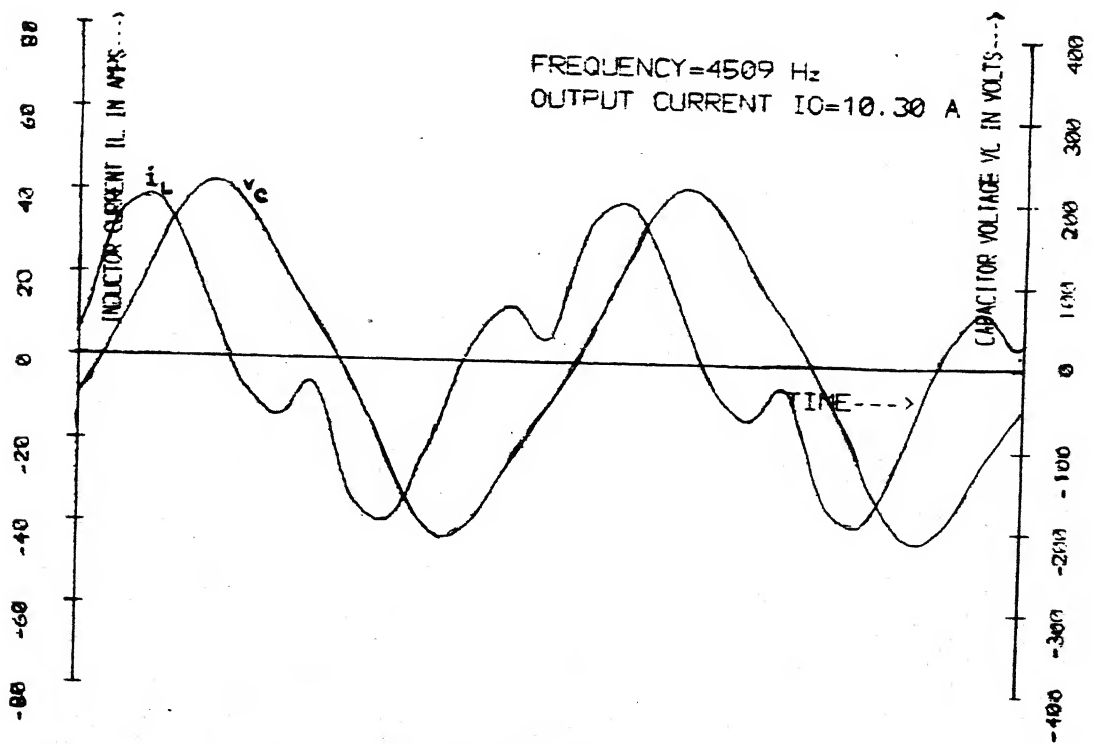


Figure 3.4(b)

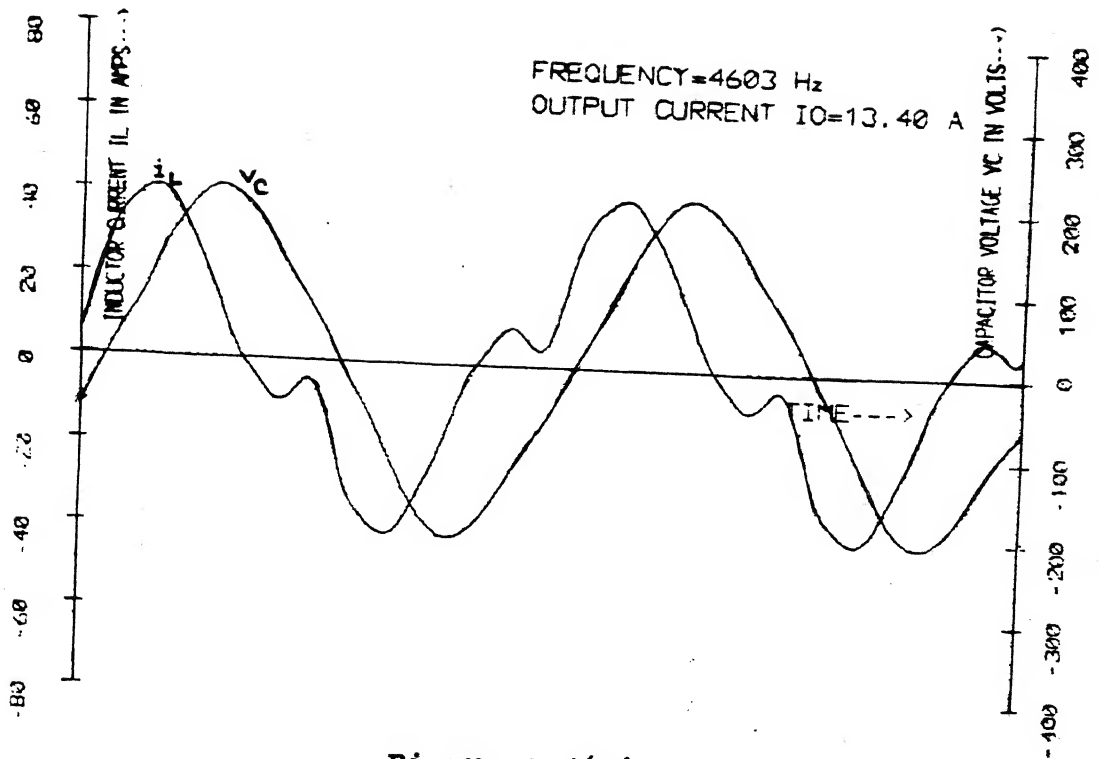


Figure 3.4(c)

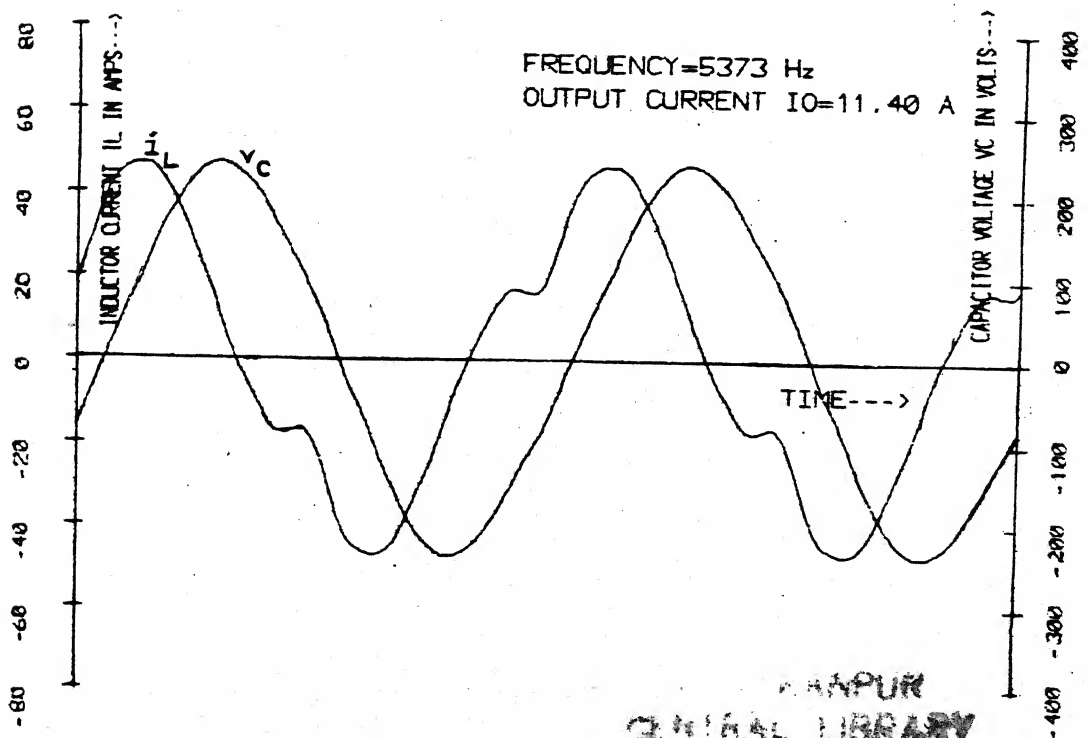


Figure 3.4(d)

CHAPUR
CENTRAL LIBRARY
92045
A

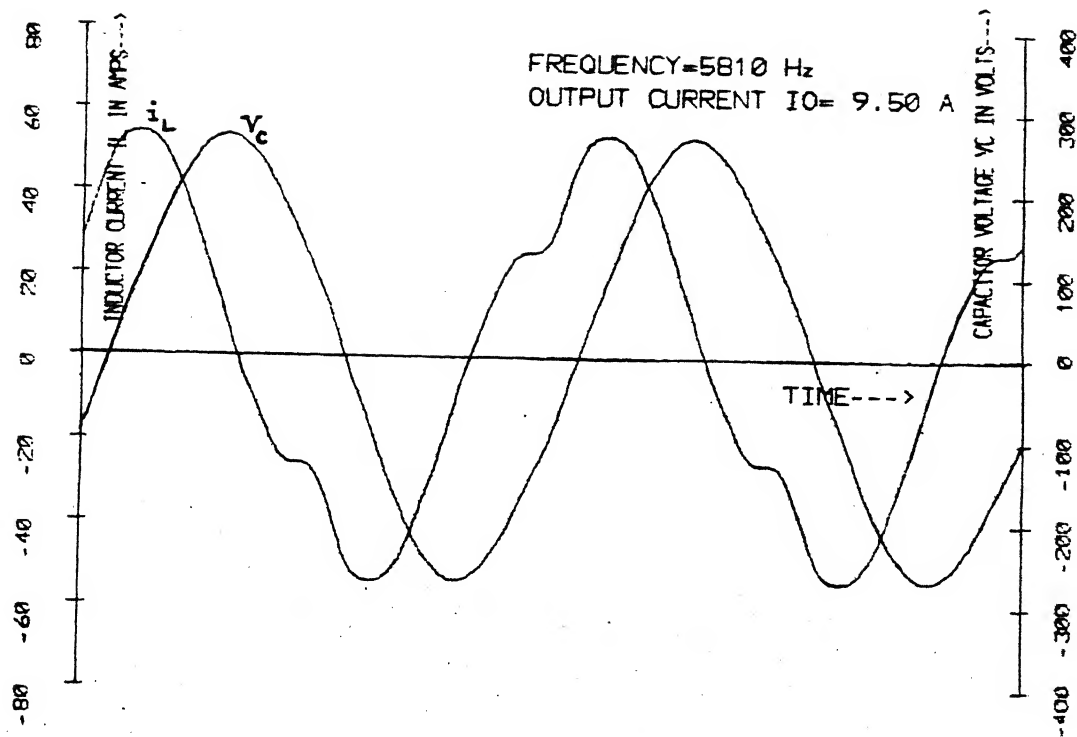


Figure 3.4(e)

Figure 3.4. Inductor current and capacitor voltage waveforms obtained from the model of Figure 3.1 for $L = 73 \mu\text{H}$, $C = 5 \mu\text{F}$, $Q = 7.3$ and $V_s = 120$ V.

Figure 1.2(a). In this mode the power switch S_1 or S_2 conducts twice in each half cycle. Such a mode has been illustrated in Figure 3.5 for $f = 4.6$ KHz and $I_o = 19$ A.

The conduction sequence over a full cycle in the multiple continuous conduction mode has been sketched in Figure 3.6. At the start of the first half cycle at $t = 0$ the inductor current i_L is negative. The device conducting then is the feedback diode D_1 . When i_L becomes positive, conduction passes to the switch S_1 . When i_L reverses again, the diode D_1 takes over. Before the half cycle is complete, i_L becomes positive again and S_1 starts to conduct once more. At the end of the first half cycle S_1 is turned off by forced commutation and i_L , which is still positive, now flows through the feedback diode D_2 . When i_L reverses in direction, the switch S_2 starts to conduct. The conduction sequence in the second half cycle is similar to that in the first.

It should be noted that when the converter is operating in the multiple continuous conduction mode, the power switches S_1 and S_2 cannot be turned off by natural commutation. S_1 and S_2 must be turned off by forced commutation or gate control when they are still conducting current. Also, the switches S_1 and S_2 must be turned on slightly after the beginning of each half cycle so that a short circuit of the input voltage sources through S_1 and S_2 is prevented. The switch S_1 or S_2 should be turned on only when the switch that was conducting at the end of the previous half cycle has been completely turned off.

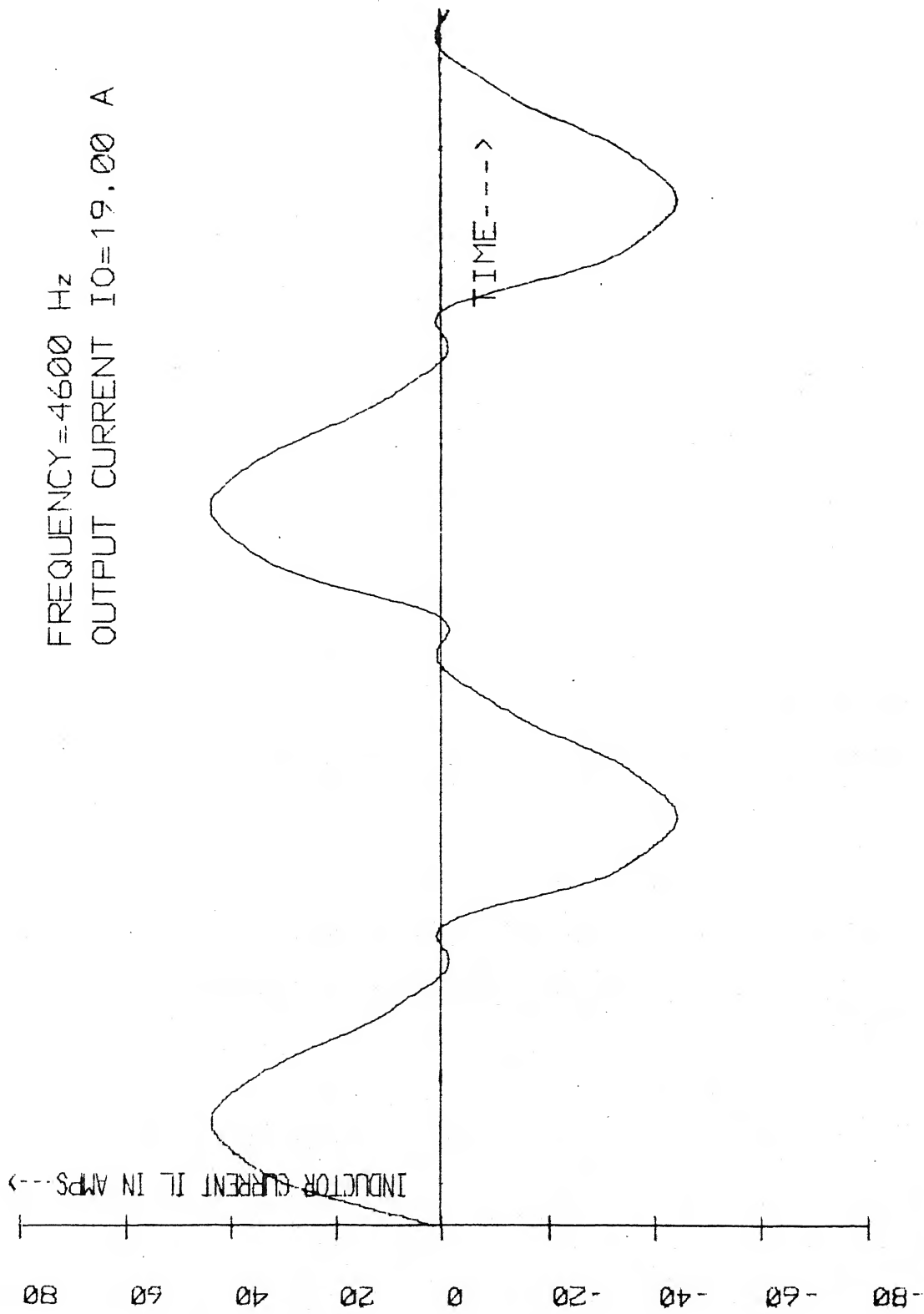


Figure 3.5. Inductor current and capacitor voltage waveforms in the multiple continuous conduction mode
 ($L = 73 \mu\text{H}$, $C = 5 \mu\text{F}$, $Q = 7.3$ and $V_s = 120 \text{ V}$).

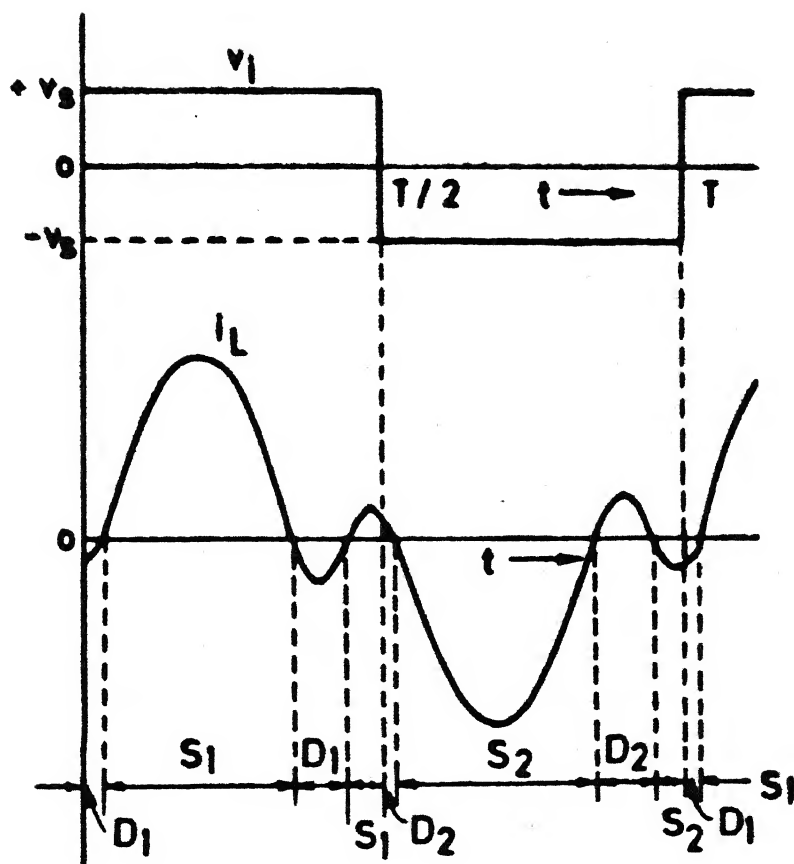


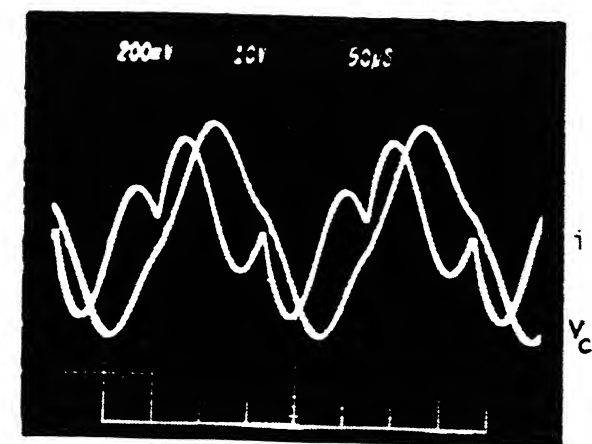
FIG.3.6. Inductor current waveform in the multiple continuous conduction mode

It was observed that as the frequency is raised, the magnitude of output current I_o at which the converter just enters into this mode is also correspondingly increased. This increase continues till frequencies near the resonant frequency after which there is a decrease in the value of I_o required to enter into this mode.

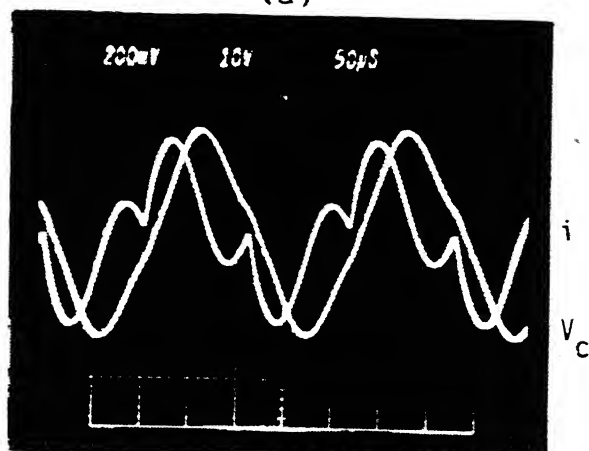
It should be noted that the continuous conduction mode is possible only if the power switches S_1 and S_2 are gated continuously in the first and second half cycles respectively. If, however, pulse gating is used the converter will enter into discontinuous conduction mode at higher values of I_o instead of entering into the multiple continuous conduction mode discussed above. In such cases there is an upper limit on the value of output current I_o for which continuous conduction is possible at a given frequency. For pulse gating, however, the exact behaviour of the converter for values of I_o above this specified limit cannot be predicted from the frequency domain model, since discontinuous conduction violates the basic assumption on which the model is based.

3.3 COMPARISON OF THE RESULTS OBTAINED FROM THE SIMPLER MODEL, THE MODIFIED MODEL AND EXPERIMENTAL RESULTS REPORTED IN LITERATURE [11]

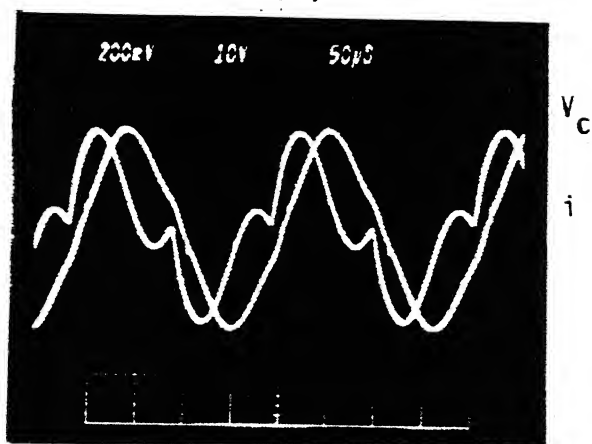
Experimental waveforms of inductor current i_L and capacitor voltage v_C reported in [11] have been reproduced in Figure 3.7. These waveforms have been obtained for the same circuit parameters and the same five sets of frequency and output current I_o as those of Figure 3.4.



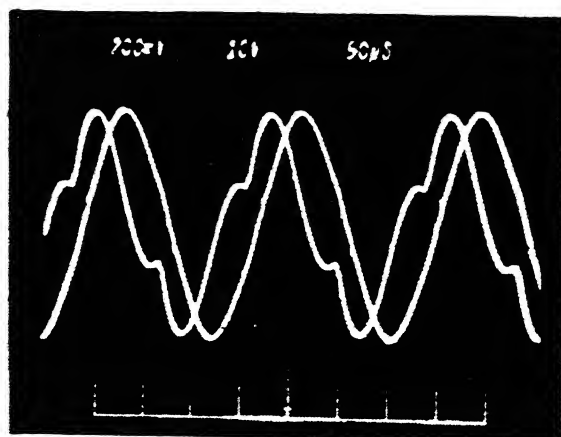
(a)



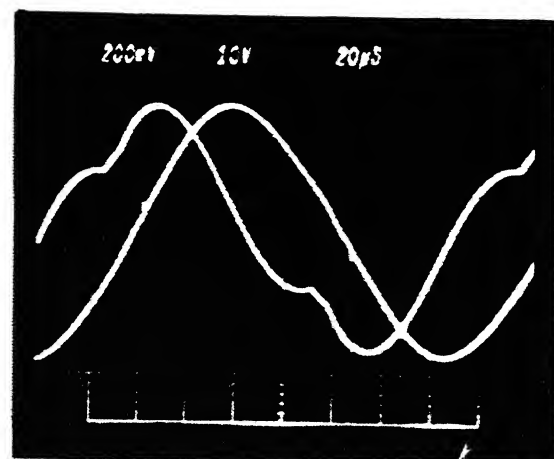
(b)



(c)



(d)



(e)

Fig. 3.7. Experimental waveforms for the inductor current and the capacitor voltage for $L = 73 \mu\text{H}$, $C = 5 \mu\text{F}$, $Q = 7.3$ and $V_s = 120 \text{ V}$ (Reproduced from [11]).

y - scales are current = 20 A/cm; voltage = 100 V/cm

(a) Frequency = 4446 Hz, $I_o = 7.28 \text{ A}$

(b) Frequency = 4509 Hz, $I_o = 10.3 \text{ A}$

(c) Frequency = 4603 Hz, $I_o = 13.4 \text{ A}$

(d) Frequency = 5373 Hz, $I_o = 11.4 \text{ A}$

(e) Frequency = 5810 Hz, $I_o = 9.5 \text{ A}$

A comparison of the Figures 3.4 and 3.7 reveals the striking resemblance of the two sets of waveforms. The only discrepancy is that the values of currents and voltages for Figure 3.4 at some points are slightly greater than the corresponding values of Figure 3.7. This difference is particularly obvious from the waveform of i_L at the instant when the conduction passes from a feedback diode to a power switch. This discrepancy, however, is only to be expected since in the analysis of Chapter 3 stray circuit resistances have not been considered and voltage drops across conducting devices have also been neglected.

A comparison of Figure 2.4 with Figures 3.4 and 3.7 shows that the values of currents and voltages are somewhat greater in Figure 2.4 than those in Figures 3.4 and 3.7. The discrepancy discussed in the previous paragraph is much more pronounced for Figure 2.4. This is so, because in the analysis of Chapter 2 the resistance of the resonant circuit was altogether neglected.

3.4 CONCLUSIONS

The frequency domain model described in Chapter 2 has been further refined by including the effects of the resonant circuit resistance. An analysis similar to the one of Chapter 2 has been carried out. The existence of a continuous conduction mode at higher values of output current in which each power switch conducts twice in each half cycle has been pointed out. Variations of inductor current and capacitor

voltage with time have been plotted and these have been compared with known experimental results. The proposed model is validated by the close agreement between the predicted and the experimental waveforms.

SOME IMPORTANT PERFORMANCE CHARACTERISTICS

4.1 INTRODUCTION

The proposed frequency domain model has been described in Chapters 2 and 3. The validity of the model has been demonstrated by comparison with experimental results reported in literature. In this chapter using the results obtained from the modified model of Chapter 3, several interesting and useful relationships have been given in the form of graphs. These curves, together with those given in Chapter 5, can be used to design a parallel resonant converter (a design example has been given in Chapter 6).

The variation of phase difference ϕ as a function of $I_{o_{pu}} X_{L1_{pu}}$ has been discussed in Section 4.2, first taking ω_{pu} as a parameter, and then taking Q as a parameter. The maximum possible value of $I_{o_{pu}} X_{L1_{pu}}$ at different frequencies has been plotted in Section 4.3 for different values of Q . The boundary of the multiple conduction mode discussed in Section 3.2.3.1 has been obtained in Section 4.4. The variations of peak capacitor voltage and output voltage at different frequencies have been discussed in Sections 4.5 and 4.6 respectively. Finally, the turn-off time available to the power switches has been calculated in Section 4.7.

While plotting the curves the quantity $I_{o_{pu}} X_{L1_{pu}}$ has been taken as either the independent or the dependent variable. With this choice, the effects of variations of output

current, frequency of operation and circuit components can all be incorporated in the same variable. The expressions for the inductor current (equation (3.23)), the capacitor voltage (equation (3.24)), and the phase difference ϕ (equation (3.38)) can be written conveniently in terms of the quantity $I_{o_{pu}} X_{L1_{pu}}$. If Q and ω_{pu} are known, the expressions for the capacitor voltage $V_{C_{pu}}$ (equation (3.24)) and the phase difference ϕ (equation 3.38) can be completely determined by assigning values to $I_{o_{pu}} X_{L1_{pu}}$. It is then not necessary to assign separate values to $I_{o_{pu}}$, L_{pu} or C_{pu} . The various quantities in (3.24) and (3.38) can be expressed in terms of Q and ω_{pu} as follows

$$A_n = \frac{4}{\pi Z'_n} = \frac{4}{\pi \{ \alpha_n^2 + (\beta_n - 1)^2 \}^{1/2}} \quad (4.1)$$

$$\beta_n = n^2 \omega_{pu}^2 \quad (4.2)$$

$$\alpha_n = \frac{\beta_n}{Q_n} \quad (4.3)$$

$$Q_n = n Q \omega_{pu} \quad (4.4)$$

$$Z'_{Ln} = (\gamma_n^2 + 1)^{1/2} \quad (4.5)$$

$$\gamma_n = \frac{1}{Q_n} \quad (4.6)$$

$$\theta_{Zn} = \tan^{-1} \{ Q_n (1 - \frac{1}{\beta_n}) \} \quad (4.7)$$

$$\theta_{Ln} = \tan^{-1}(Q_n) \quad (4.8)$$

$$I_{o_{pu}} X_{Ln_{pu}} = n I_{o_{pu}} X_{L1_{pu}} \quad (4.9)$$

While plotting these curves as well as those given in Chapter 5, the effects of all harmonics upto the 9th were

considered. The various graphs in this chapter have been drawn using the PLOT-10 and the GPGS.

4.2 VARIATION OF PHASE DIFFERENCE \emptyset

The variation of the phase difference \emptyset with $I_{o_{pu}} X_{L1_{pu}}$ has been plotted first taking ω_{pu} as a parameter. Subsequently the effect of variation of Q on \emptyset at a particular frequency has been examined.

4.2.1 Variation of \emptyset with ω_{pu} as a Parameter

The value of \emptyset corresponding to a given value of $I_{o_{pu}} X_{L1_{pu}}$ can be obtained using the technique described in Section 3.2.2. For this it is necessary to solve the non-linear equation (3.38). This, however, requires considerable computer time. Moreover, it was observed that equation (3.38) could not be solved for higher values of $I_{o_{pu}} X_{L1_{pu}}$ using the usual IMSL and NAG subroutines used for solving non-linear equations. Also, whether $I_{o_{pu}} X_{L1_{pu}}$ is a single or multi-valued function of \emptyset cannot be determined using this technique.

By using an alternative technique the corresponding values of \emptyset and $I_{o_{pu}} X_{L1_{pu}}$ can be obtained more conveniently. Equation (3.38) may be written as

$$I_{o_{pu}} X_{L1_{pu}} = \frac{\sum_n \frac{A_n}{n} \cos(\theta_{zn} - n\emptyset)}{\sum_n \frac{A_n}{n} \frac{Z'_{Ln}}{Z'_{Ln}} \cos(\theta_{Ln} - \theta_{zn})} \quad (4.10)$$

From this expression it is observed that for a given value of \emptyset , the corresponding value of $I_{o_{pu}} X_{L1_{pu}}$ can be determined by simply evaluating the right hand side of equation.

(4.10). It is then not necessary to solve any complicated non-linear equation. Consequently, instead of determining the value of ϕ corresponding to a given value of $I_{o_{pu}} X_{L1_{pu}}$ it is much easier to proceed in the reverse direction.

ϕ is assigned values from 0° onwards and the corresponding values of $I_{o_{pu}} X_{L1_{pu}}$ are determined using equation (4.10). The corresponding values of ϕ and $I_{o_{pu}} X_{L1_{pu}}$ have been plotted in Figure 4.1 for different values of per unit frequency ω_{pu} . These curves have been obtained assuming the value of Q to be 10. The curves of Figure 4.1(a) are for the values of ω_{pu} which lie in the normal operating region $0.5 < \omega_{pu} < 1.0$. Figure 4.1(b) is an expanded version of Figure 4.1(a) for values of $I_{o_{pu}} X_{L1_{pu}}$ in the range 0 to 0.8. Figure 4.1(c) shows the curves for $\omega_{pu} \leq 0.5$ and $\omega_{pu} \geq 1.0$. Only the values of ϕ corresponding to positive values of $I_{o_{pu}} X_{L1_{pu}}$ have been shown in these figures. The curve obtained from the relationship given by equation (2.32) which has been obtained using the simplified model for fundamental components only is also given in Figures 4.1(a) and 4.1(b).

4.2.1.1 Conclusions: The following conclusions can be drawn from Figure 4.1:

- (1) For ω_{pu} lying in the range $0.5 < \omega_{pu} < 1.0$ and also for frequencies above resonance ($\omega_{pu} > 1.0$), ϕ is a double-valued function of $I_{o_{pu}} X_{L1_{pu}}$.
- (2) For a given value of ω_{pu} there is a maximum value of $I_{o_{pu}} X_{L1_{pu}}$.

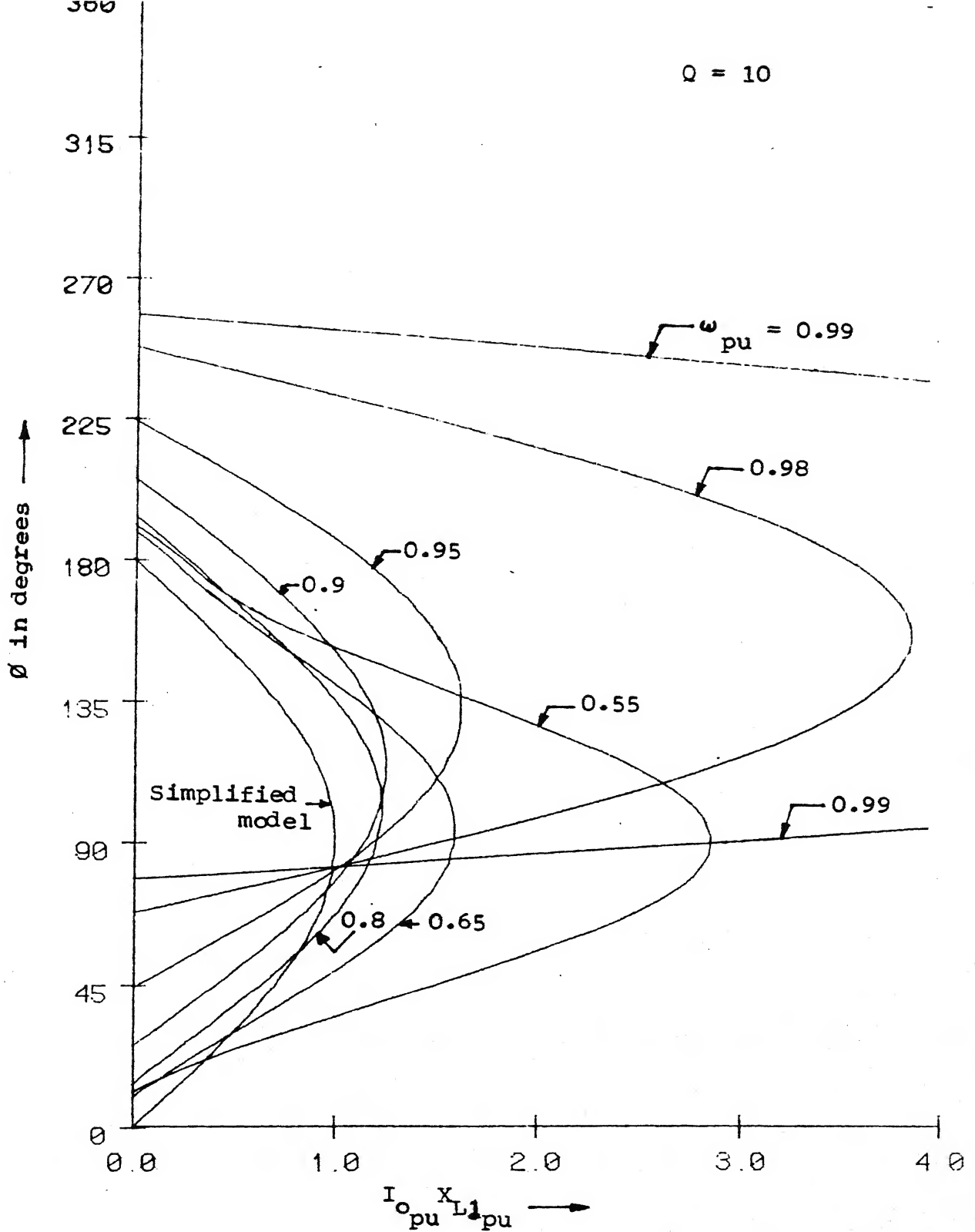


Figure 4.1(a). Variation of ϕ with $I_{o_pu} X_{L1_pu}$ for $0.5 < \omega_{pu} < 1.0$

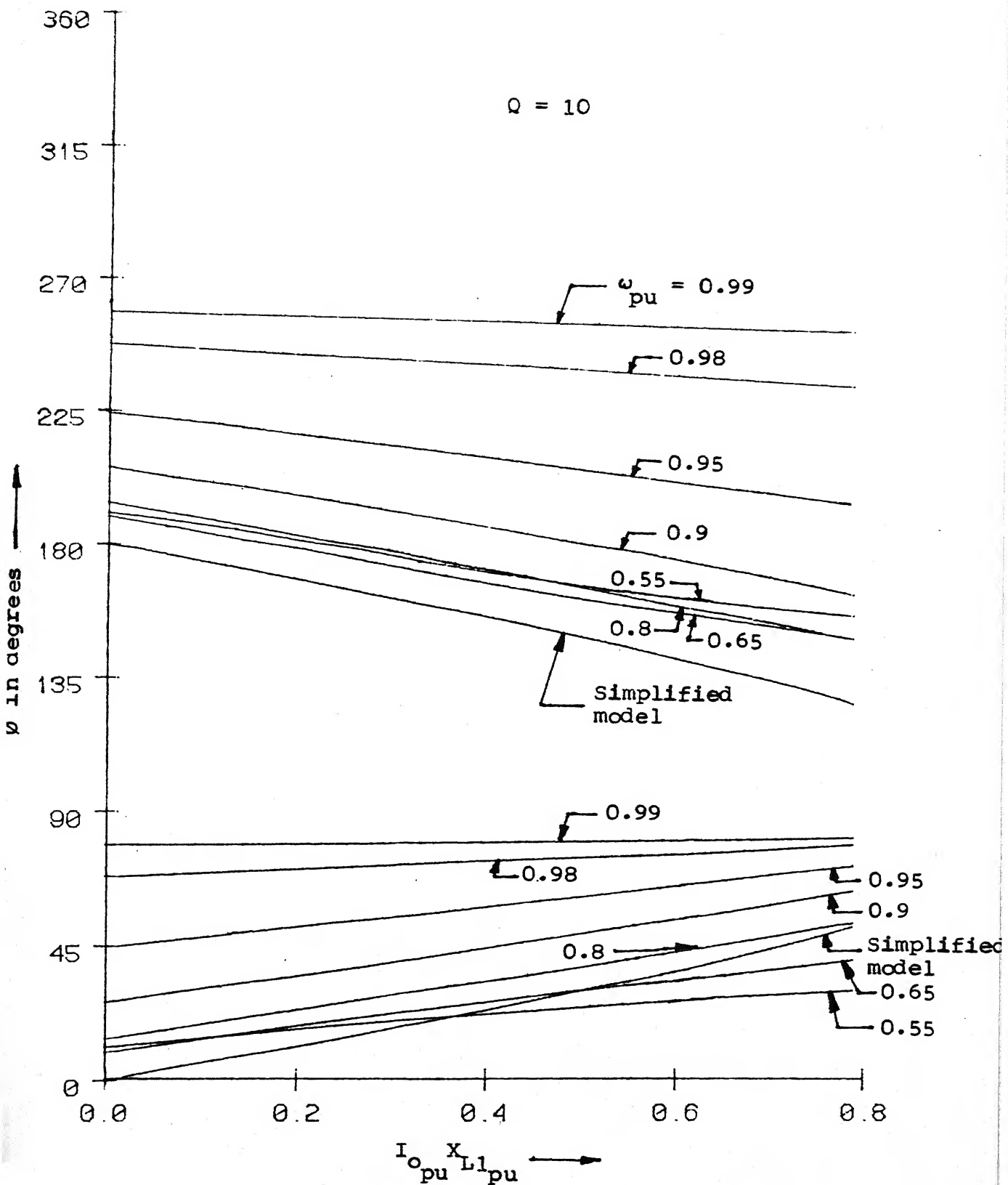


Figure 4.1(b). Variation of ϕ with $I_{o_{pu}} X_{L1_{pu}}$ for $0.5 < \omega_{pu} < 1.0$ (expanded version of Figure 4.1(a)).

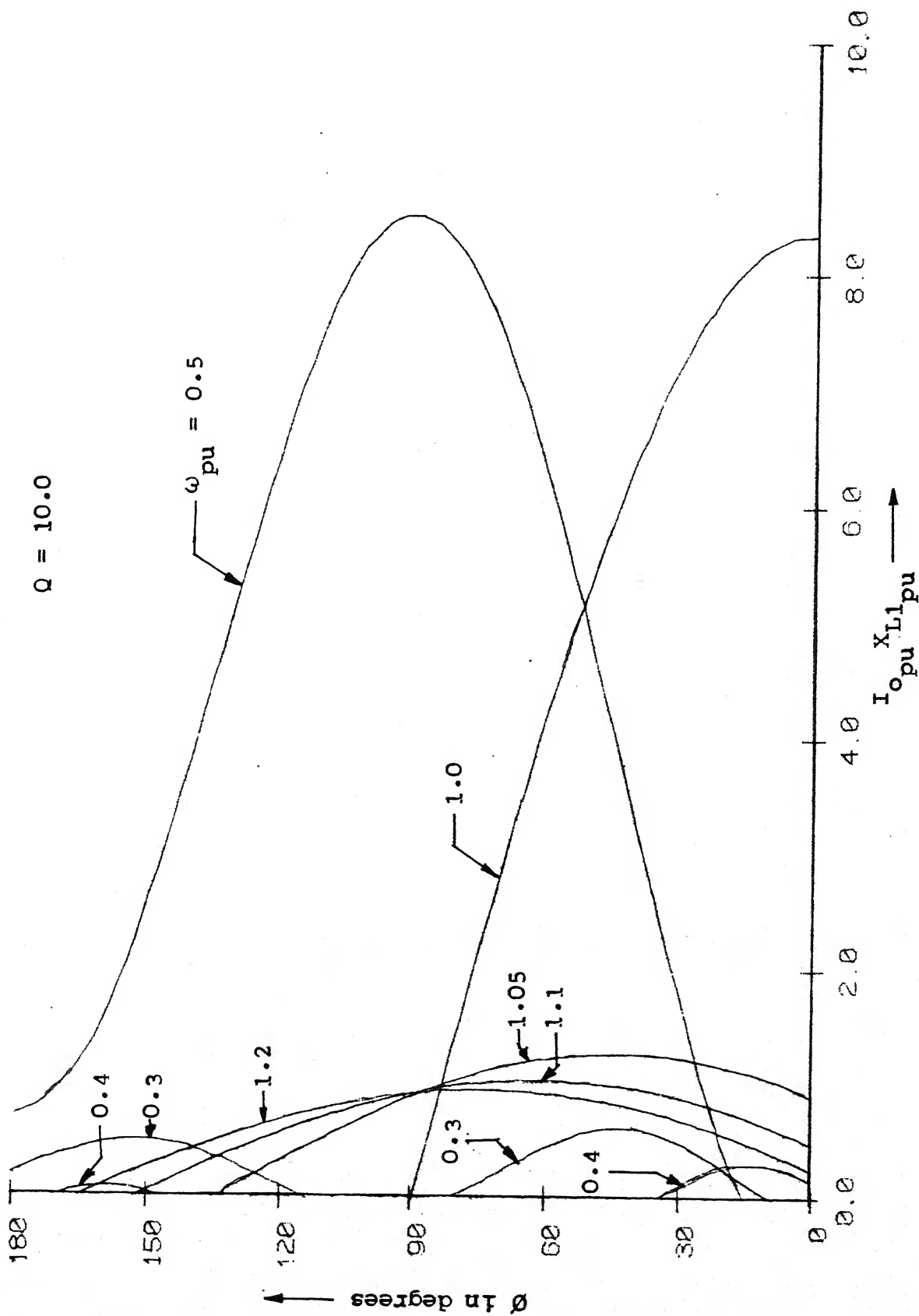


Figure 4.1(c). Variation of δ with $I_0 X_L L_1 / pu$ for $\omega_{pu} \leq 0.5$ and $\omega_{pu} \geq 1.0$.

$Q = 10$

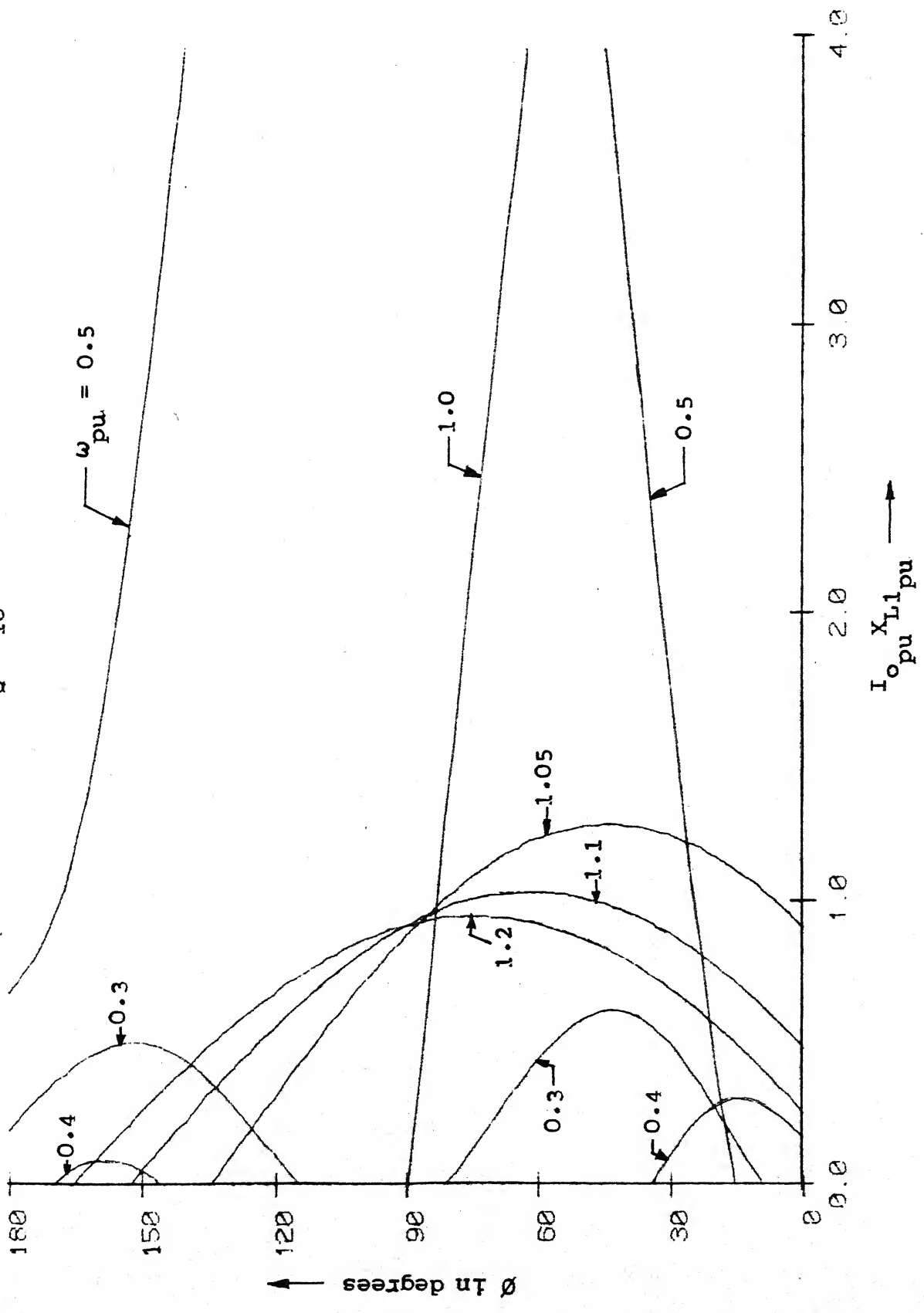


Figure 4.1(d). Variation of δ with $I_{0p} X_{L1p} / pu$ for $\omega_{pu} \leq 0.5$ and $\omega_{pu} \geq 1.0$

- (3) When ω_{pu} lies in the range $0.5 < \omega_{pu} < 1.0$, all values of ϕ lie above a certain minimum value. This minimum possible value of ϕ which occurs for zero output current increases for increasing values of frequency.

4.2.2 Variation of ϕ at a Constant Frequency with Q as a Parameter

With ω_{pu} constant at 0.65 the variation of ϕ with $I_{o_{pu}} X_{L1_{pu}}$ for different values of Q has been shown in Figure 4.2. These curves have been obtained from equation (4.10) using the same technique as that described in Section 4.2.1.

4.2.2.1 Conclusions: From Figure 4.2 it is observed that at a given frequency ϕ is a relatively weak function of Q . For the usual practical values of Q in the range of 5 to 10, there is relatively small change in the value of ϕ even for appreciable changes in the value of Q .

4.3 VARIATION OF MAXIMUM POSSIBLE VALUE OF $I_{o_{pu}} X_{L1_{pu}}$, ($I_{o_{pu}} X_{L1_{pu}} \max$) WITH FREQUENCY

As pointed out in Section 4.2.1, for a given frequency there is an upper limit to the value of $I_{o_{pu}} X_{L1_{pu}}$. Taking Q as a parameter the variation of ($I_{o_{pu}} X_{L1_{pu}} \max$) with ω_{pu} has been shown in Figure 4.3.

4.3.1 Method of Calculation

There is no easy analytical relationship between ($I_{o_{pu}} X_{L1_{pu}} \max$) and ω_{pu} . So to calculate ($I_{o_{pu}} X_{L1_{pu}} \max$) corresponding to a given value of ω_{pu} , values of $I_{o_{pu}} X_{L1_{pu}}$ are calculated using equation (4.10) by varying ϕ within the

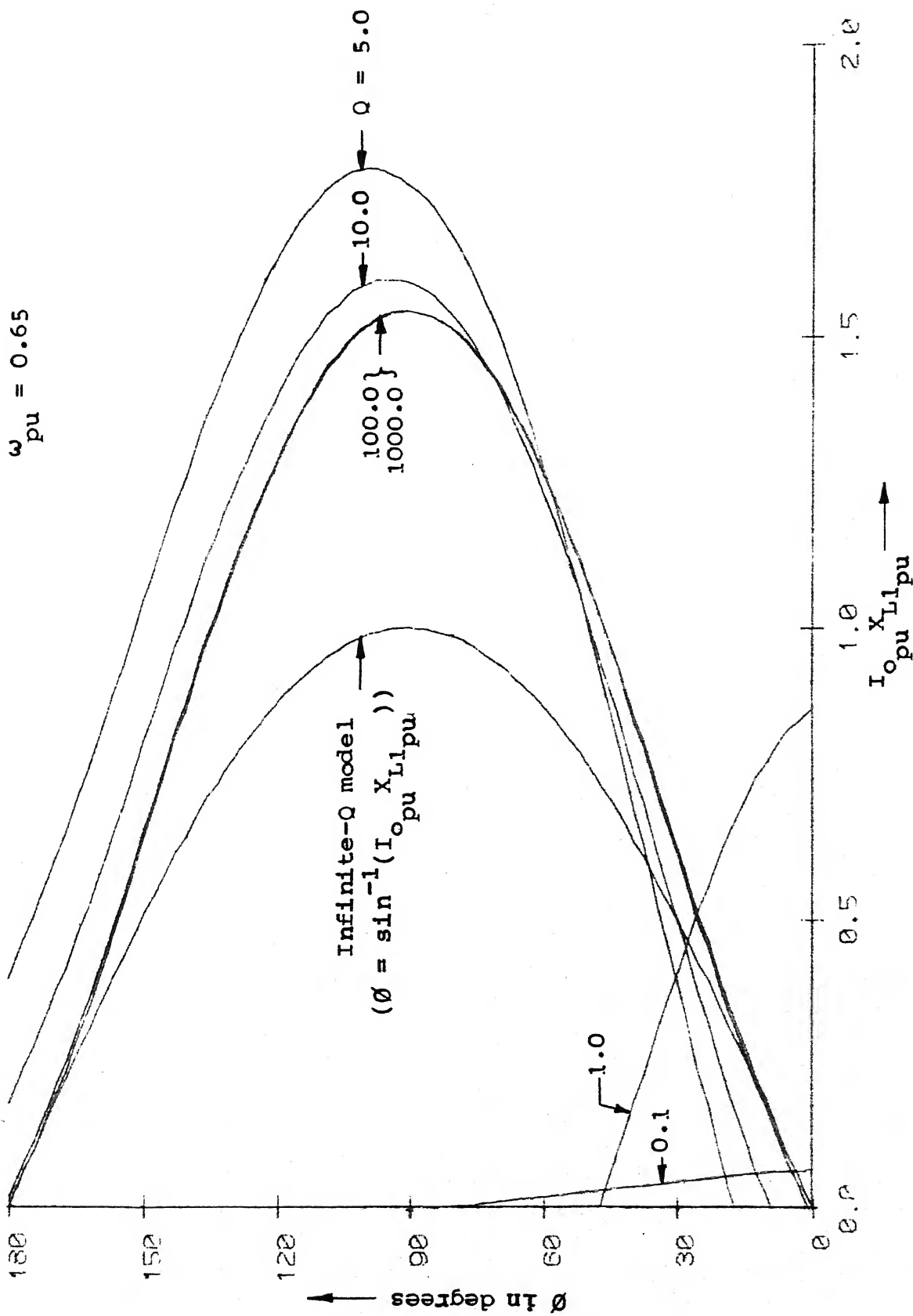


Figure 4.2. Variation of δ with $I_{0_{pu}}$ $X_{L1_{pu}}$ at $\omega_{pu} = 0.65$ with Q as a parameter.

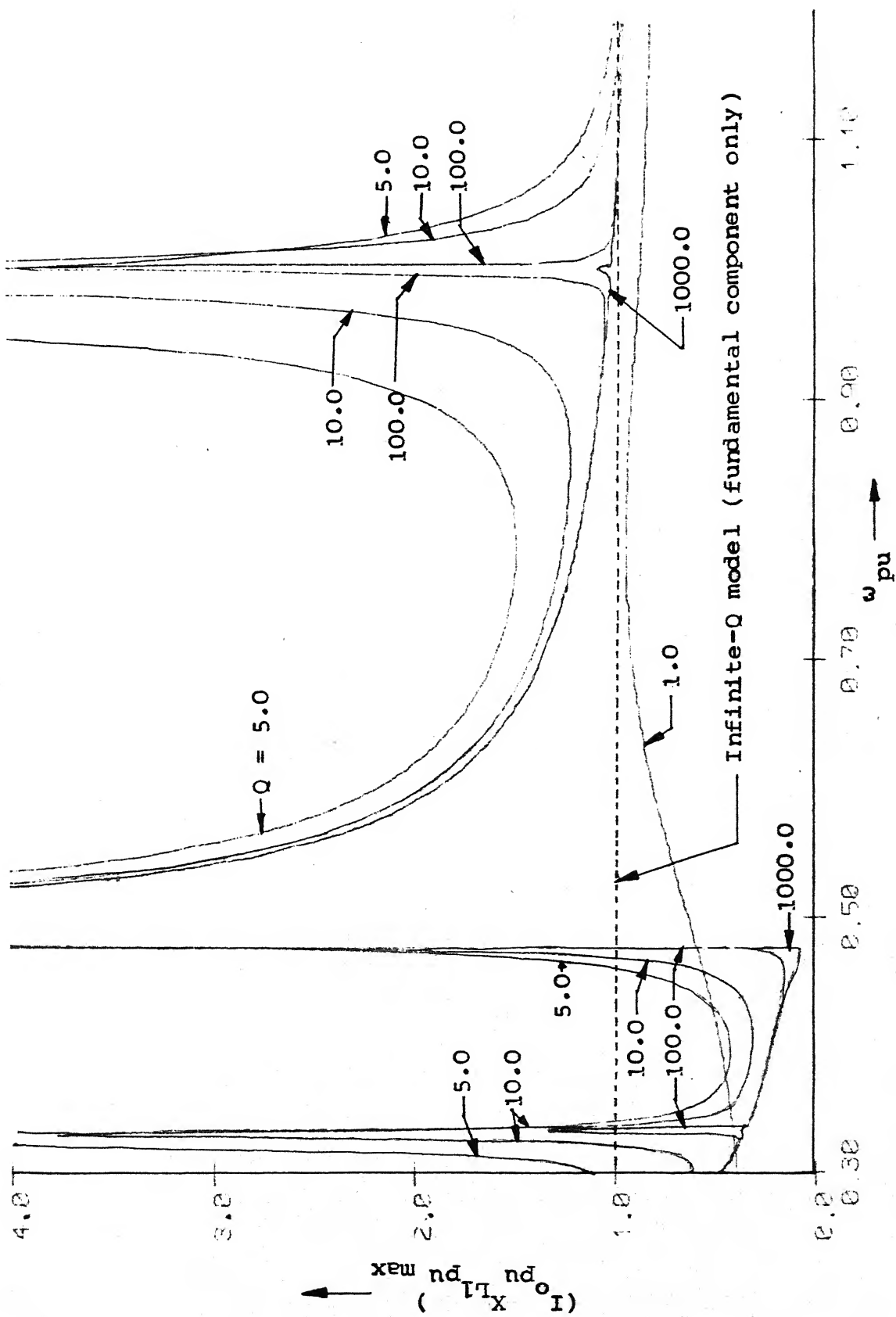


Figure 4.3. Variation of $(I_o X_{L1})_{pu \max}$ with ω_{pu} taking Q as a parameter.

range of 0° to 180° in steps of 0.333 degrees. The maximum of these values is taken as the $(I_o X_{L1})_{pu \text{ max}}$ corresponding to the given value of ω_{pu} .

4.3.2 Conclusions

From Figure 4.3 it is observed that $(I_o X_{L1})_{pu \text{ max}}$ has peaks for $\omega_{pu} = 0.33, 0.5$ and 1.0 . The peak at $\omega_{pu} = 1.0$ can be explained by the fact that at resonance the impedance of the L-C circuit is minimum and so the circuit current is limited by only resistance in the circuit.

The existence of the peaks at $\omega_{pu} = 0.33, 0.5$ and 1.0 implies that it is theoretically possible to operate the converter at higher currents at or near these frequencies. However, at high values of I_o the converter is likely to enter into the multiple conduction mode that has been pointed out in Section 3.2.3.1. Moreover, limitations imposed by the turn-off times of the power switches S_1 and S_2 will also have to be taken into consideration before operating the converters at such high currents.

4.4 BOUNDARY OF MULTIPLE CONDUCTION MODE

The multiple conduction mode (m.c.m.) that has been discussed in Section 3.2.3.1 is of critical importance to the system designer. When the converter is operating in the m.c.m., natural commutation cannot be made use of. The power switches S_1 and S_2 must be turned off by forced commutation. From Figure 3.6 it follows that in order to prevent the short circuit of the input voltage sources through S_1 and S_2 , the

turn off of S_1 and S_2 must be accomplished within the time intervals for which D_2 and D_1 respectively conduct at the beginning of each half cycle. It is obvious from Figure 3.5 that these time intervals are usually small. Consequently it is advantageous to ensure that the converter operates in the normal continuous conduction mode and does not enter into the m.c.m.

In this section the boundary of the m.c.m. has been determined. The values of $I_{o_{pu}} X_{L1_{pu}}$ at which the converter just enters into the m.c.m. at different frequencies in the normal operating range of $0.5 < \omega_{pu} < 1.0$ have been shown in Figure 4.4 for $Q = 10$.

4.4.1 Method of Calculation

In the limiting case when the converter just enters into the m.c.m. the inductor current i_L is zero at the end of each half cycle. This is so, because then the conduction passes from D_1 or D_2 to S_2 or S_1 at the end of each half cycle with the switch S_1 or S_2 just about to conduct. So the value of $I_{o_{pu}} X_{L1_{pu}}$ corresponding to a given value of ω_{pu} can be determined by equating the expression for $i_{L_{pu}}$ given by equation (3.23) to zero at $\omega t = 0$ and solving for $I_{o_{pu}} X_{L1_{pu}}$.

From equation (3.23) with the help of equation (2.19) one can write

$$i_{L_{pu}} \Big|_{\omega t=0} = - \frac{1}{X_{C1_{pu}}} \left[\sum_n A_n \{ \sin \theta_{Zn} + \frac{I_{o_{pu}} X_{L1_{pu}}}{n \omega_{pu}^2} \cos(n\theta + \theta_{Zn}) \} \right] \quad (4.11)$$

since $nX_{Cn_{pu}} = X_{C1_{pu}}$, which is independent of n .

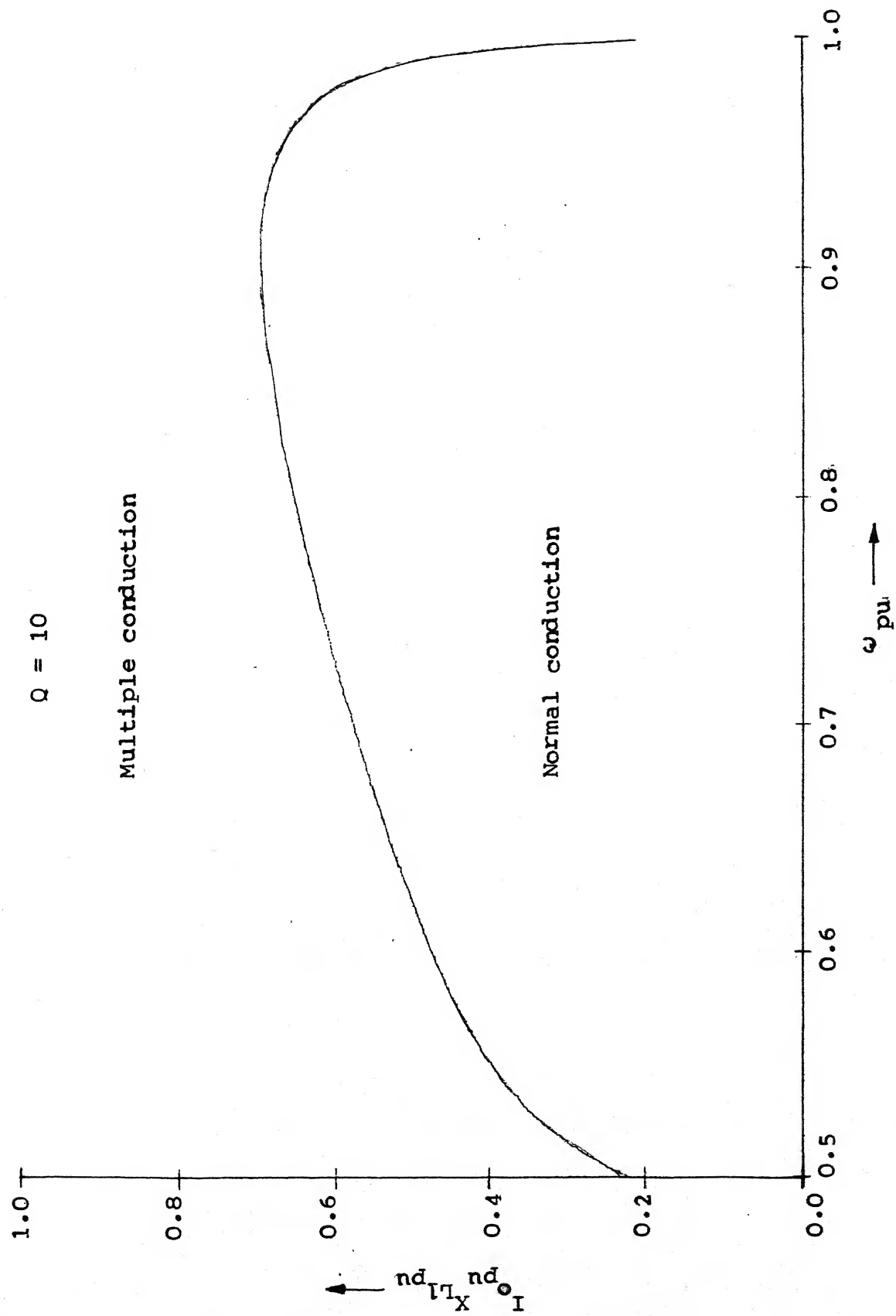


Figure 4.4. Boundary of multiple conduction mode.

Equating $i_{L_{pu}}|_{\omega t=0}$ to zero gives the following non-linear equation

$$\sum_n A_n \left[\sin \theta_{zn} + \frac{I_{o_{pu}} X_{L1_{pu}}}{n \omega_{pu}^2} \cos(n\theta + \theta_{zn}) \right] = 0 \quad (4.12)$$

For given values of Q and ω_{pu} equation (4.12) can be solved for $I_{o_{pu}} X_{L1_{pu}}$ using the usual techniques used for solution of non-linear equations. This, however, requires that every time the left hand side of (4.12) is evaluated, the value of θ corresponding to the value of the variable $I_{o_{pu}} X_{L1_{pu}}$ has to be determined by solving the complicated non-linear equation (3.38). The amount of numerical computations required for solving equation (4.12) can be reduced considerably by solving equation (4.12) for θ instead. Then for each function evaluation the value of $I_{o_{pu}} X_{L1_{pu}}$ corresponding to the value of θ at that point can easily be determined from equation (4.10).

Using this technique equation (4.12) has been solved for θ by means of the IMSL subroutine ZFALSE. The corresponding value of $I_{o_{pu}} X_{L1_{pu}}$ has been obtained from equation (4.10). This gives the boundary of the m.c.m. corresponding to the given value of ω_{pu} .

4.4.2 Observations

As pointed out at the beginning of Section 4.4, the converter would preferably be operated such that it does not enter the m.c.m. So from Figure 4.4 it follows that at a given frequency there is an upper limit to the value of

$I_{o_pu} X_{L1_pu}$ (and, therefore, to output current I_o) below which the converter must be operated such that it does not enter the m.c.m. There is, thus, a limit to the maximum output current a parallel resonant converter can provide at a given frequency.

4.5 VARIATION OF PER UNIT PEAK CAPACITOR VOLTAGE $v_{C_peak_pu}$

To determine the voltage rating of the capacitor it is necessary to determine the peak value of the voltage across it. The per unit peak capacitor voltage $v_{C_peak_pu}$ at any frequency of operation can be determined from curves similar to those given in Figure 4.5. Figure 4.5 shows the variation of peak capacitor voltage with $I_{o_pu} X_{L1_pu}$ for six different values of frequencies. These curves have been obtained assuming a Q of 10.

4.5.1 Method of Calculation

The expression for the capacitor voltage v_{C_pu} is given by equation (3.24). However, no numerical technique is available which can be used to maximize a function such as the one given by (3.24). To determine $v_{C_peak_pu}$, therefore, v_{C_pu} as given by (3.24) is evaluated at a number of points by varying ωt in the range $0 < \omega t < (180^\circ + \phi)$. The maximum of these values is taken as the peak value of per unit capacitor voltage. Since the capacitor voltage is a smooth function of ωt , the error produced by this method is negligible if the number of points is sufficiently high.

$Q = 10$

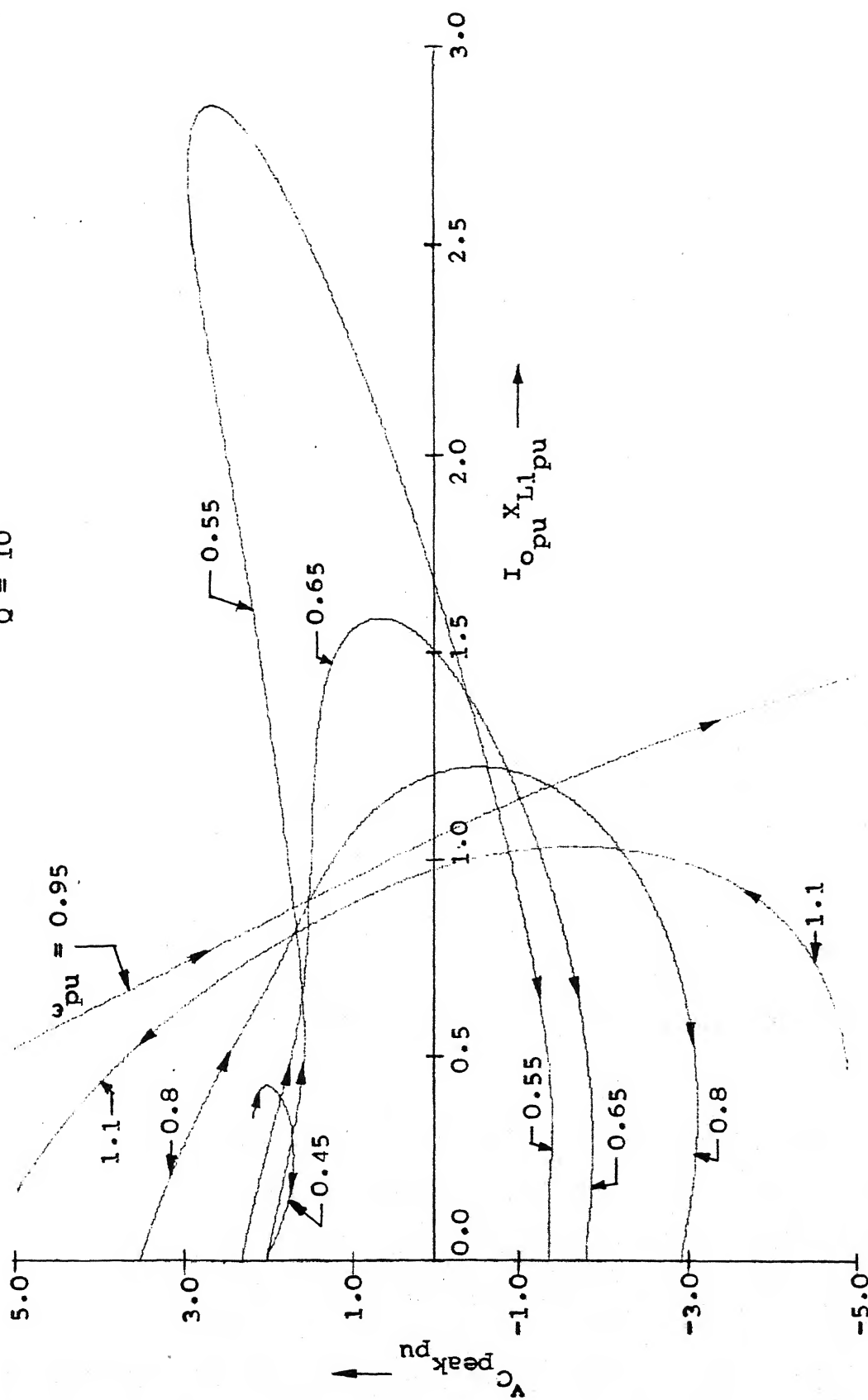


Figure 4.5. Variation of per unit peak capacitor voltage $v_C^{\text{peak}} \text{ pu}$ with $I_{o \text{ pu}} X_{L1 \text{ pu}}$ (Arrowhead indicates increasing values of δ).

In order to evaluate $v_{C_{pu}}$ as a function of $I_{o_{pu}} X_{L1_{pu}}$ as given by equation (3.24), it is necessary that the value of ϕ corresponding to the chosen value of $I_{o_{pu}} X_{L1_{pu}}$ be determined. However, instead of calculating the value of ϕ for a given $I_{o_{pu}} X_{L1_{pu}}$, it is much more advantageous to calculate $I_{o_{pu}} X_{L1_{pu}}$ for a given value of ϕ using equation (4.10). So at each frequency ϕ is varied from 0° onwards and the corresponding values of $I_{o_{pu}} X_{L1_{pu}}$ are calculated using equation (4.10). The corresponding pairs of values of $I_{o_{pu}} X_{L1_{pu}}$ and ϕ have been then substituted in expression (3.24) to calculate $v_{C_{pu}}$. Only the values of ϕ corresponding to positive values of $I_{o_{pu}} X_{L1_{pu}}$ have been taken into consideration.

4.5.2 Conclusions

The following conclusions can be drawn from curves of Figure 4.5.

- (1) The peak capacitor voltage is a double valued function of $I_{o_{pu}} X_{L1_{pu}}$. The two values of $v_{C_{peak_{pu}}}$ correspond to the two values of ϕ that exist for a given value of $I_{o_{pu}} X_{L1_{pu}}$.
- (2) For small values of $I_{o_{pu}} X_{L1_{pu}}$, $v_{C_{peak_{pu}}}$ takes considerably higher values at higher frequencies of operation. This suggests that if the converter is operated as a current source whose magnitude is small, it is advantageous to operate the converter at frequencies slightly above $0.5 \omega_o$, so that the peak capacitor voltage is reduced.

4.6 VARIATION OF PER UNIT OUTPUT VOLTAGE $V_{o_{pu}}$

In order to determine the usefulness of the parallel resonant converter as a dc power supply, it is necessary to examine the regulation of the output voltage as the converter is loaded. Figure 4.6(a) shows the variation of the per unit dc output voltage as a function of $I_{o_{pu}} X_{L1_{pu}}$ at different frequencies. Figure 4.6(b) is the expanded version of Figure 4.6(a) for values of $I_{o_{pu}} X_{L1_{pu}}$ lying in the range 0 to 0.8. The Q of the circuit, as before, was taken as 10.

4.6.1 Method of Calculation

The output voltage in the parallel resonant converter is obtained by rectifying and filtering the voltage across the resonant capacitor. So the output voltage can be determined by calculating the average value of the capacitor voltage over a half cycle. The expression for $v_{C_{pu}}$ given by equation (3.24) has been numerically integrated from \emptyset to $\emptyset + 180^\circ$ and the result has been divided by π to obtain the per unit output voltage $V_{o_{pu}}$ corresponding to the given values of ω_{pu} and $I_{o_{pu}} X_{L1_{pu}}$. The numerical integration has been carried out with the help of the NAG subroutine D01AJF.

As described in Section 4.4.1, \emptyset was varied from 0° onwards and the corresponding values of $I_{o_{pu}} X_{L1_{pu}}$, obtained using equation (4.10), were substituted in (3.24) before $v_{C_{pu}}$ was evaluated at each point during the integration.

4.6.2 Conclusions

The following conclusions may be drawn from the curves of Figure 4.6.

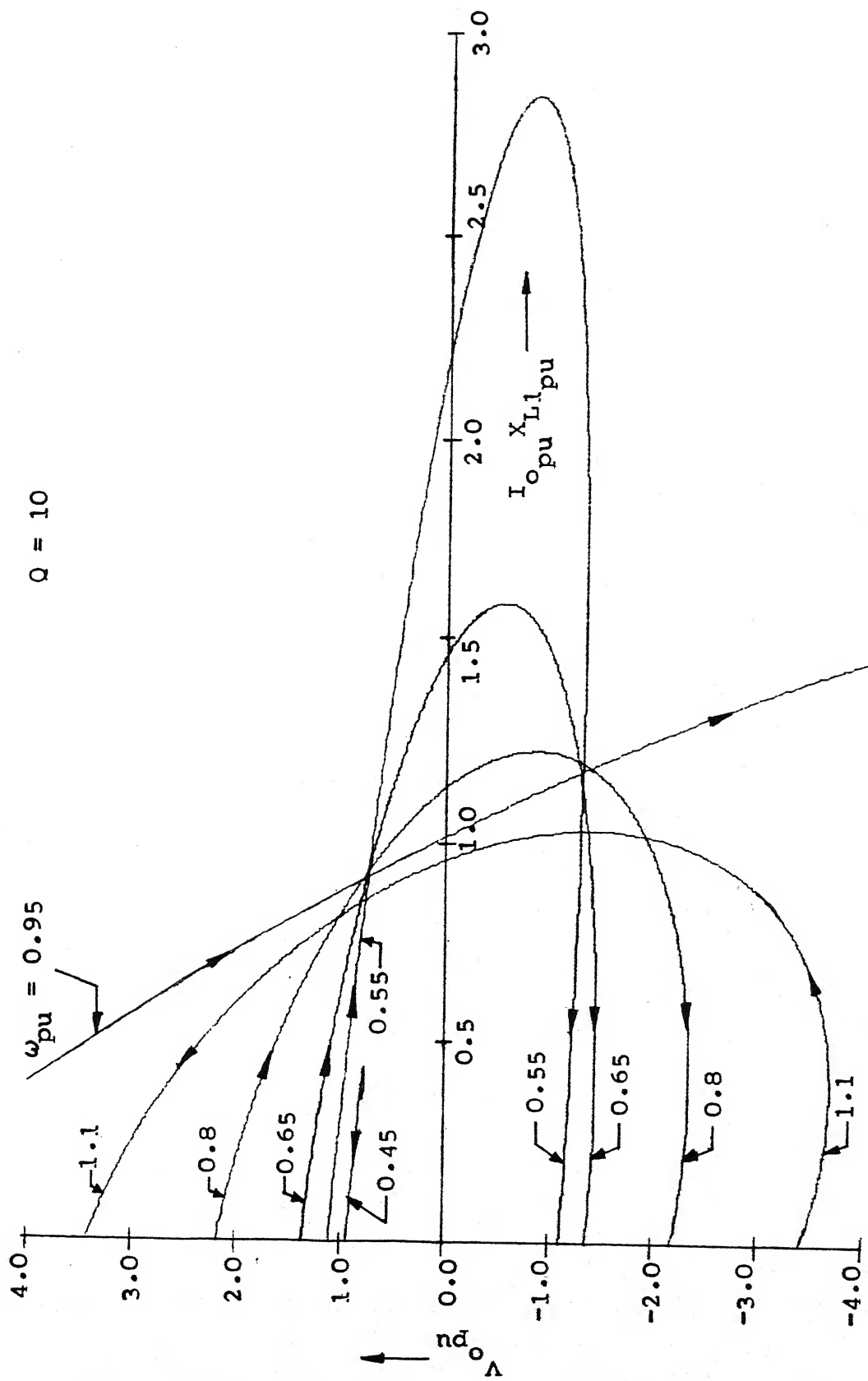


Figure 4.6(a), Variation of per unit dc output voltage $V_{o,pu}$ with $I_{o,pu} X_{L1,pu}$
 (Arrowhead indicates increasing values of ω).

$$Q = 10$$

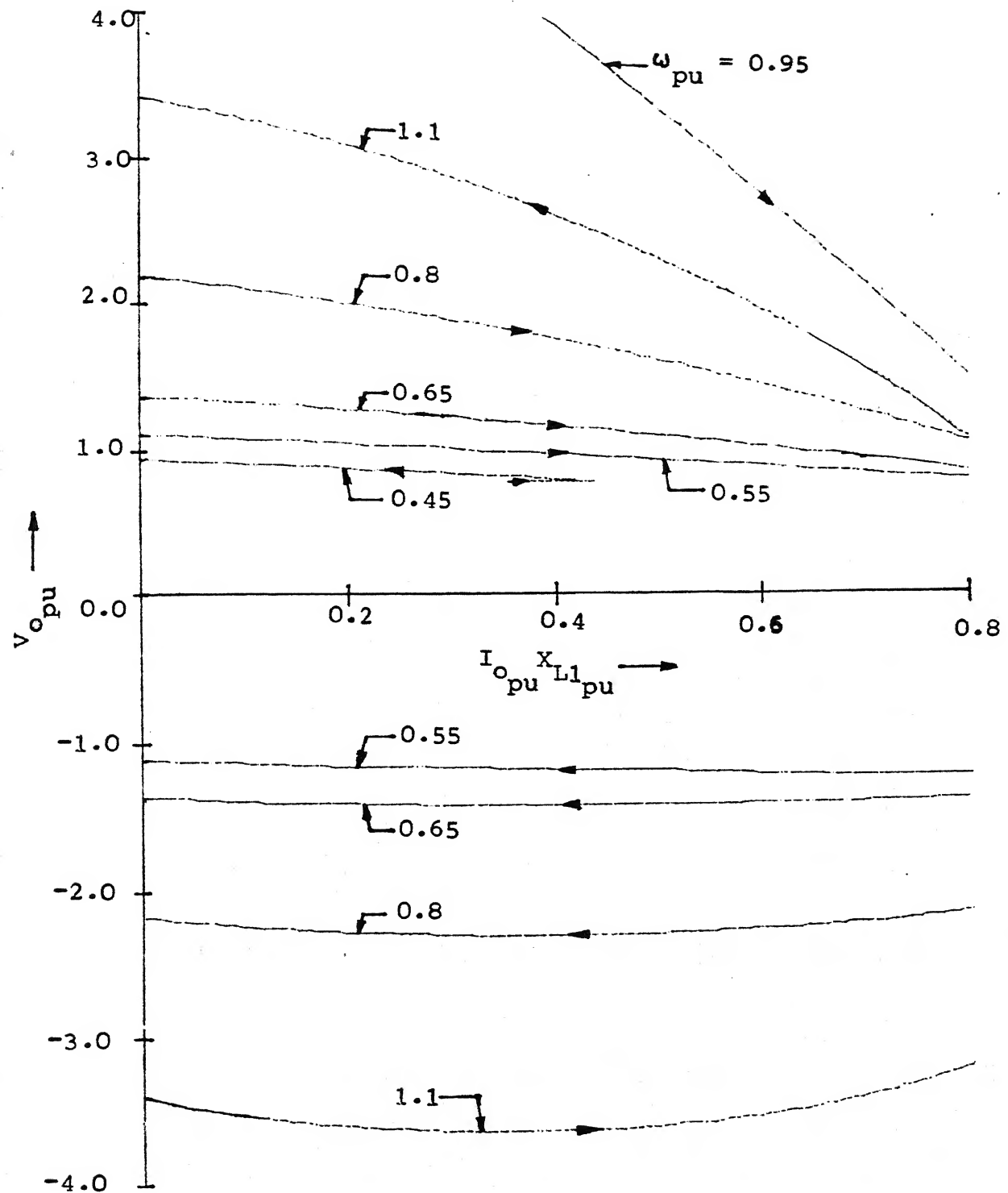


Figure 4.6(b). Variation of per unit dc output voltage v_{o_pu} with $I_{o_pu} X_{L1_pu}$ (expanded version of Figure 4.6(a)).

- (1) The nature of variation of $V_{o_{pu}}$ with $I_{o_{pu}} X_{L1_{pu}}$ is essentially the same as that of $V_{C_{peak_{pu}}}$. This implies that the voltage across the resonant capacitor is essentially sinusoidal.
- (2) The capacitor voltage may depart from sinusoidal waveform at higher values of $I_{o_{pu}} X_{L1_{pu}}$ for some frequencies. This may be noted by comparing the curves of Figure 4.5 with those of Figure 4.6. For example, for $\omega_{pu} = 0.55$ and $\omega_{pu} = 0.65$ at higher values of $I_{o_{pu}} X_{L1_{pu}}$, $V_{C_{peak_{pu}}}$ is positive while the output voltage $V_{o_{pu}}$ is negative. This implies that the capacitor voltage is highly distorted for very high values of load current at these frequencies.
- (3) At low values of output current I_o if the frequency is increased the average output voltage also increases.
- (4) The regulation of the output voltage with respect to load current is much better at lower frequencies than at higher frequencies. This suggests that when used as a power supply, the converter should preferably be operated at frequencies slightly above $0.5 \omega_o$.
- (5) When the output voltage is negative, i.e. the converter is operating in the regenerative mode, the regulation of output voltage is excellent, specially at lower frequencies around $0.55 \omega_o$.

4.7 VARIATION OF PER UNIT TURN-OFF TIME $t_{q_{pu}}$

Figure 4.7 shows the per unit turn-off time available to the power switches S_1 and S_2 as a function of $I_{o_{pu}} X_{L1_{pu}}$ at seven different frequencies.

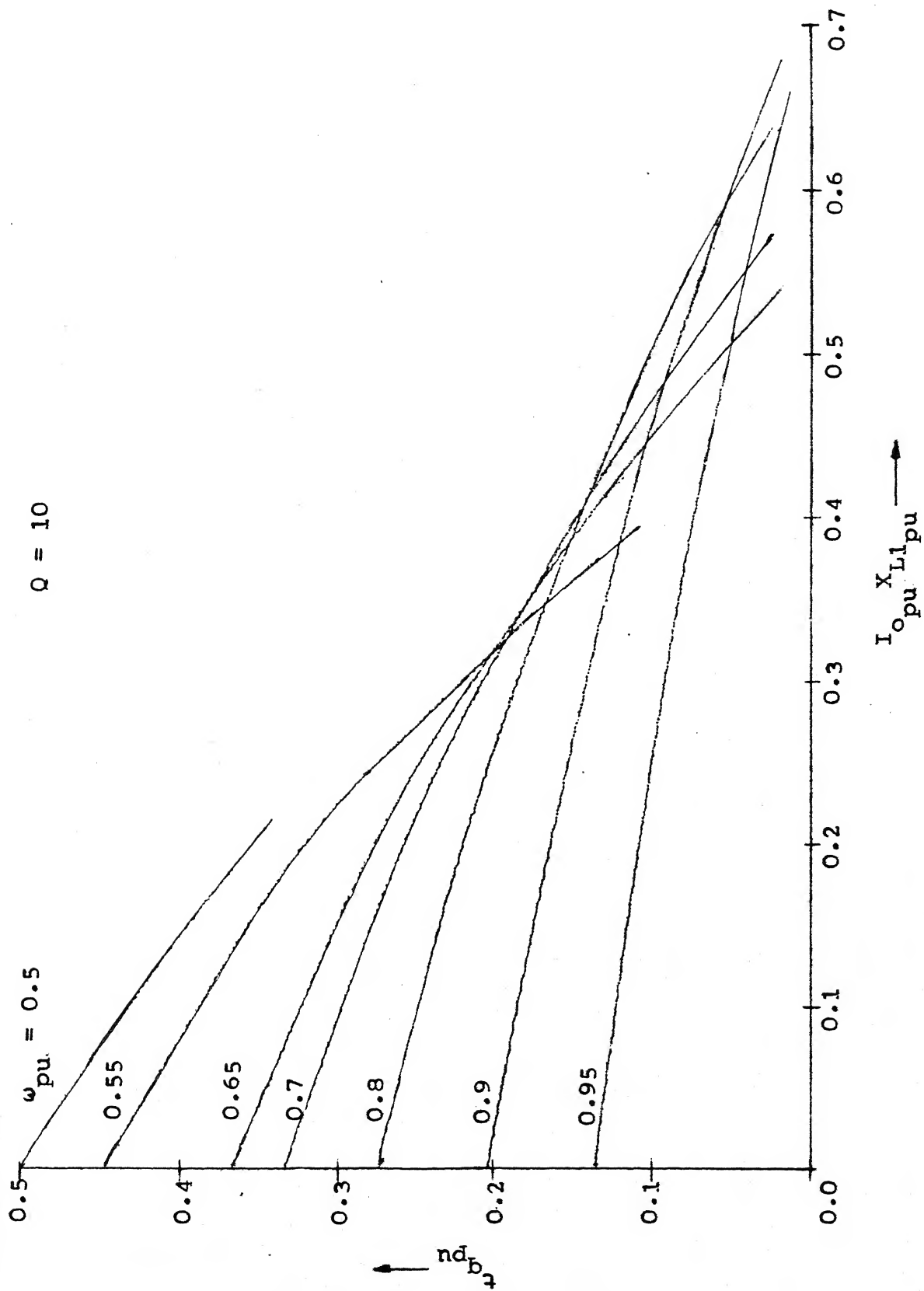


Figure 4.7. Variation of per unit turn-off time $t_{q_{pu}}$ with $I_o X_{L1_{pu}}$ at different frequencies.

4.7.1 Method of Calculation

When the converter is operating in the normal continuous conduction mode ($0.5 < \omega_{pu} < 1$), it is observed from Figure 1.2(a) that the turn-off time t_q available to the power switches S_1 or S_2 is the time interval for which the corresponding feedback diode conducts. So one can write

$$t_q = \frac{T}{2} - t_1 \quad (4.13)$$

With the help of equation (2.19) t_q may be expressed in terms of per unit quantities as

$$t_{q_{pu}} = \frac{\frac{T}{2} - t_1}{\frac{2\pi}{\omega_o}}$$

or,

$$t_{q_{pu}} = \frac{1}{\omega_{pu}} \left(0.5 - \frac{\omega t_1}{2\pi} \right) \quad (4.14)$$

The quantity ωt_1 can be determined by observing that at $\omega t = \omega t_1$ the expression for $i_{L_{pu}}$ as given by (3.23) becomes zero, i.e.

$$i_{L_{pu}} \Big|_{\omega t = \omega t_1} = 0 \quad (4.15)$$

Substituting the expression for $i_{L_{pu}}$ from (3.23) in (4.15) gives

$$\sum_n A_n \left[\sin(n \omega t_1 - \theta_{zn}) + \frac{I_{o_{pu}} X_{L1_{pu}}}{n \omega_{pu}^2} \sin(n \omega t_1 - n\phi - \frac{\pi}{2} - \theta_{zn}) \right] = 0 \quad (4.16)$$

For given values of Q and ω_{pu} the non-linear equation (4.16) can be solved for ωt_1 for different values of $I_{o_{pu}} X_{L1_{pu}}$.

Equation (4.16) has been solved using the IMSL subroutine ZFALSE. The region within which the root will lie was specified as from 0 to π .

The value of ωt_1 obtained by solving equation (4.16) is substituted in equation (4.14) to determine the per unit turn-off time corresponding to the given value of $I_{o_{pu}} X_{L1_{pu}}$.

The turn-off time has been determined for values of $I_{o_{pu}} X_{L1_{pu}}$ upto the value at which the converter enters into the multiple conduction mode. Once the converter enters the m.c.m., the turn-off time available is zero for all higher values of $I_{o_{pu}} X_{L1_{pu}}$.

4.7.2 Conclusions

From Figure 4.7 it is observed that higher turn-off time is available at lower frequencies of operation. Also, the turn-off time available at a given frequency decreases as the output load current is increased.

4.8 CONCLUSIONS

The variations of several important variables have been obtained in this chapter. By choosing $I_{o_{pu}} X_{L1_{pu}}$ as the variable, the effects of variations in both the output current and the component values have been incorporated in the same variable. The curves that have been given in this chapter lead to a better understanding of the operation and a superior evaluation of performance of the converter. These curves are also useful for the design of the converter. From the conclusions

that have been obtained in Sections 4.5, 4.6 and 4.7 it is seen that when used as a power supply it is advantageous to operate the converter at relatively lower frequencies that are a little above $0.5 \omega_0$.

CHAPTER 5

VARIATION OF POWER AND EFFICIENCY FOR DIFFERENT CONTROL SCHEMES

5.1 INTRODUCTION

In order to have a proper insight into the performance of the parallel resonant converter, it is necessary to determine the variations of power and efficiency in addition to the performance characteristics that have been obtained in Chapter 4. In this chapter the variations of output power, input power, circuit losses and converter efficiency for different control schemes have been examined.

Two types of control schemes — the open-loop frequency control and the closed-loop phase control — have been briefly discussed in Section 5.2. Generalised expressions for output power, input power, circuit losses and efficiency in terms of the variable $I_{o_{pu}} X_{L1_{pu}}$ have been derived in Section 5.3. The variations of power and efficiency for both the frequency and the phase control have been examined in Section 5.4. The variations have been first examined as a function of the variable $I_{o_{pu}} X_{L1_{pu}}$. Subsequently the variations of power and efficiency with per unit output current for a given set of circuit parameters have been observed. Finally, a comparison of the frequency and the phase control scheme has been made in Section 5.5.

While performing the various calculations the value of the circuit Q has been taken as 10 throughout this chapter.

Like the graphs in Chapter 4, the graphs in this chapter have also been drawn using the PLOT-10 and the GPGS.

5.2 CONTROL SCHEMES FOR THE PARALLEL RESONANT CONVERTER

In order to ensure satisfactory performance of the parallel resonant converter, some kind of control must be employed. In this section two possible control schemes — namely, frequency control (f-control) and phase control (ϕ -control) have been briefly discussed.

5.2.1 Frequency Control (f-control)

In the frequency control scheme the open-loop control is employed. The converter output is controlled by varying directly the frequency at which the power switches S_1 and S_2 are operated.

5.2.2 Phase Control (ϕ -control)

In this control scheme the phase difference ϕ between the square wave voltage source v_i and the square wave current source i_o of Figure 3.1 is the control variable. This is a closed-loop control with the error in the phase controlling the frequency. An example of implementation of this control scheme has been given in [11].

It may be pointed out here that in all the control schemes that may be employed in the parallel resonant converter, the frequency at which the power switches S_1 and S_2 are turned on is the ultimate variable that is controlled. This frequency is controlled explicitly in the open-loop f-control scheme. In the closed-loop control schemes such as the ϕ -control, the frequency is controlled in an implicit manner.

5.3 EXPRESSIONS FOR OUTPUT POWER, INPUT POWER, CIRCUIT LOSSES AND EFFICIENCY

The expressions for power can be obtained by summing the power due to the respective harmonic components. Thus one can write

$$P_{o_{pu}} = \sum_{n=1,3,5}^{\infty} P_{on_{pu}} \quad (5.1)$$

$$P_{i_{pu}} = \sum_{n=1,3,5}^{\infty} P_{in_{pu}} \quad (5.2)$$

$$P_{l_{pu}} = \sum_{n=1,3,5}^{\infty} P_{ln_{pu}} \quad (5.3)$$

where $P_{o_{pu}}$, $P_{i_{pu}}$ and $P_{l_{pu}}$ represent respectively the per unit output power, input power and power loss due to the resistance of the inductor. $P_{on_{pu}}$, $P_{in_{pu}}$ and $P_{ln_{pu}}$ are the corresponding n^{th} harmonic power components.

From equation (3.24) the expression for the n^{th} harmonic component of the per unit capacitor voltage $v_{Cn_{pu}}$ may be written as

$$v_{Cn_{pu}} = v_{pn_{pu}} \sin(n\omega t - \phi_{V_{Cn}}) \quad (5.4)$$

where
$$v_{pn_{pu}} = \frac{A_n}{n} (x_{V_{Cn}}^2 + y_{V_{Cn}}^2)^{1/2} \quad (5.5)$$

$$\phi_{V_{Cn}} = \tan^{-1} \left(\frac{y_{V_{Cn}}}{x_{V_{Cn}}} \right) \quad (5.6)$$

$$x_{V_{Cn}} = \cos(\phi_{V_{Cn1}}) - B_{V_{Cn}} \cos(\phi_{V_{Cn2}}) \quad (5.7)$$

$$y_{V_{Cn}} = \sin(\phi_{V_{Cn1}}) - B_{V_{Cn}} \sin(\phi_{V_{Cn2}}) \quad (5.8)$$

$$\phi_{V_{Cn1}} = \frac{\pi}{2} + \theta_{Zn} \quad (5.9)$$

$$\phi_{V_{Cn2}} = n\phi + \frac{\pi}{2} - \theta_{Ln} + \theta_{Zn} \quad (5.10)$$

$$B_{V_{Cn}} = n I_{o_{pu}} X_{L1_{pu}} Z'_{Ln} \quad (5.11)$$

From equation (3.23) the expression for $i_{Ln_{pu}}$, the n^{th} harmonic component of the per unit inductor current may similarly be written as

$$i_{Ln_{pu}} = I_{pn_{pu}} \sin(n\omega t - \phi_{I_{Ln}}) \quad (5.12)$$

where
$$I_{pn_{pu}} = \frac{A_n}{X_{Cl_{pu}}} (X_{I_{Ln}}^2 + Y_{I_{Ln}}^2)^{1/2} \quad (5.13)$$

$$\phi_{I_{Ln}} = \tan^{-1}\left(\frac{Y_{I_{Ln}}}{X_{I_{Ln}}}\right) \quad (5.14)$$

$$X_{I_{Ln}} = \cos(\phi_{I_{Ln1}}) + B_{I_{Ln}} \cos(\phi_{I_{Ln2}}) \quad (5.15)$$

$$Y_{I_{Ln}} = \sin(\phi_{I_{Ln1}}) + B_{I_{Ln}} \sin(\phi_{I_{Ln2}}) \quad (5.16)$$

$$\phi_{I_{Ln1}} = \theta_{Zn} \quad (5.17)$$

$$\phi_{I_{Ln2}} = n\phi + \frac{\pi}{2} + \theta_{Zn} \quad (5.18)$$

$$B_{I_{Ln}} = \frac{I_{o_{pu}} X_{L1_{pu}}}{n \omega_{pu}^2} \quad (5.19)$$

The per unit expressions for the n^{th} harmonic components of the voltage source v_i and current source i_o of Figure 3.1 are respectively given by

$$v_{in_pu} = \frac{4}{n\pi} \sin n \omega t \quad (5.20)$$

$$i_{on_pu} = \frac{4I_o}{n\pi} \sin(n \omega t - n\phi) \quad (5.21)$$

From (5.4) and (5.21) the expression for the per unit output power due to the n^{th} harmonic components may be written as

$$P_{on_pu} = \frac{V_{pn_pu}}{\sqrt{2}} \cdot \frac{1}{\sqrt{2}} \left(\frac{4I_o}{n\pi} \right) \cos(\phi_{V_{Cn}} - n\phi) \quad (5.22)$$

$$\therefore P_{on_pu} = \frac{2V_{pn_pu} I_o}{n\pi} \cos(\phi_{V_{Cn}} - n\phi) \quad (5.23)$$

Similarly, with the help of equations (5.12) and (5.20), the per unit input power due to the n^{th} harmonic components may be expressed as

$$P_{in_pu} = \frac{2I_{pn_pu}}{n\pi} \cos(\phi_{I_{Ln}}) \quad (5.24)$$

The expression for the n^{th} harmonic component of the power loss due to resistance of the inductor coil may be written in terms of per unit quantities as

$$P_{ln_pu} = \left(\frac{I_{pn_pu}}{\sqrt{2}} \right)^2 R_{pu} \quad (5.25)$$

$$\text{i.e. } P_{ln_pu} = \frac{I_{pn_pu}^2 R_{pu}}{2} \quad (5.26)$$

The expressions for $P_{on_{pu}}$, $P_{in_{pu}}$ and $P_{ln_{pu}}$ as given by equations (5.23), (5.24) and (5.26) respectively may be substituted in equations (5.1), (5.2) and (5.3) to calculate the output power, the input power and the circuit losses.

The efficiency η of the converter may be determined from the following relationship

$$\eta(\%) = \frac{P_{o_{pu}}}{P_{i_{pu}}} \cdot 100 \quad (5.27)$$

It should be noted that in order to evaluate $P_{o_{pu}}$, $P_{i_{pu}}$ and $P_{l_{pu}}$ for a given value of the independent variable $I_{o_{pu}} X_{L1_{pu}}$, specific values of $I_{o_{pu}}$, $X_{L1_{pu}}$, $X_{C1_{pu}}$ and R_{pu} have to be substituted in the expressions of $P_{on_{pu}}$, $P_{in_{pu}}$ and $P_{ln_{pu}}$. If, however, both sides of equations (5.23), (5.24) and (5.26) are multiplied by $X_{L1_{pu}}$, more generalised expressions may be obtained. For given values of Q and ω_{pu} it is then possible to evaluate these expressions for a given value of $I_{o_{pu}} X_{L1_{pu}}$ without assigning specific values to R , L , C and I_o .

Multiplying both sides of equations (5.23), (5.24) and (5.26) by $X_{L1_{pu}}$ and using equation (2.22) the following expressions are obtained from equations (5.1), (5.2) and (5.3).

$$P_{o_{pu}} X_{L1_{pu}} = \sum_n \frac{2V_{pn} I_{o_{pu}} X_{L1_{pu}}}{n\pi} \cos(\phi_{V_{Cn}} - n\phi) \quad (5.28)$$

$$P_{i_{pu}} X_{L1_{pu}} = \sum_n \frac{2I'_{pn}}{n\pi} \cos(\phi_{I_{Ln}}) \quad (5.29)$$

$$P_{l_{pu}} X_{L1_{pu}} = \sum_n \frac{(I'_{pn})^2}{2Q_1} \quad (5.30)$$

where $I'_{pn_{pu}} = I_{pn_{pu}} X_{L1_{pu}}$

$$= A_n \omega_{pu}^2 (X_{I_{Ln}}^2 + Y_{I_{Ln}}^2)^{1/2} \quad (5.31)$$

and $Q_1 = \omega_{pu} Q \quad (5.32)$

i.e. Q_1 is the quality factor of the coil at the frequency of operation.

The efficiency η of the converter can be obtained with the help of the following relationship

$$\eta(\%) = \frac{P_{o_{pu}}}{P_{i_{pu}}} \cdot 100$$

or, $\eta(\%) = \frac{P_{o_{pu}} X_{L1_{pu}}}{P_{i_{pu}} X_{L1_{pu}}} \cdot 100 \quad (5.33)$

5.4 VARIATION OF OUTPUT POWER, INPUT POWER, CIRCUIT LOSSES AND EFFICIENCY

The variations of power and efficiency as a function of $I_{o_{pu}} X_{L1_{pu}}$ have first been obtained in this section for both f-control and ϕ -control. Subsequently the variations of power and efficiency with $I_{o_{pu}}$ have been examined for these two control schemes.

5.4.1 Variation of Power and Efficiency with $I_{o_{pu}} X_{L1_{pu}}$ for f-control

For given values Q and ω_{pu} the expressions (5.28), (5.29) and (5.30) have been evaluated for a given value of $I_{o_{pu}} X_{L1_{pu}}$ by evaluating the various quantities with the help

of equations (4.1) through (4.9) as pointed out in Section 4.1. Figures 5.1, 5.2, 5.3 and 5.4 illustrate the variation of $P_{o_{pu}} X_{L1_{pu}}$, $P_{i_{pu}} X_{L1_{pu}}$, $P_{l_{pu}} X_{L1_{pu}}$ and η respectively for six different values of frequencies. To evaluate expressions (5.28), (5.29) and (5.30) for a given value of ω_{pu} , ϕ is increased from 0° onwards and the corresponding values of $I_{o_{pu}} X_{L1_{pu}}$ are calculated using equation (4.10) as in Chapter 4.

5.4.2 Variation of Power and Efficiency with $I_{o_{pu}} X_{L1_{pu}}$ for ϕ -control

Figures 5.5, 5.6, 5.7 and 5.8 show the variation of $P_{o_{pu}} X_{L1_{pu}}$, $P_{i_{pu}} X_{L1_{pu}}$, $P_{l_{pu}} X_{L1_{pu}}$ and η as a function of $I_{o_{pu}} X_{L1_{pu}}$ for ϕ -control. Each of the curves in these figures has been obtained for a fixed value of ϕ . For a given value of ϕ , ω_{pu} is varied from 0.5 to 1.0 and the corresponding values of $I_{o_{pu}} X_{L1_{pu}}$ are calculated using equation (4.10). The corresponding values of ω_{pu} and $I_{o_{pu}} X_{L1_{pu}}$ then have been used to evaluate the expressions (5.28), (5.29) and (5.30) for the given value of ϕ . Only those values of ω_{pu} for which the corresponding values of $I_{o_{pu}} X_{L1_{pu}}$ are positive have been taken into consideration.

5.4.3 Variation of Power and Efficiency as a Function of $I_{o_{pu}}$ for f-control

In this section the variation of per unit output power, input power, power loss and efficiency as a function of the per unit output current have been obtained for a given set of circuit parameters. The circuit parameters are chosen such that $X_{L1_{pu}} = 0.25$ at $\omega_{pu} = 0.5$. The value of $X_{L1_{pu}}$ at any frequency is then given by

$$X_{L1_{pu}} = 0.25 \cdot \frac{\omega_{pu}}{0.5}$$

$$\text{i.e. } X_{L1_{pu}} = 0.5 \omega_{pu} \quad (5.34)$$

$X_{C1_{pu}}$ may be calculated from equation (2.22) as follows

$$X_{C1_{pu}} = \frac{X_{L1_{pu}}}{\omega_{pu}^2} \quad (5.35)$$

Having calculated $X_{L1_{pu}}$ and $X_{C1_{pu}}$, $P_{o_{pu}}$, $P_{i_{pu}}$ and $P_{l_{pu}}$ have been calculated from equations (5.23), (5.24), (5.26) and (5.1), (5.2), (5.3). η has been obtained from equation (5.27). The variations of $P_{o_{pu}}$, $P_{i_{pu}}$, $P_{l_{pu}}$ and η with $I_{o_{pu}}$ have been shown in Figures 5.9, 5.10, 5.11 and 5.12 respectively for six different values of frequencies. For a given value of ω_{pu} \emptyset is increased from 0° onwards and the corresponding values of $I_{o_{pu}}$ are calculated from equation (4.10) as in Section 5.4.1.

5.4.4 Variation of Power and Efficiency as a Function of $I_{o_{pu}}$ for \emptyset -control

In this case also the circuit parameters are chosen such that $X_{L1_{pu}} = 0.25$ at $\omega_{pu} = 0.5$. After calculating $X_{L1_{pu}}$ and $X_{C1_{pu}}$ with the help of equations (5.34) and (5.35) respectively, ω_{pu} is varied as in Section 5.4.2 from 0.5 to 1.0 and the corresponding values of $I_{o_{pu}}$ are calculated from equation (4.10) for the given value of \emptyset . Values of $P_{o_{pu}}$, $P_{i_{pu}}$, $P_{l_{pu}}$ and η have been then calculated from equations (5.23), (5.24), (5.26), (5.27) and (5.1), (5.2), (5.3) as before. Figures 5.13, 5.14, 5.15 and 5.16 show the variations of $P_{o_{pu}}$, $P_{i_{pu}}$, $P_{l_{pu}}$ and η respectively with $I_{o_{pu}}$ for different values of \emptyset .

$Q = 10$

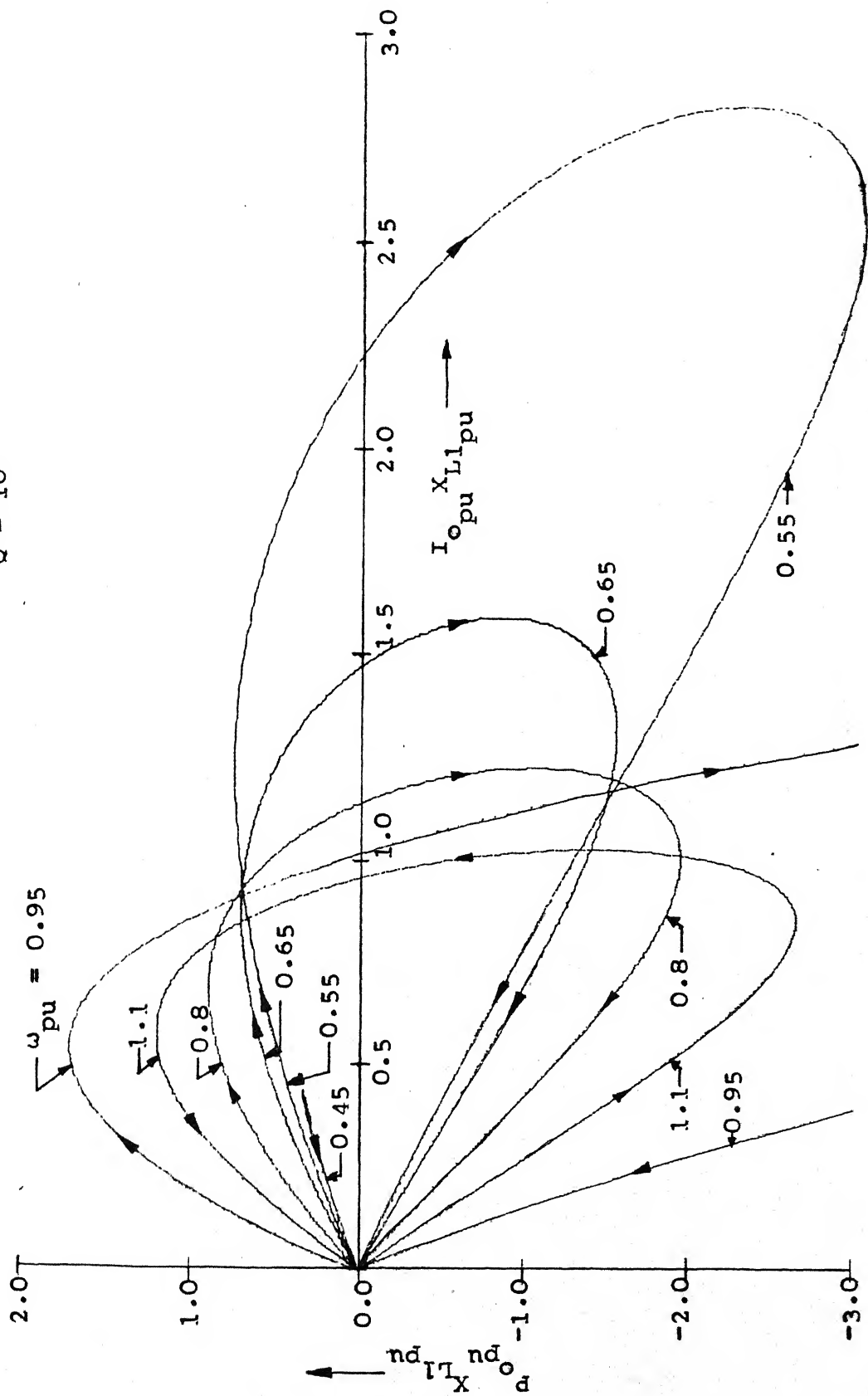


Figure 5.1(a). Variation of $P_0 X_{L1}^{pu}$ with $I_{0pu} X_{L1}^{pu}$ for f -control
(Arrowhead indicates increasing values of \emptyset).

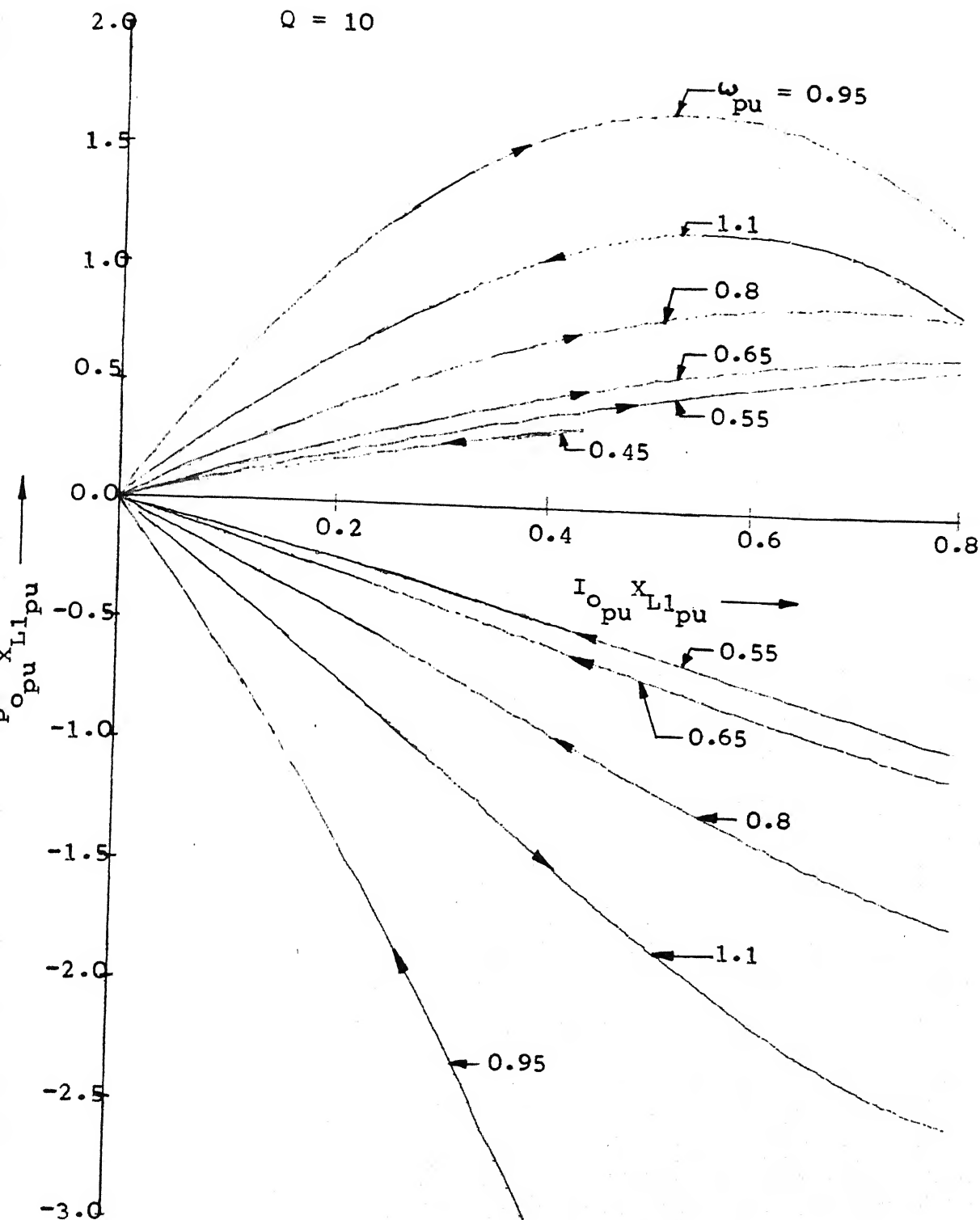


Figure 5.1(b). Variation of $P_{o_pu} X_{L1_pu}$ with $I_{o_pu} X_{L1_pu}$ for f-control (expanded version of Figure 5.1(a)).

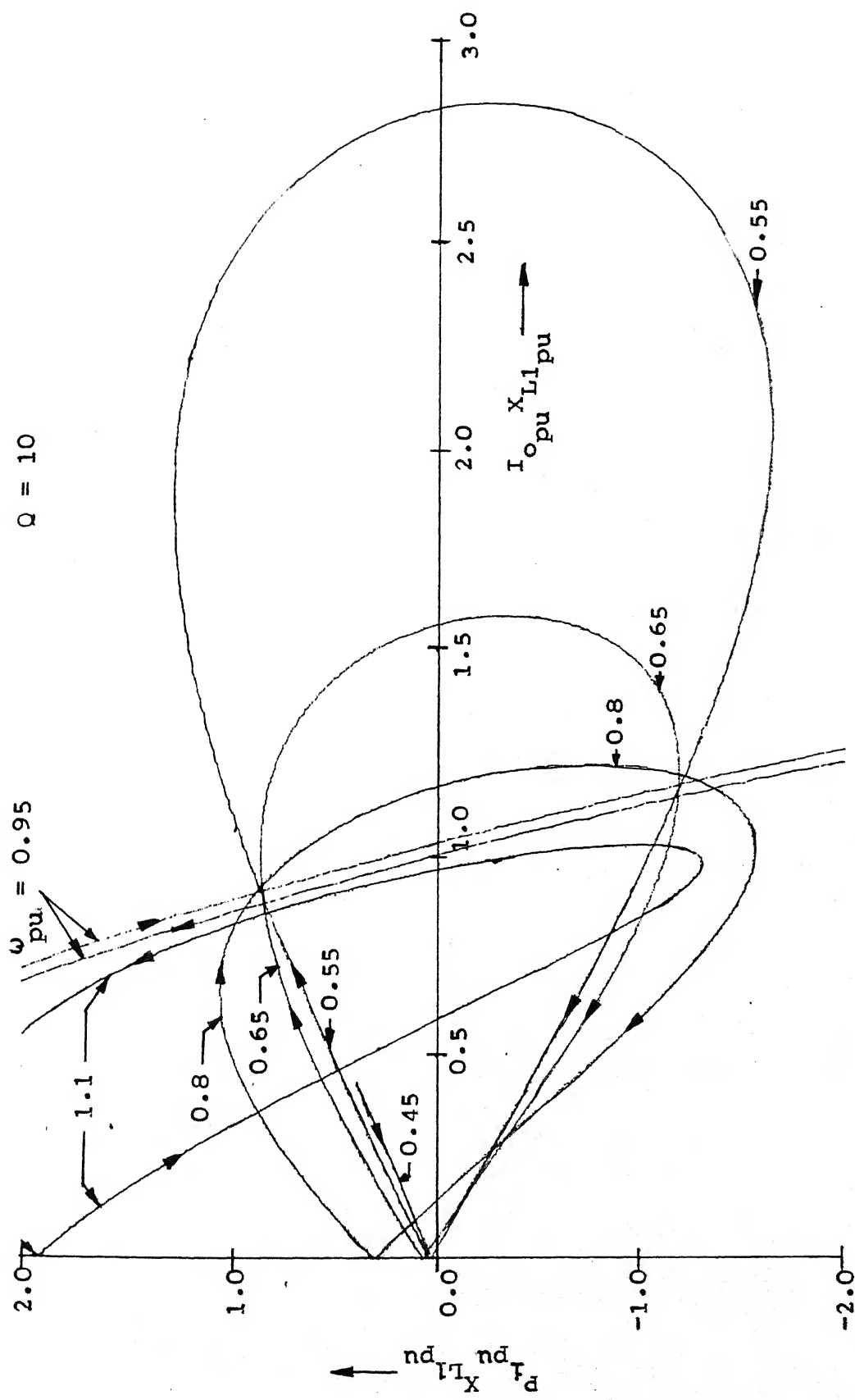


Figure 5.2(a). Variation of $P_L X_{L1} \text{ pu}$ with $I_o X_{L1} \text{ pu}$ for f-control (Arrowhead indicates increasing values of δ).

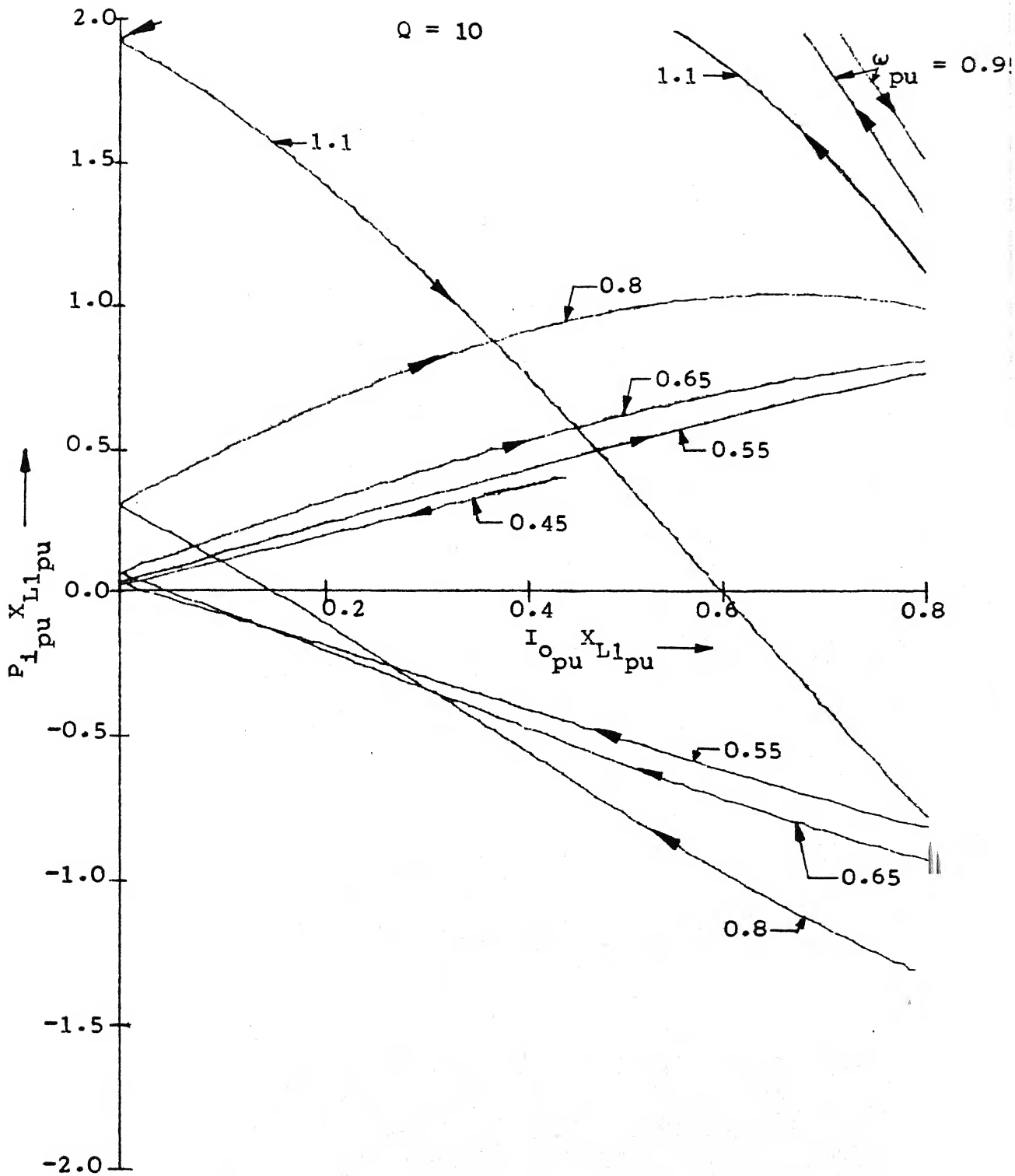


Figure 5.2(b). Variation of $P_i X_{L1 pu}$ with $I_o X_{L1 pu}$ for f-control (expanded version of Figure 5.2(a)).

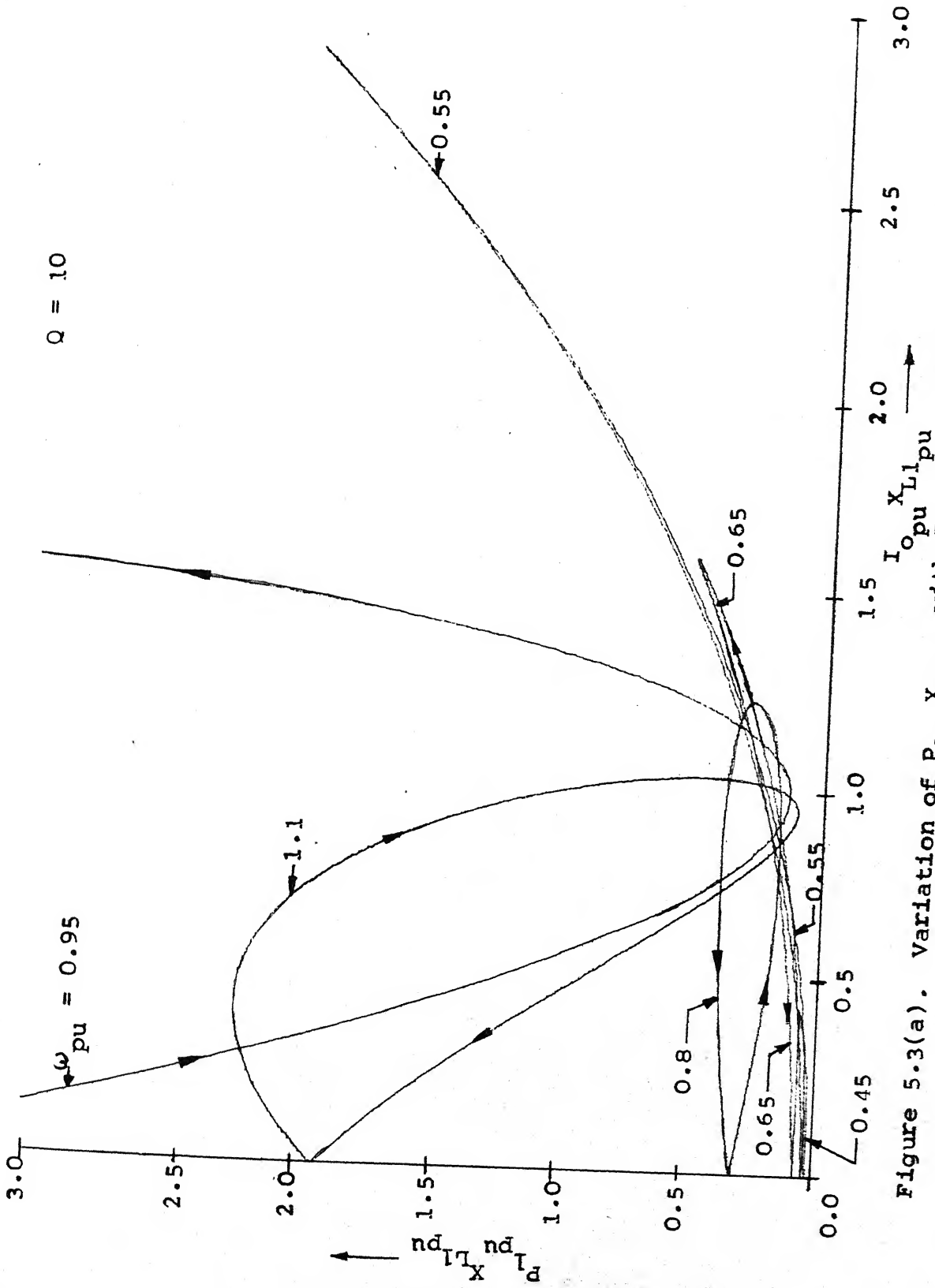


Figure 5.3(a). Variation of $P_{1\text{pu}} X_{L1\text{pu}}$ with $I_{\text{Opu}} X_{L1\text{pu}}$ for f-control (Arrowhead indicates increasing values of \emptyset).

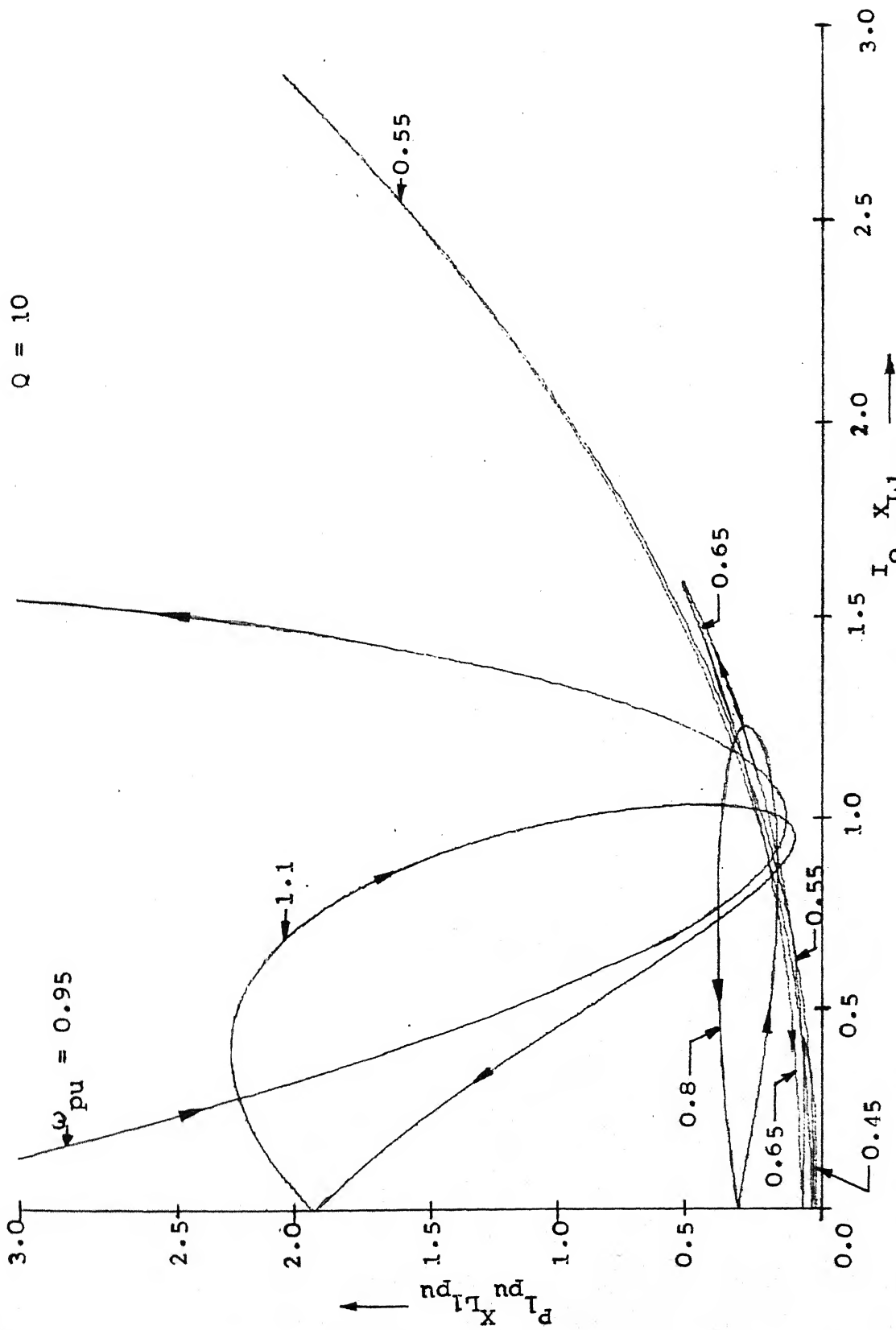


Figure 5.3(a). Variation of P_1 , X_{L1} with $I_o L_1$ pu for f-control
(Arrowhead indicates increasing values of ϕ).

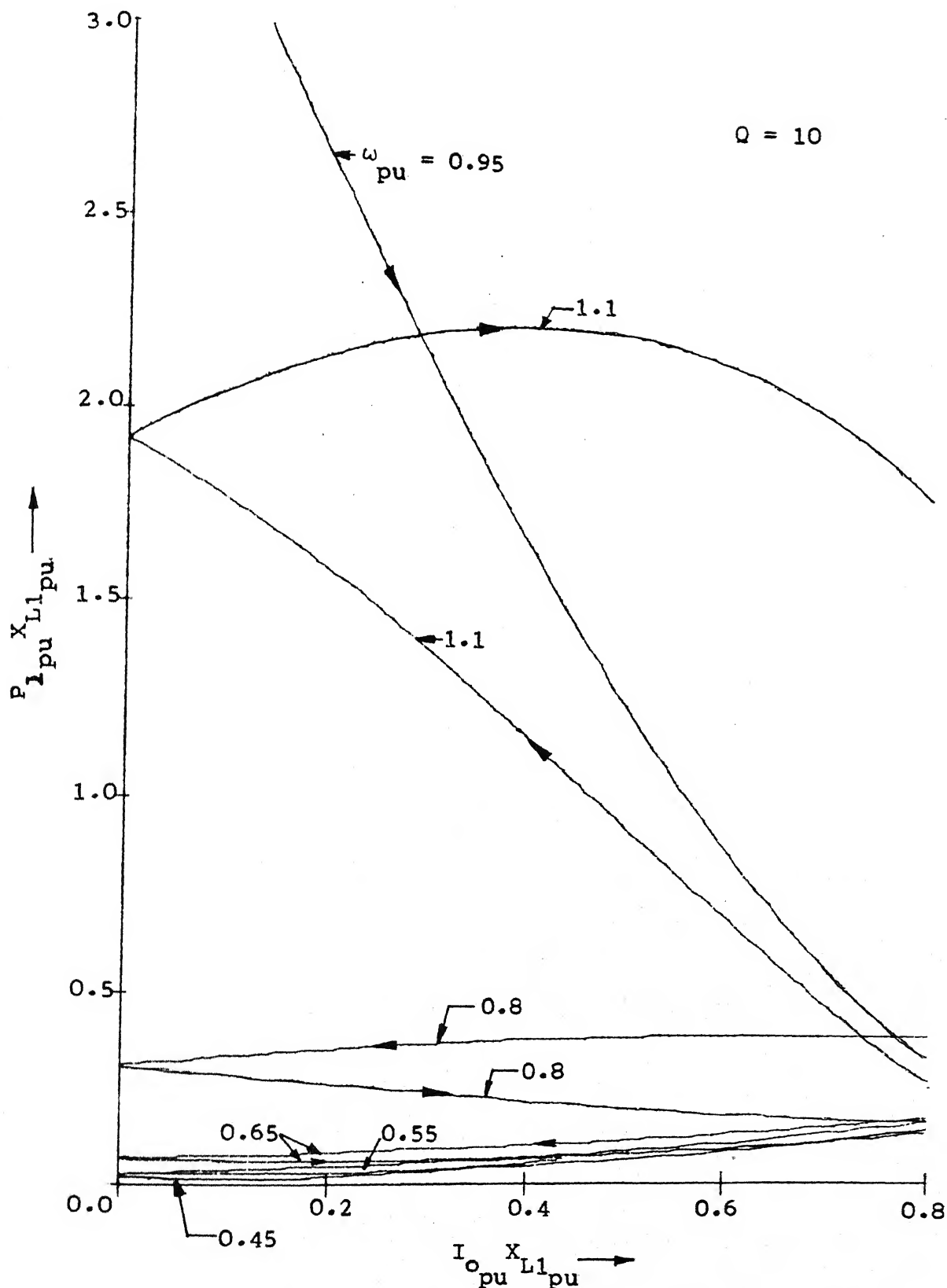


Figure 5.3(b). Variation of $P_1 X_{L1_{pu}}$ with $I_{o_{pu}} X_{L1_{pu}}$ for f-control (expanded version of Figure 5.3(a)).

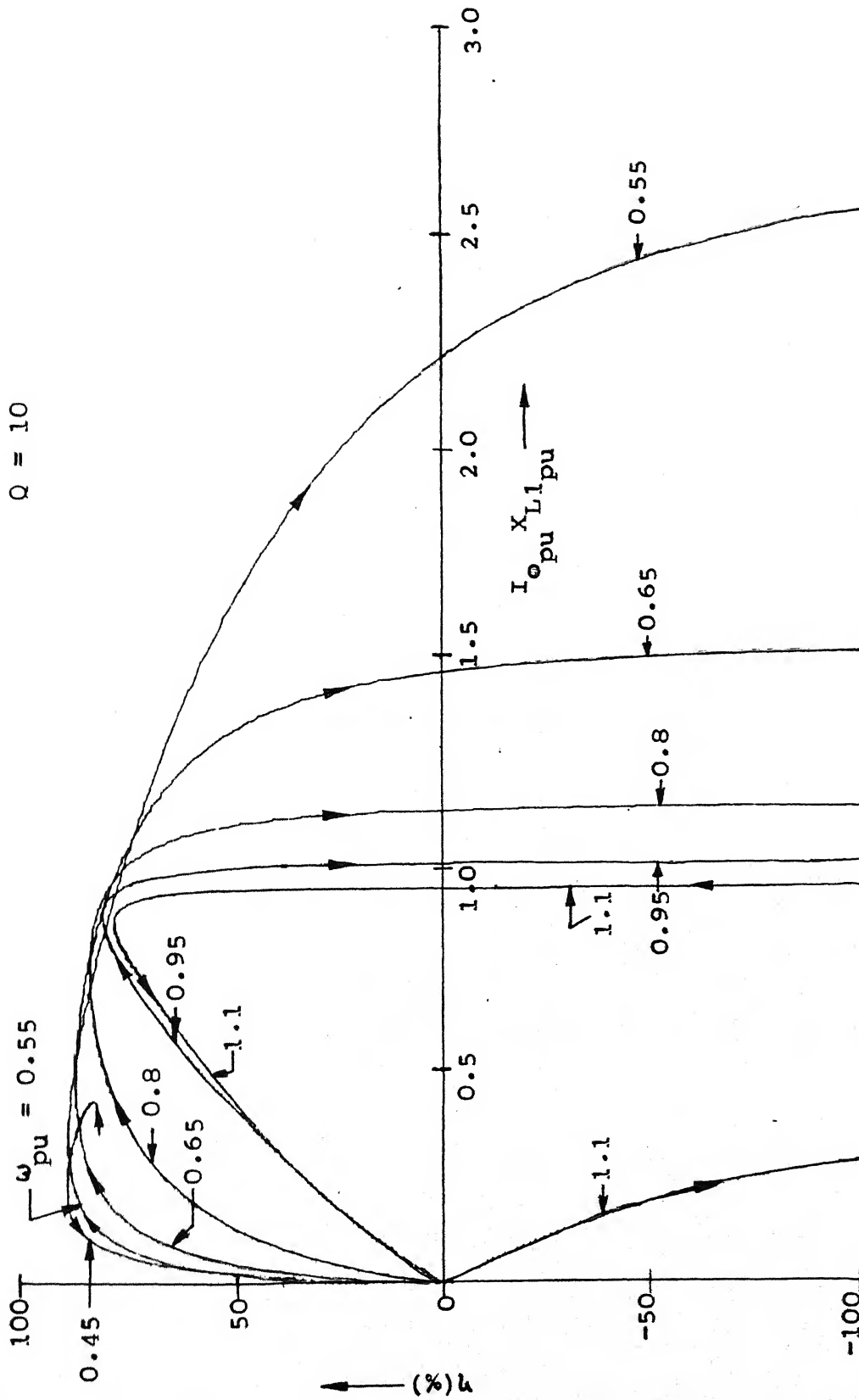


Figure 5.4(a). Variation of efficiency η with $I_o X_{L1}$ pu for f-control (Arrowhead indicates increasing values of ω).

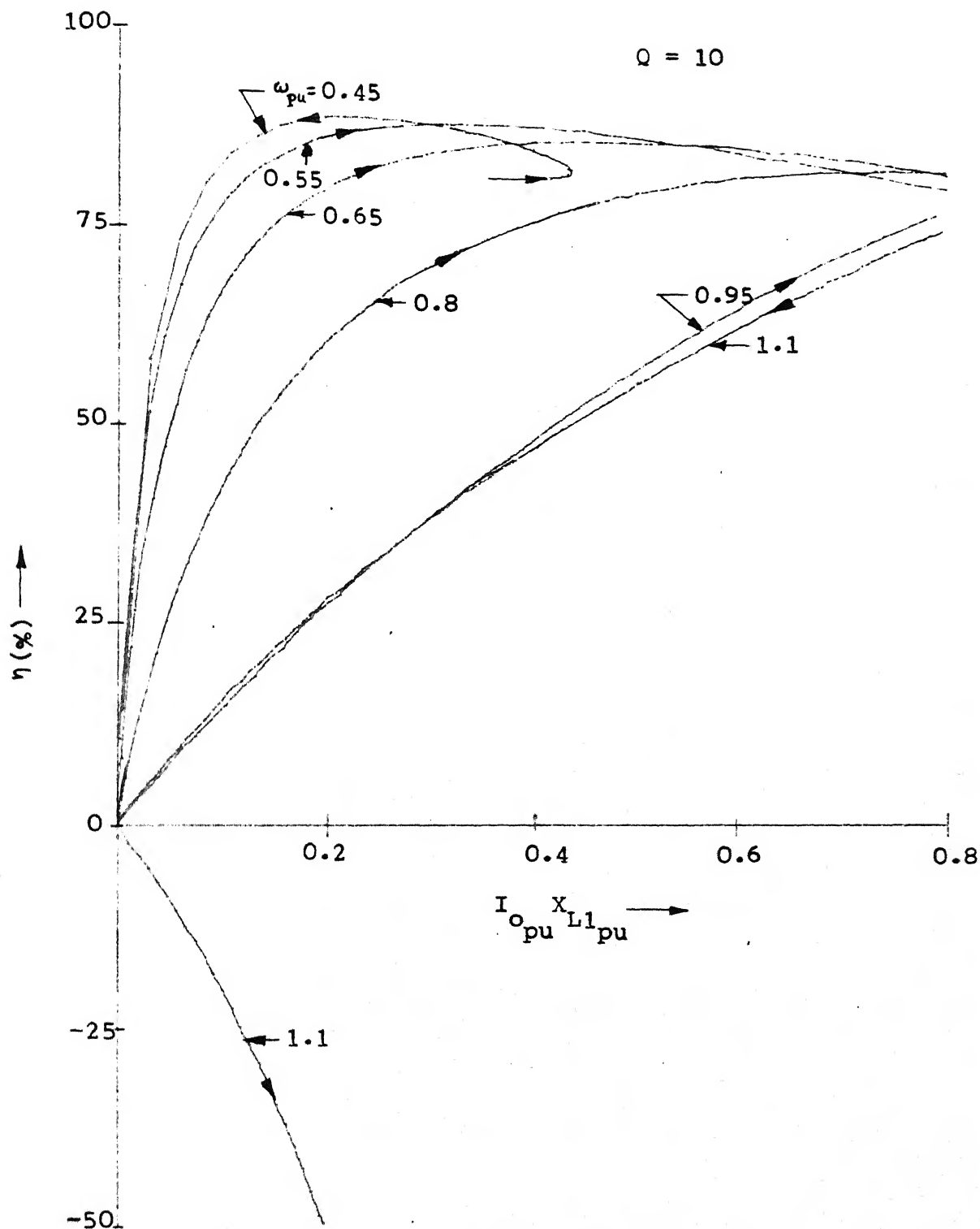


Figure 5.4(b). Variation of efficiency η with $I_{o_pu} X_{L1_pu}$ for f-control (expanded version of Figure 5.4(a)).

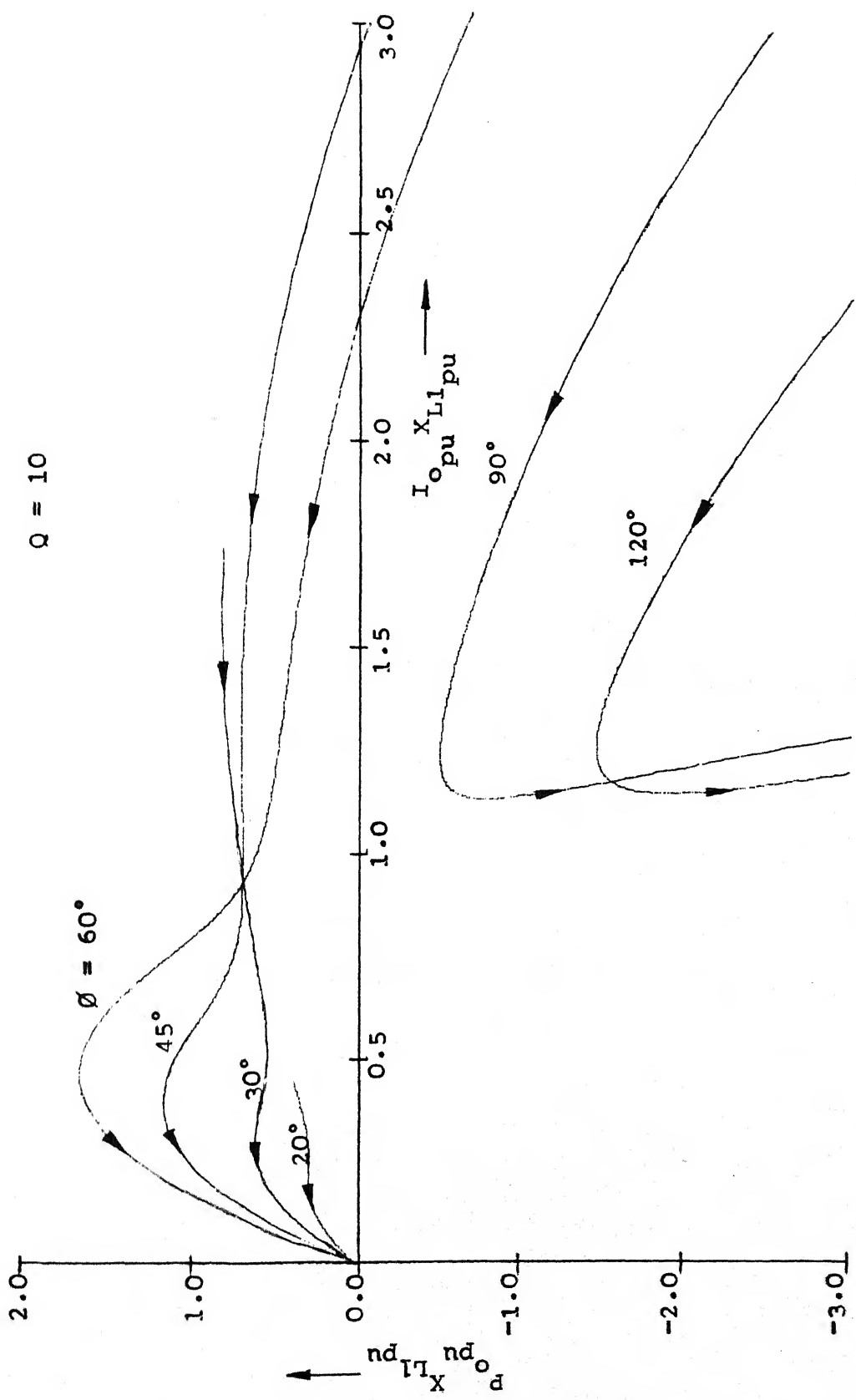


Figure 5.5(a). Variation of $P_o X_{L1} pu$ with $I_o X_{L1} pu$ for ϕ -control (Arrowhead indicates increasing values of ω_{pu}).

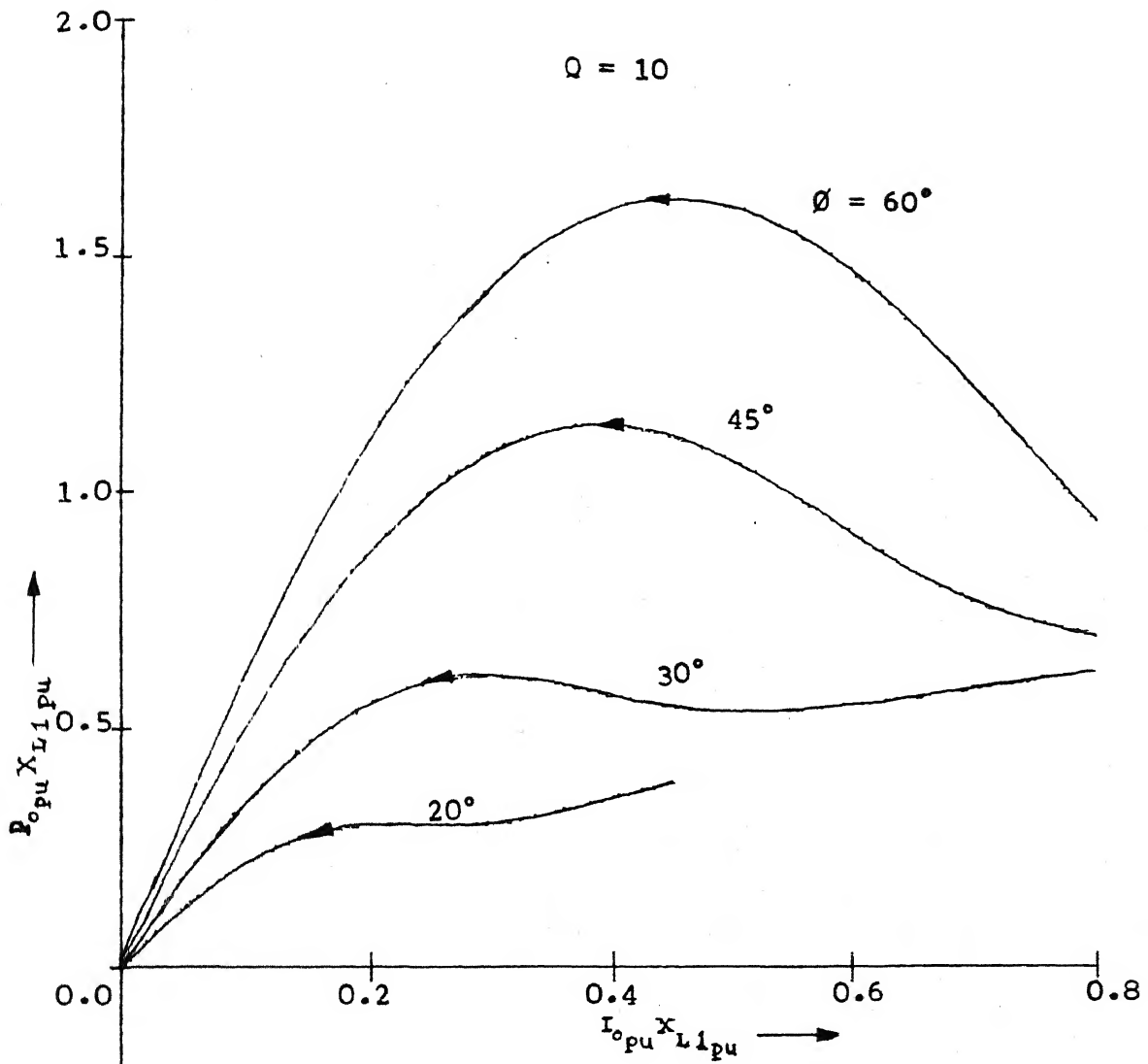


Figure 5.5(b). Variation of $P_{0pu} X_{L1pu}$ with $I_{0pu} X_{L1pu}$ for θ -control (expanded version of Figure 5.5(a)).

$$Q = 10$$

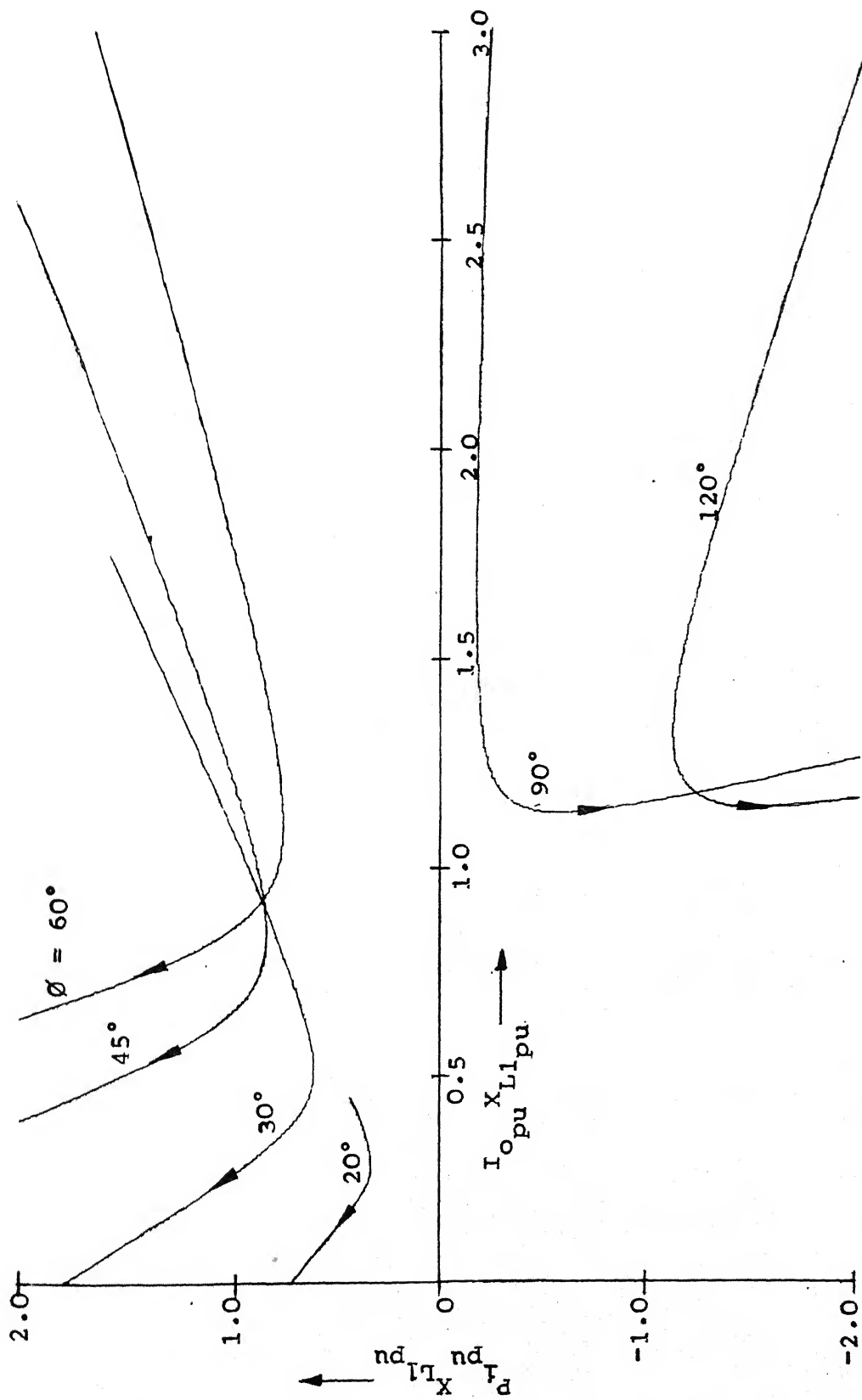


Figure 5.6(a). Variation of P_1 and X_1 with I_0 and X_1 for θ -control (Arrowhead indicates increasing values of ω_{pu}).

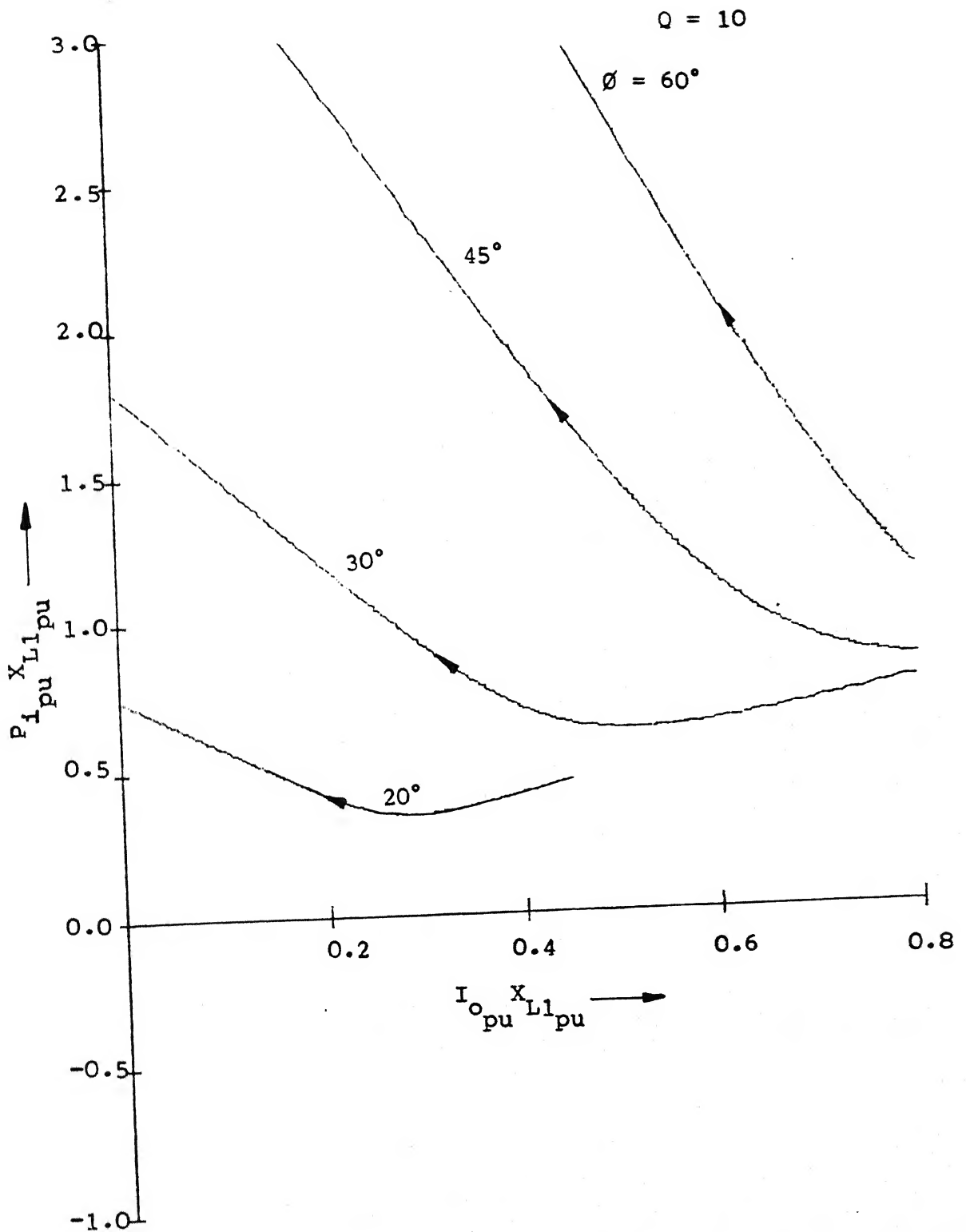


Figure 5.6(b). Variation of $P_{I_{pu} X_{L1_{pu}}}$ with $I_{O_{pu} X_{L1_{pu}}}$ for ϕ -control (expanded version of Figure 5.6(a))

$Q = 10$

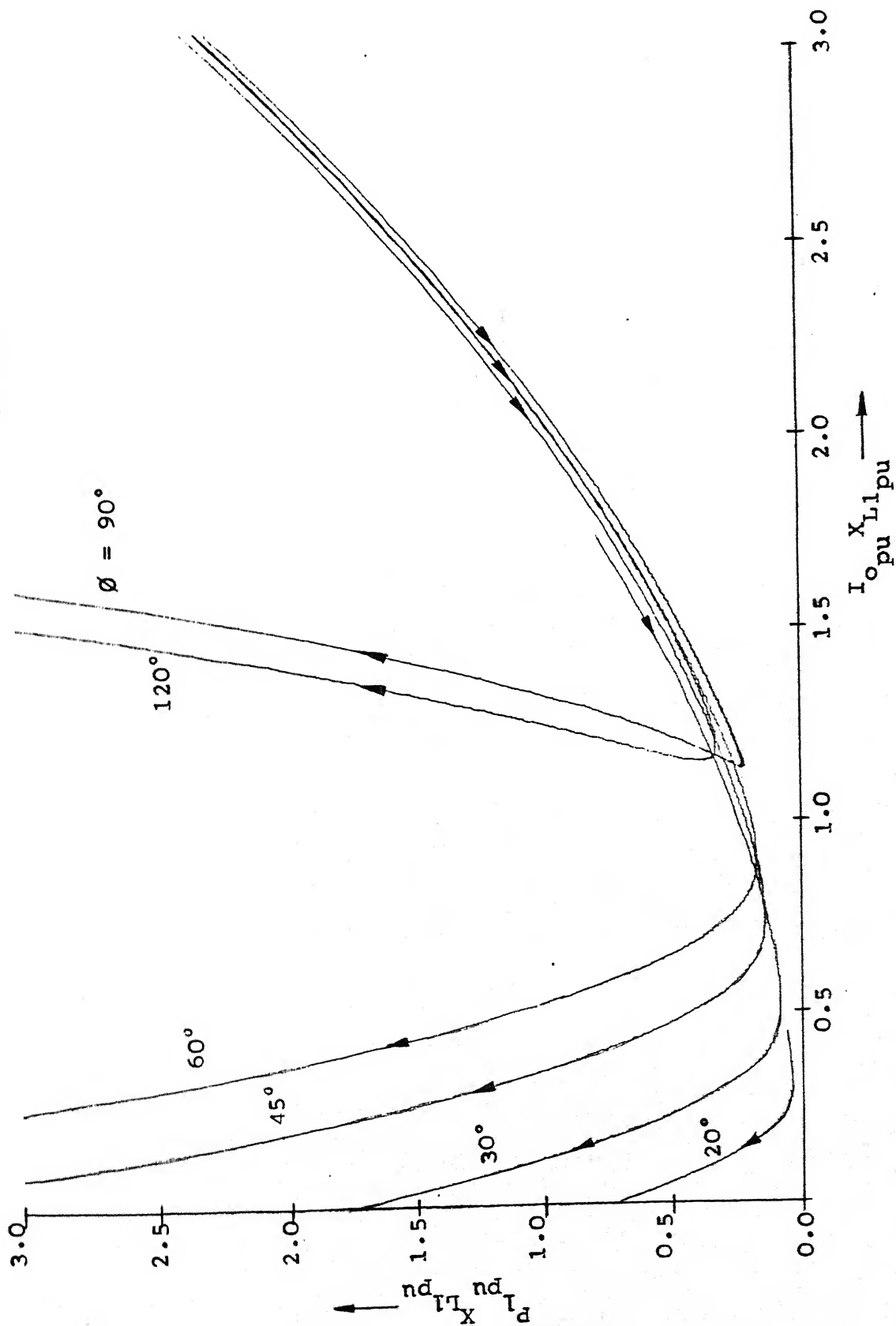


Figure 5.7(a). Variation of $P_L X_{L1} \text{ pu}$ with $I_O X_{L1} \text{ pu}$ for δ -control (Arrowhead indicates increasing values of ω_{pu}).

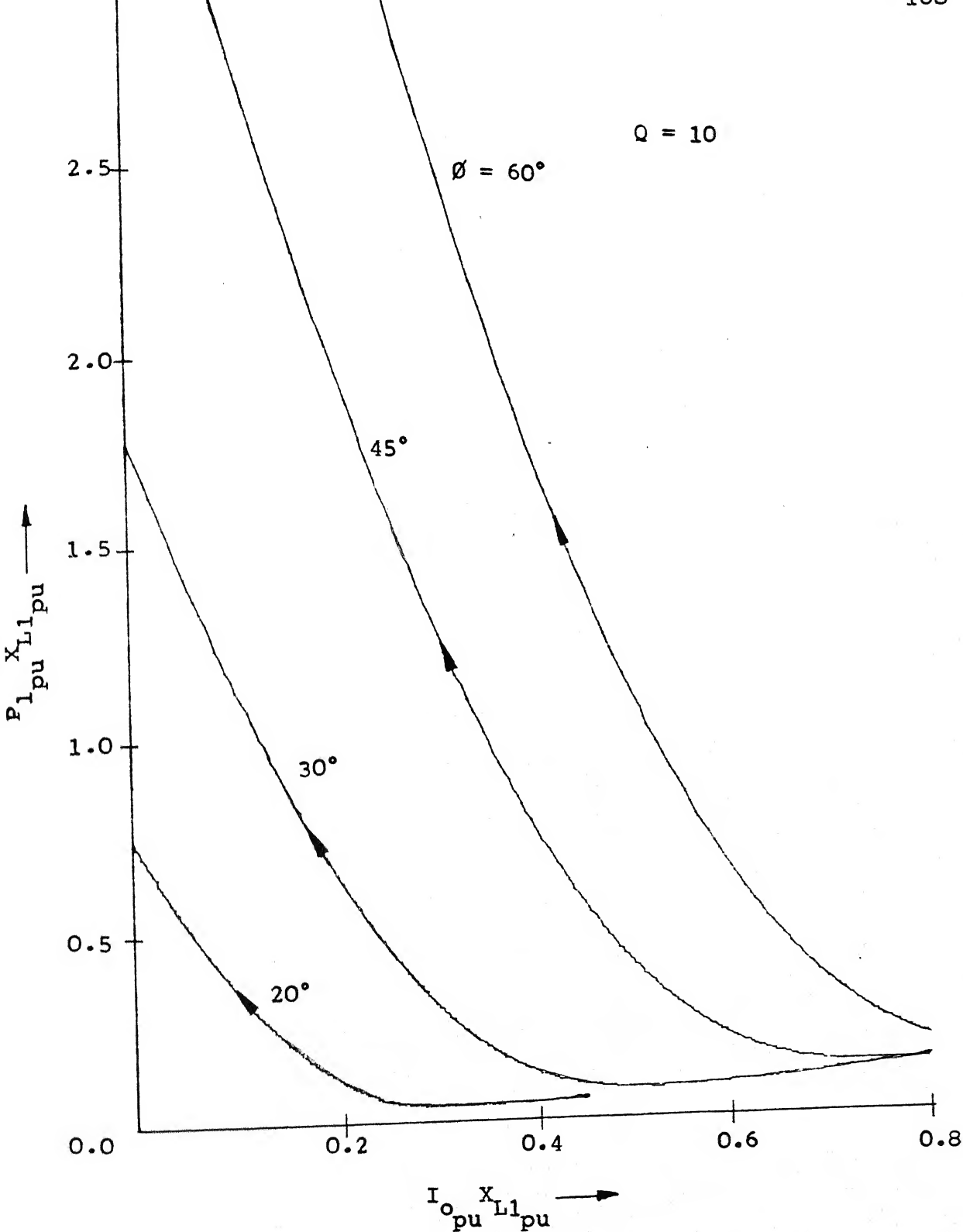


Figure 5.7(b). Variation of $P_{l_{pu}} X_{l_{pu}}$ with $I_{o_{pu}} X_{l_{pu}}$ for ϕ -control (expanded version of Figure 5.7(a)).

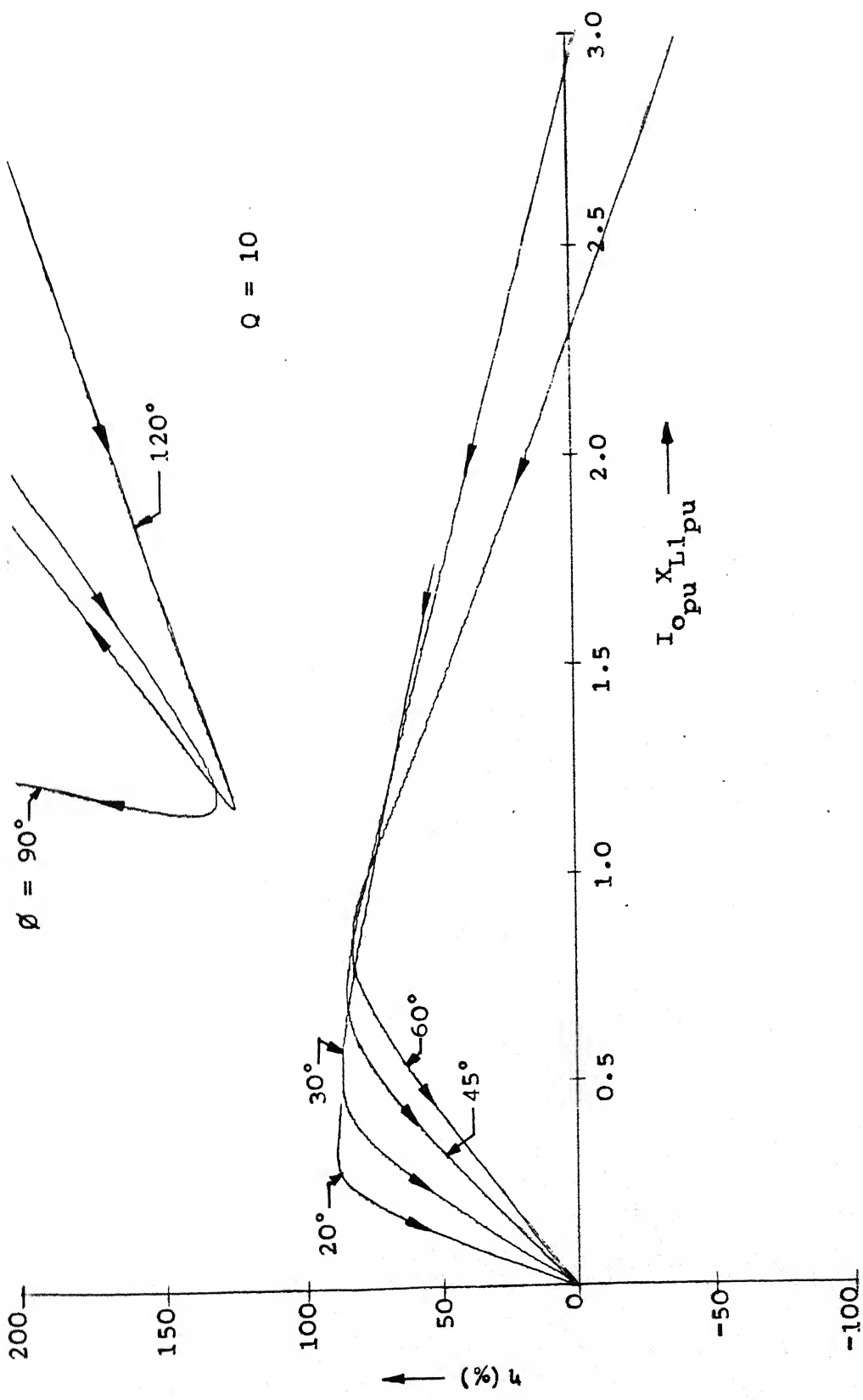


Figure 5.8(a). Variation of efficiency η with $I_{opu} X_{L1_pu}$ for δ -control (Arrowhead indicates increasing values of ω_{pu}).

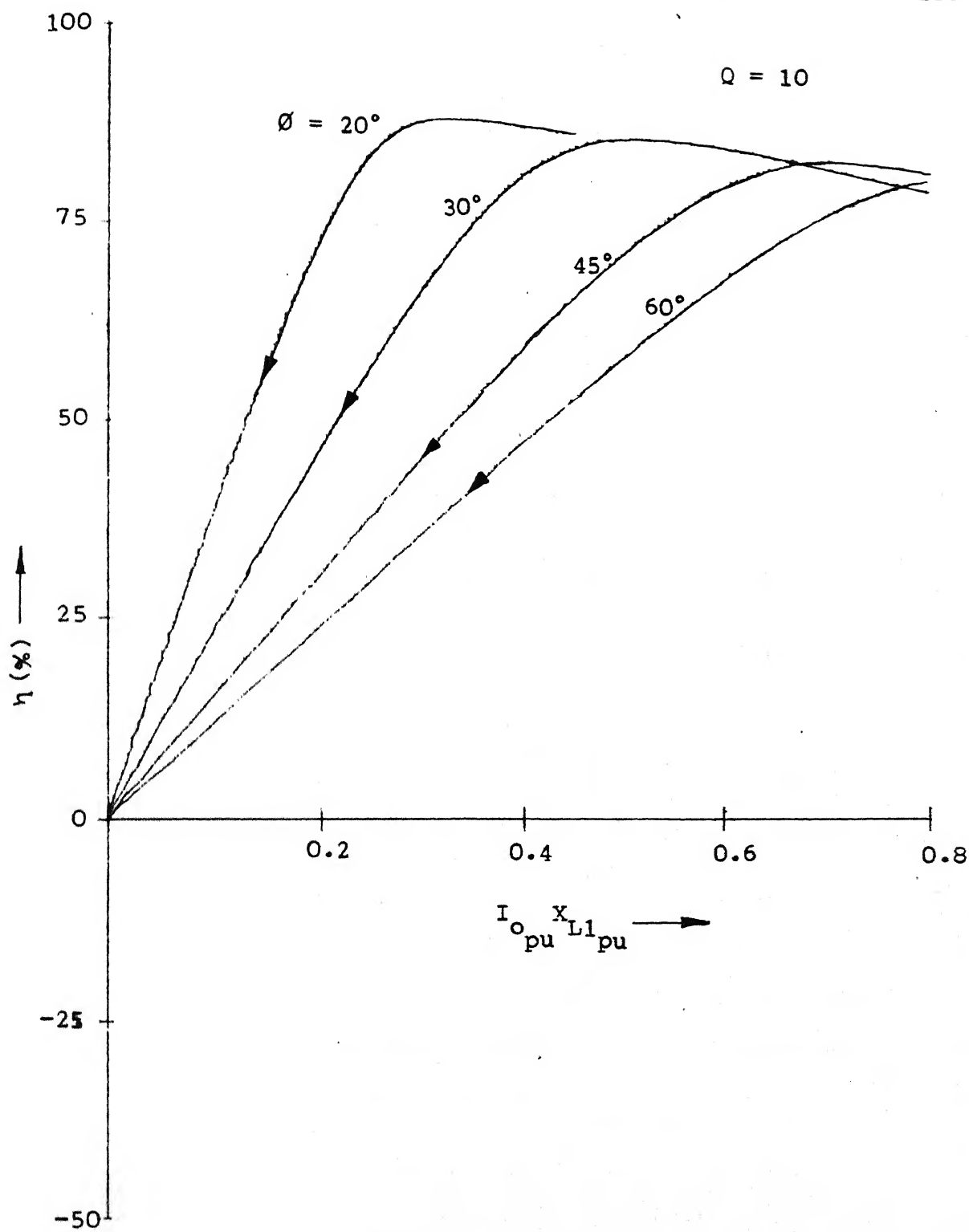


Figure 5.8(b). Variation of efficiency η with $I_o X L1 / I_{pu}$ for \emptyset -control (expanded version of Figure 5.8(a)).

$Q = 10$
 $X_{L1_pu} = 0.25$ at $\omega_{pu} = 0.5$

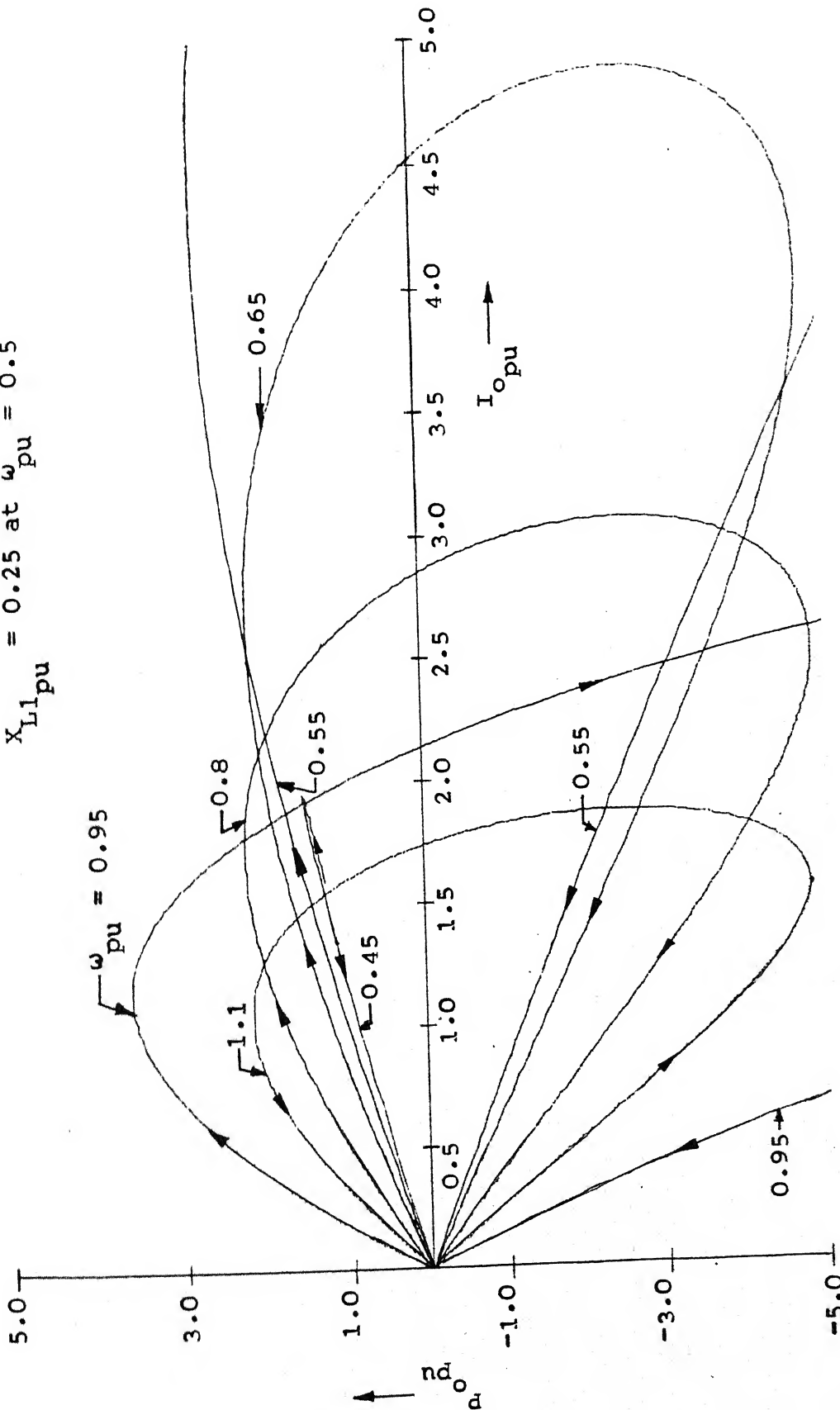


Figure 5.9. Variation of per unit output power P_{Opu} with I_{Opu} for f-control for a given set of circuit parameters (Arrowhead indicates increasing values of ϕ).

$Q = 10$
 $X_{L1_{pu}} = 0.25$ at $\omega_{pu} = 0.5$

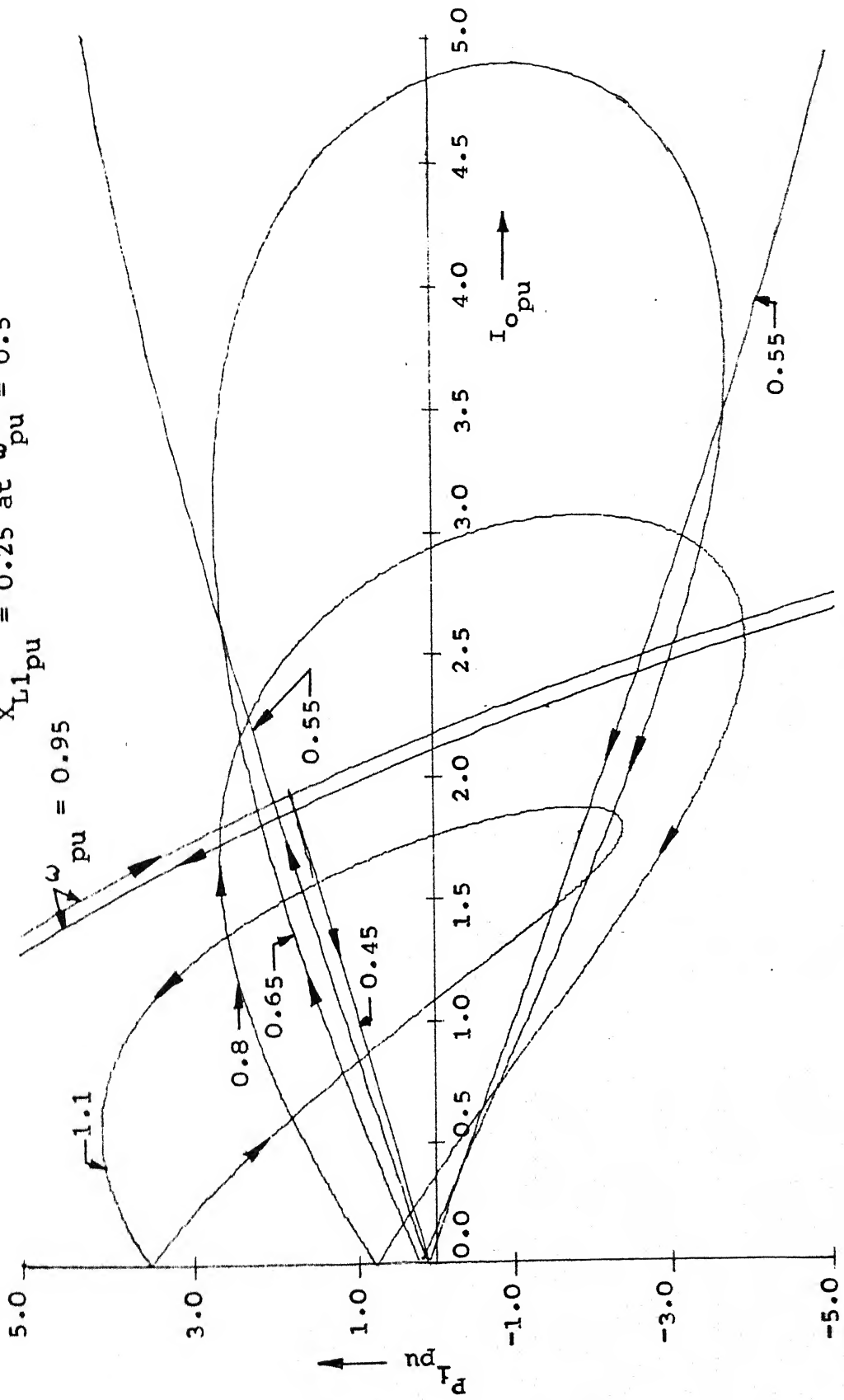


Figure 5.10. Variation of per unit input power $P_{i_{pu}}$ with $I_{o_{pu}}$ for f-control for a given set of circuit parameters (Arrowhead indicates increasing values of ϕ).

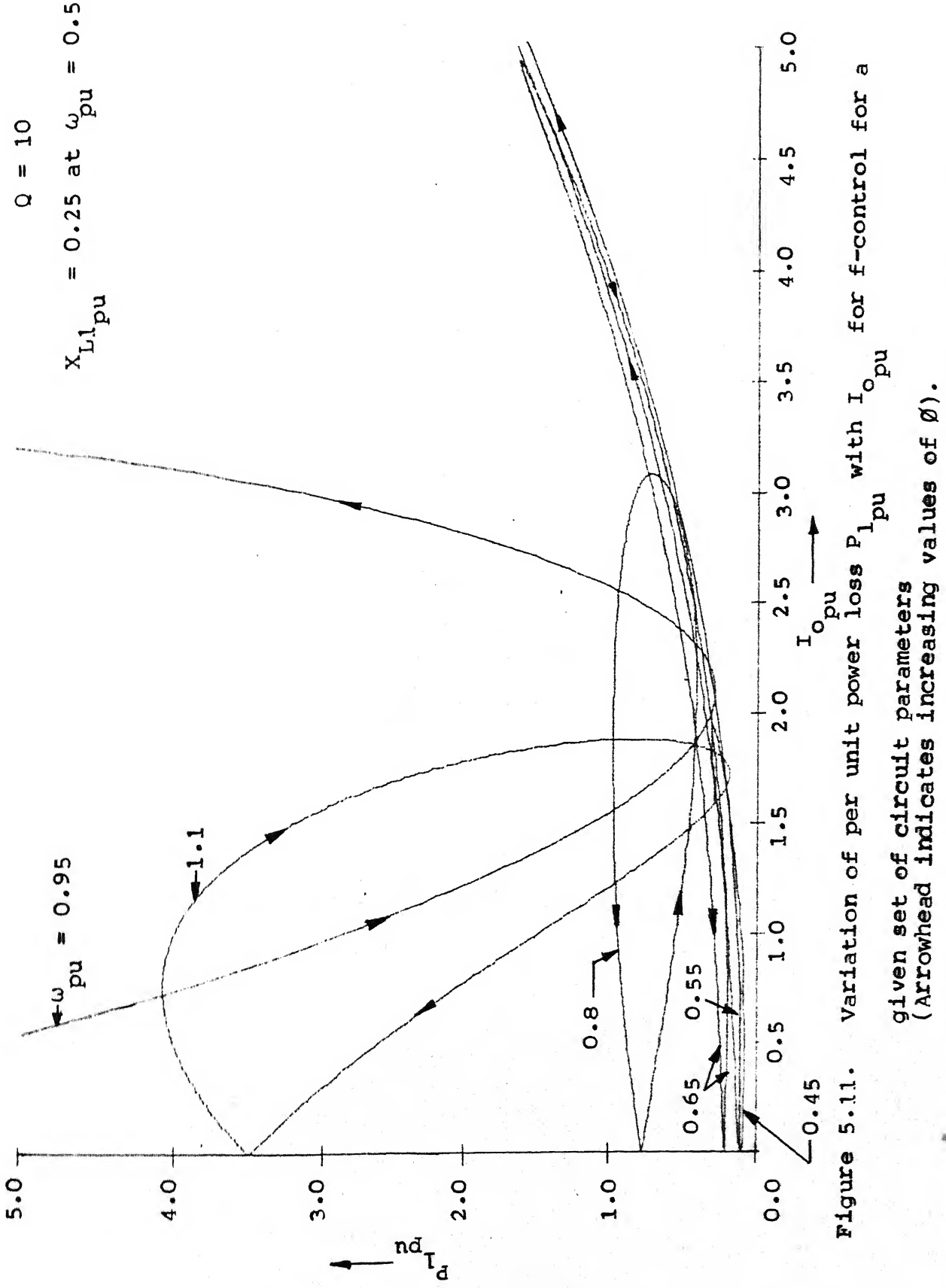


Figure 5.11. Variation of per unit power loss $P_{L1_{pu}}$ with $I_{O_{pu}}$ for f-control for a given set of circuit parameters (Arrowhead indicates increasing values of ω).

$$Q = 10$$

$$X_{L1\text{ pu}} = 0.25 \text{ at } \omega_{\text{pu}} = 0.5$$

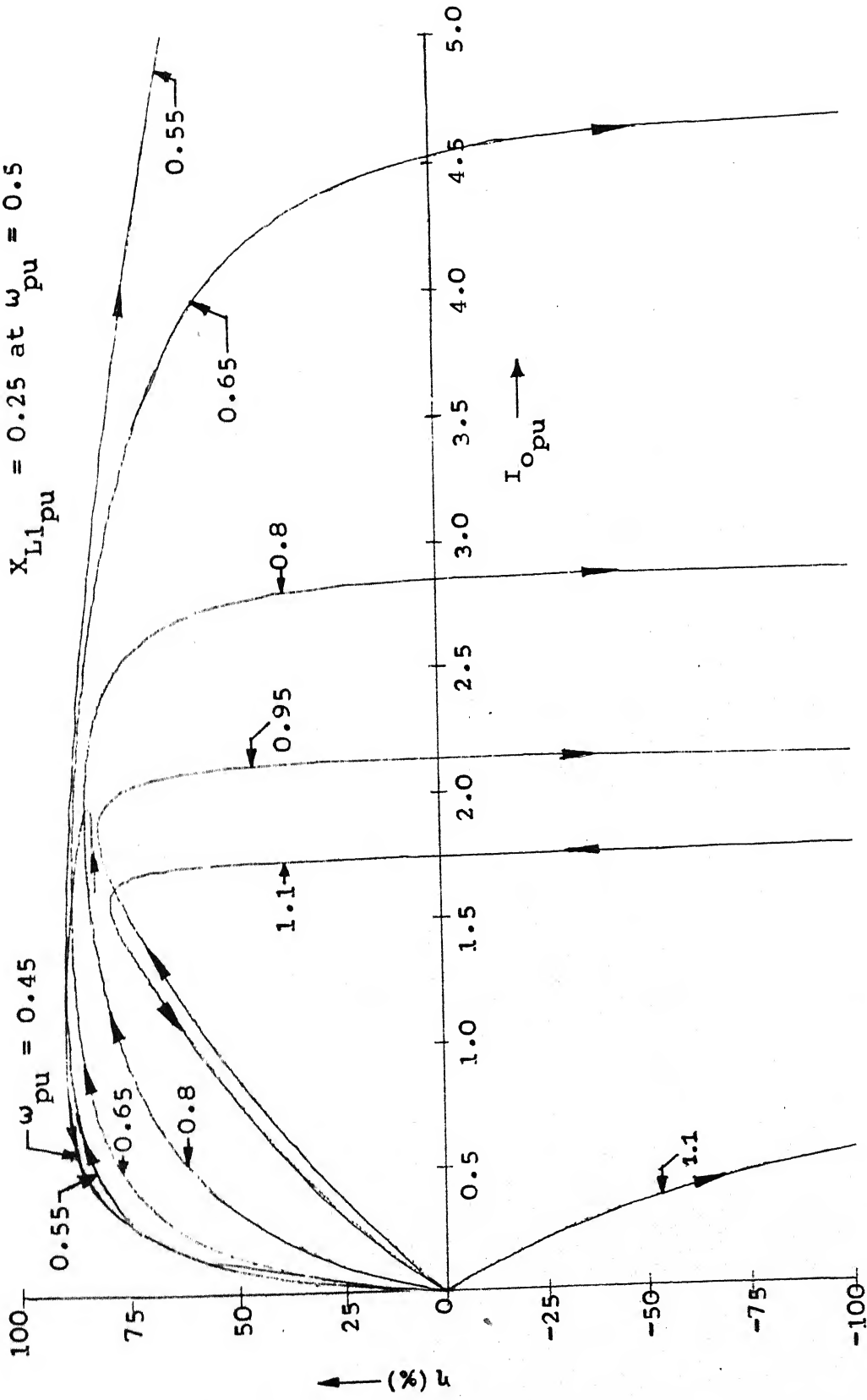


Figure 5.12. Variation of efficiency η with I_{Opu} for f-control for a given set of circuit parameters (Arrowhead indicates increasing values of δ).

$$Q = 10$$

$$X_{L1\text{ pu}} = 0.25 \text{ at } \omega_{\text{pu}} = 0.5$$

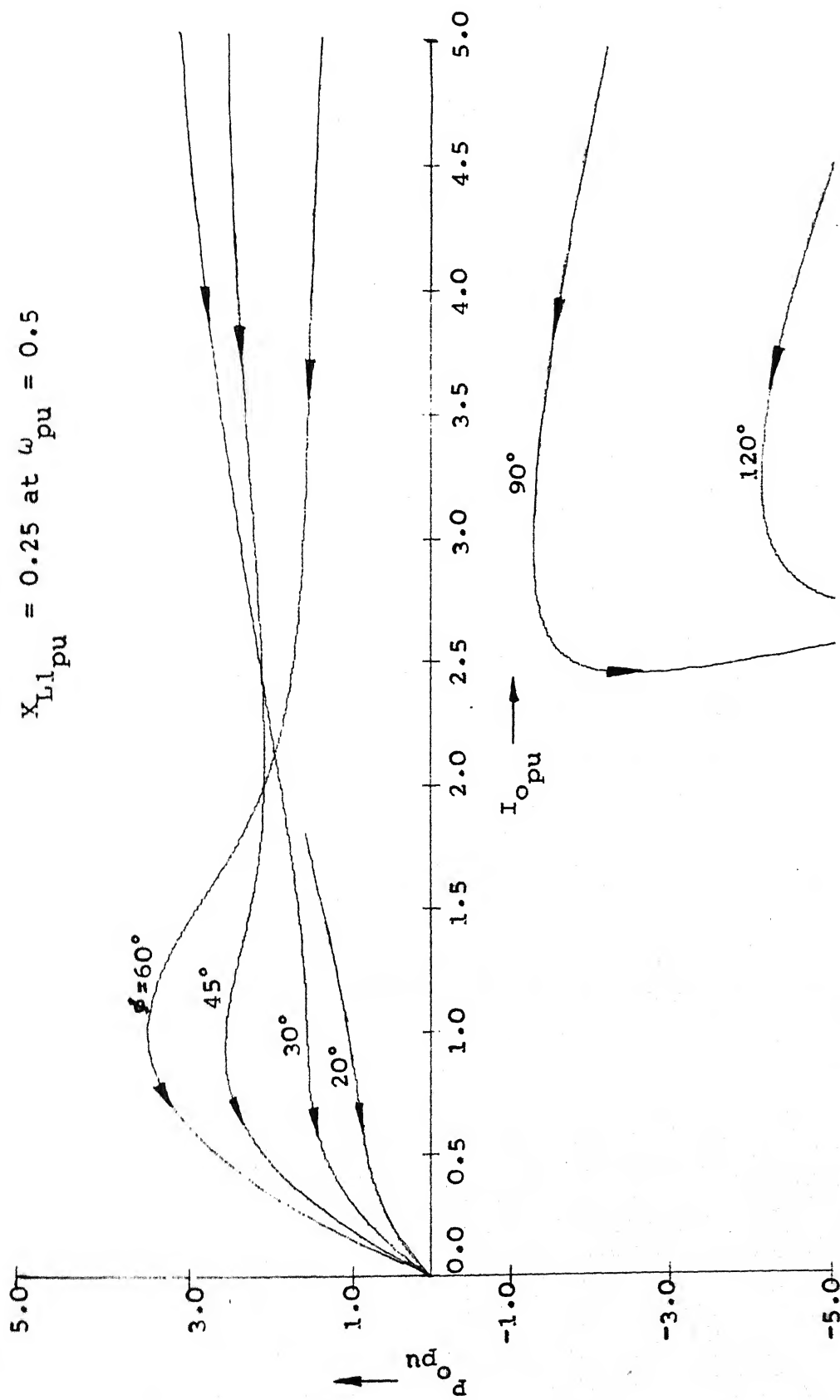


Figure 5.13. Variation of per unit output power P_{oppu} with I_{oppu} for ϕ -control for a given set of circuit parameters (Arrowhead indicates increasing values of ω_{pu}).

$Q = 10$
 $X_{L1\text{ pu}} = 0.25$ at $\omega_{\text{pu}} = 0.5$

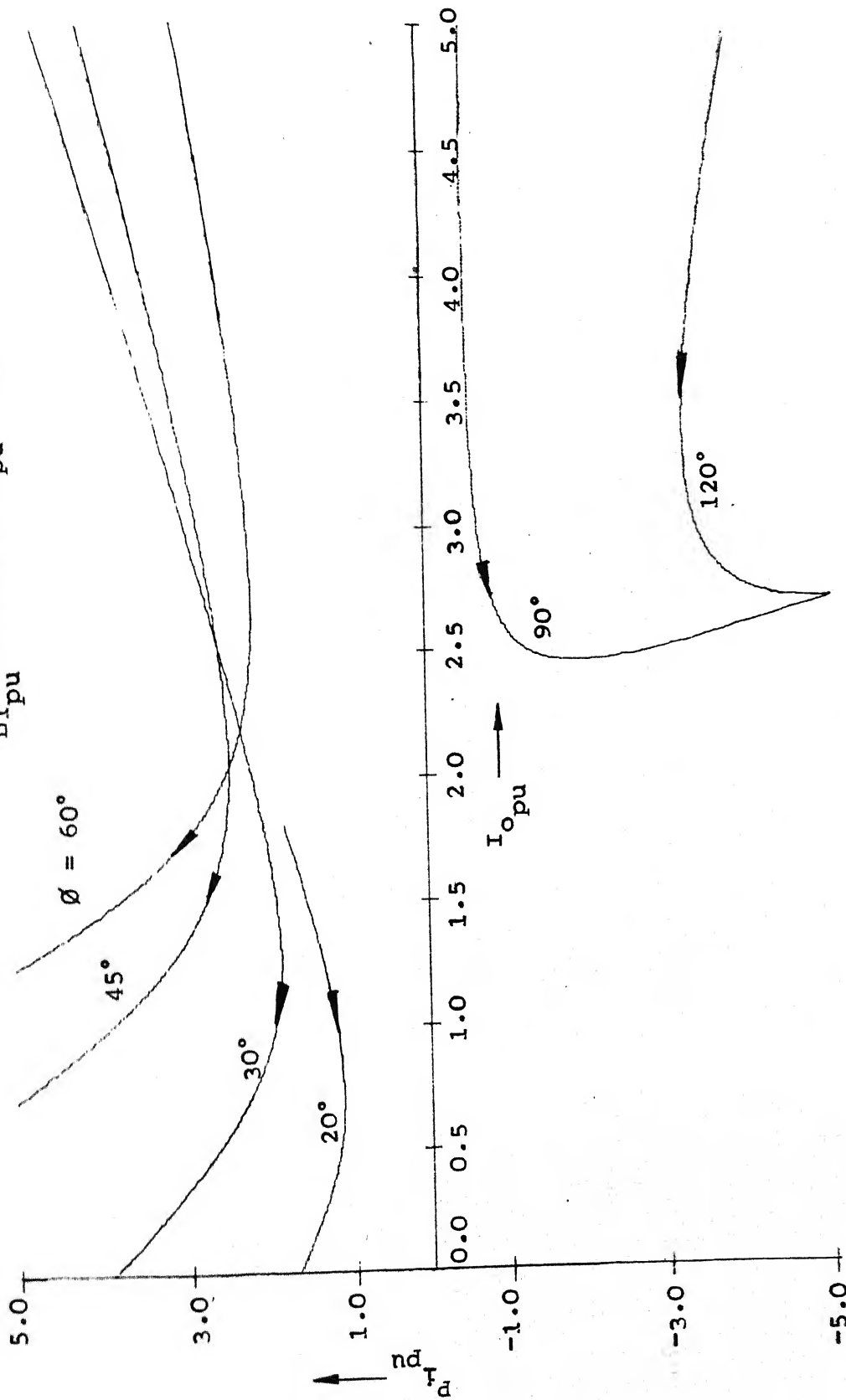


Figure 5.14. Variation of per unit input power $P_{1\text{ pu}}$ with $I_{0\text{ pu}}$ for θ -control for a given set of circuit parameters (Arrowhead indicates increasing values of ω_{pu}).

$Q = 10$
 $X_{L1,pu} = 0.25$ at $\omega_{pu} = 0.5$

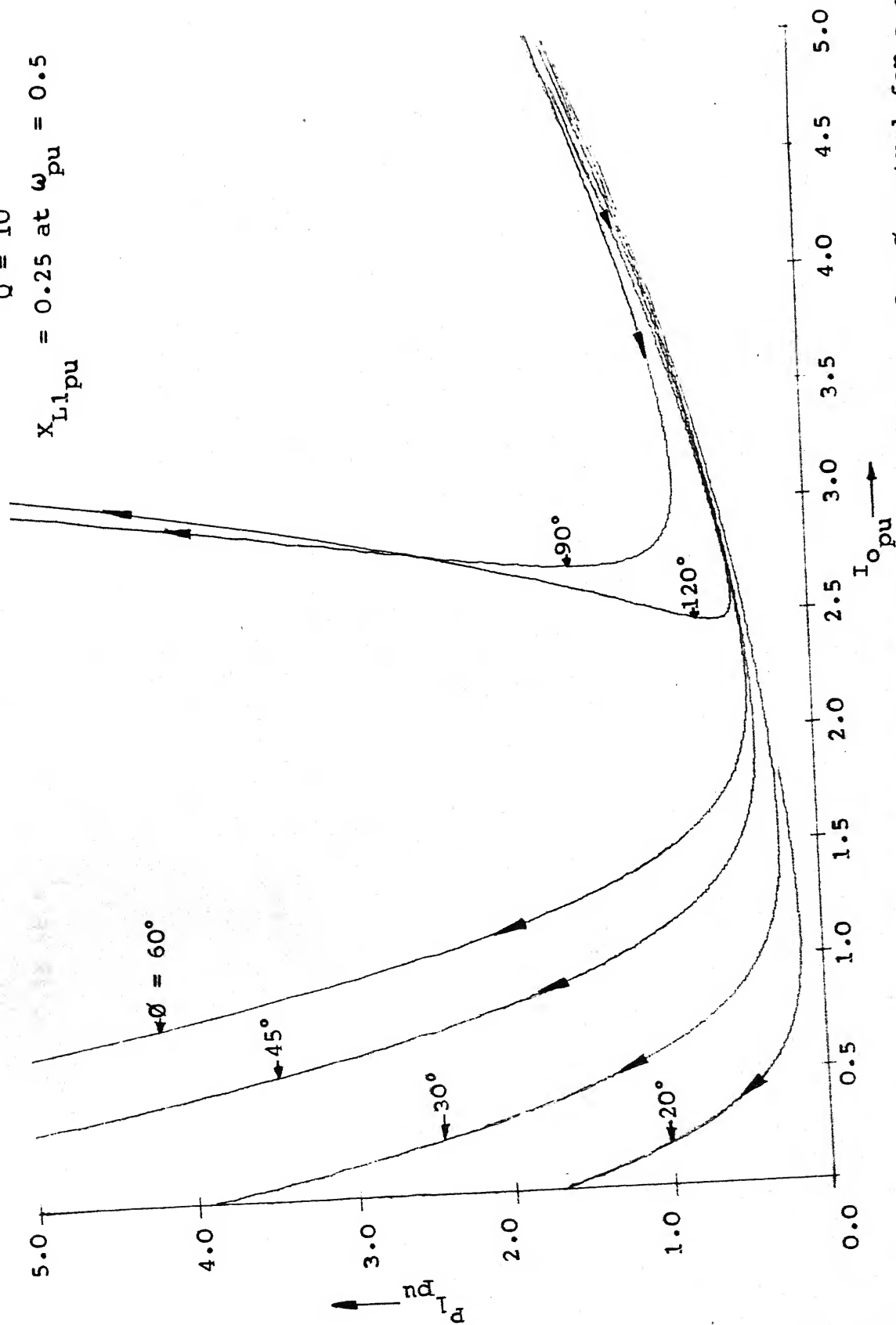


Figure 5.15. Variation of per unit power loss $P_{L,pu}$ with $I_{0,pu}$ for ϕ -control for a given

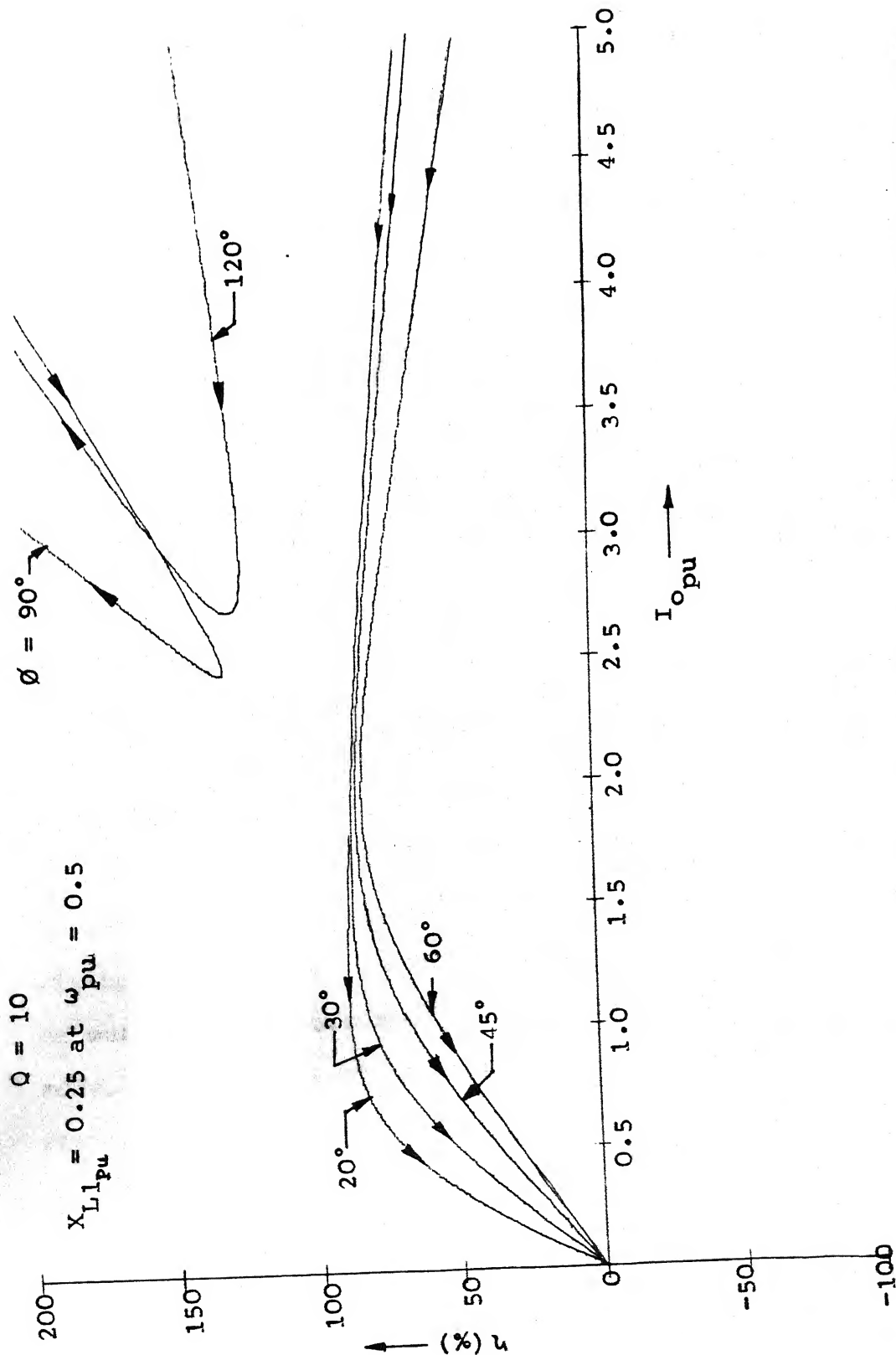


Figure 5.16. Variation of efficiency η with I_o pu for δ -control for a given set of circuit parameters (Arrowhead indicates increasing values of ω_{pu}).

5.4.5 Conclusions

Several interesting observations can be made from the curves of Figures 5.1 through 5.16.

5.4.5.1 f-control: From Figures 5.1 through 5.4 and 5.9 through 5.12 one can arrive at the following conclusions about the frequency control scheme.

(1) The output power, the input power and the power loss in the circuit are double valued functions of output current I_o .

(2) For lower value of output current the output power is greater at higher frequencies. Also, the maximum output power available at a given frequency increases with increasing frequency in the frequency range $0.5 < \omega_{pu} < 1.0$.

(3) The output power is zero when I_o is equal to zero. In the frequency range $0.5 < \omega_{pu} < 1.0$ for a given value of frequency it increases for increasing values of I_o , reaches a maximum and then starts falling. Finally it reaches to zero, reaches a maximum in the negative direction, starts rising and finally becomes zero again. The positive values of output power correspond to operation in the normal converter mode, while the negative values imply operation in the regenerative mode.

(4) The nature of variation of the input power at a given frequency is similar to that of the output power except that when I_o is equal to zero the input power is not equal to zero but is equal to the power loss at zero output current.

(5) The power loss of the inductor coil rises rapidly at higher frequencies. For small values of output current, the power loss at higher frequencies is appreciably greater than that at lower frequencies.

(6) The efficiency of the converter is zero at zero output current. In the frequency range $0.5 < \omega_{pu} < 1.0$ at a given frequency (Figures 5.4 and 5.12) the efficiency increases for increasing value of I_o , reaches a maximum, then starts falling and finally becomes negative. The negative values of efficiency at higher currents in Figures 5.4(a) and Figure 5.12 imply that in that region although the converter is operating in the regenerative mode and the output power is negative, the input voltage source is also delivering power. Both the input and the output power are then used up to supply the high power loss that is taking place in the inductor coil at such high currents.

(7) For a given value of output current, the efficiency is greater at lower values of frequency than that at higher frequencies in the normal frequency range $0.5 < \omega_{pu} < 1.0$. From this and the previous observation it is concluded that it is not desirable to operate the converter at very low values of output current and at higher values of frequencies.

5.4.5.2 ϕ -control: The following conclusions are made about the ϕ -control scheme with the help of Figures 5.5 through 5.8 and 5.13 through 5.16.

(1) For lower values of ϕ the output power is positive and for higher values it is negative, i.e. the

converter is operating in the regenerative mode.

(2) The magnitude of the output power at a given value of the output current is usually greater for higher values of ϕ . This is true in both the normal and the regenerative mode.

(3) The magnitude of the input power at a given value of ϕ passes through a minimum.

(4) Considerable power loss takes place in the inductor coil at low values of the output current and this power loss is much greater for higher values of ϕ .

(5) The efficiency is zero when the output current is zero. For lower values of ϕ the efficiency is found to increase with I_o , reach a peak and then decrease. Values of efficiency above 100 for higher values of ϕ indicate that the converter is operating in the regenerative mode in such a manner that the power delivered by the active load is used to supply power to the input voltage source as well as balance the power loss in the inductor resistance.

(6) At lower values of output current the efficiency is appreciably greater for lower values of ϕ . From this and the previous observation it is concluded that for the ϕ -control scheme it is not desirable to operate the converter at very low values of output current and at higher values of ϕ .

5.5 COMPARISON OF f -CONTROL AND ϕ -CONTROL

From Figure 4.6 it is observed that the regulation of the output voltage with the load current is quite satisfactory when the converter is operated at frequencies slightly above

$0.5 \omega_0$. From this observation it is concluded that if the converter is operated as a constant voltage source, open-loop f -control will give adequate performance. However, from Figures 5.1 and 5.9 it is observed that at low values of the load current at a given frequency, the output power varies rapidly with the load current. This suggests that if constant power output is desired, the open-loop f -control will not give satisfactory performance. However, from the curves of Figures 5.5 and 5.13 it is seen that for smaller values of ϕ the output power remains reasonably constant with load current till very low values of load current at which the output power understandably decreases. Thus it is concluded that if a constant output power is desired, closed-loop ϕ -control must be employed.

5.6 CONCLUSIONS

The variations of power and efficiency have been examined in detail in this chapter. These relationships, together with those obtained in Chapter 4, help to provide a deeper understanding of the operation and the performance of the parallel resonant converter. Several important conclusions have been reached. Suitability of the open-loop and the closed-loop control schemes to meet different requirements has also been examined.

CHAPTER 6

A DESIGN EXAMPLE

6.1 INTRODUCTION

In Chapters 4 and 5 several important performance characteristics of the parallel resonant converter have been given. These relationships can be used to design a parallel resonant converter for a specified set of input and output parameters. An example of the design of the parallel resonant converter has been given in this chapter.

Based on the values of the input and the output parameters given in Section 6.2, the values of the resonant components L and C have been determined in Section 6.3 with the help of the relationships obtained in Chapters 4 and 5. Subsequently the ratings of the power switches and the diodes have been determined in Section 6.4. A comment on the design procedure has been included at the end of the chapter in Section 6.5.

It should be noted that since all the relationships in Chapters 4 and 5 have been obtained by assuming the value of Q to be 10, the LC circuit designed also has a value of Q equal to 10.

6.2 INPUT AND OUTPUT PARAMETERS

The various input and output parameters chosen are given below

$$\begin{aligned} V_s &= 100 \text{ V}, & V_o & \text{(output dc voltage)} = 120 \text{ V} \\ I_{o_{\max}} &= 20 \text{ A}, & f_o &= 10 \text{ KHz} \end{aligned} \quad (6.1)$$

From the specifications given in equation (6.1) the following quantities are determined with the help of equation (2.19).

$$V_{\text{base}} = 100 \text{ V} \quad (6.2)$$

$$I_{\text{base}} = 20 \text{ A} \quad (6.3)$$

$$Z_{\text{base}} = 5 \Omega \quad (6.4)$$

$$T_{\text{base}} = 100 \mu\text{s} \quad (6.5)$$

$$V_{o_{\text{pu}}} = 1.2 \quad (6.6)$$

6.3 SELECTION OF COMPONENT VALUES

The normal operating range of frequencies for the parallel resonant converter is $0.5 < \omega_{\text{pu}} < 1.0$. When the converter is operated in this range, there are several advantages if the frequency of operation is as low as possible. As pointed out in Chapters 4 and 5, these include better regulation, higher efficiency and greater turn off time for the power switches. This suggests that the frequency of operation should be the lowest possible at which the rated per unit output voltage is obtained. From Figure 4.6 it is observed that the maximum per unit output voltage is obtained for zero output current, i.e. when $I_{o_{\text{pu}}} X_{L1_{\text{pu}}}$ is zero. However, from the variation of efficiency with $I_{o_{\text{pu}}} X_{L1_{\text{pu}}}$ shown in Figure 5.4 it is observed that at low values of $I_{o_{\text{pu}}} X_{L1_{\text{pu}}}$ the efficiency of the converter is also very small. So the frequency of operation should be chosen such that when the converter is operating to produce the rated output voltage, the corresponding value of $I_{o_{\text{pu}}} X_{L1_{\text{pu}}}$ should be such that the efficiency also has a reasonably high value (Figure 5.4).

From Figure 4.6 it is observed that the maximum possible values of per unit output voltage corresponding to $\omega_{pu} = 0.55$ and $\omega_{pu} = 0.65$ are 1.1 and 1.36 respectively. This suggests $\omega_{pu} = 0.65$ can be a satisfactory choice as the operating frequency. It is observed from Figure 4.6 that in order to have $V_{o_{pu}} = 1.2$ at $\omega_{pu} = 0.65$, the corresponding value of $I_{o_{pu}} X_{L1_{pu}}$ must be equal to 0.34. From Figure 5.4 the value of the efficiency corresponding to $I_{o_{pu}} X_{L1_{pu}} = 0.34$ for $\omega_{pu} = 0.65$ can be seen to be 86%. This is close to the peak efficiency obtainable for $\omega_{pu} = 0.65$ and is a reasonably satisfactory value. From Figure 5.4 it is observed that the value of $I_{o_{pu}} X_{L1_{pu}}$ at which the converter enters into the m.c.m. at $\omega_{pu} = 0.65$ is 0.52. Consequently if the converter is operated to produce the rated output voltage at $\omega_{pu} = 0.65$, there is no danger of the converter entering into the m.c.m. So it is concluded that the choice of $\omega_{pu} = 0.65$ as the operating frequency is a satisfactory one.

It is assumed that when the converter is operating at $\omega_{pu} = 0.65$ to produce the rated output voltage, the output load current is also equal to the maximum specified value, i.e. $I_o = I_{o_{max}}$. From Figure 4.6 it can be concluded that in the region of interest the output voltage increases for decreasing values of $I_{o_{pu}} X_{L1_{pu}}$ and decreases for decreasing values of frequency. So at values of output current less than $I_{o_{max}}$ the converter should be operated by means of feedback at frequencies slightly lower than $\omega_{pu} = 0.65$ in order to keep the output voltage constant at its rated value of 120 V.

It has already been determined that when the converter is producing the rated output voltage at the operating frequency of $\omega_{pu} = 0.65$, it does not enter into the m.c.m. If the design procedure discussed in the previous paragraph is followed, it is ensured that the converter does not enter into the m.c.m. for all values of output current. At values of the load current less than $I_{o_{max}}$, the value of $I_{o_{pu}} X_{L1_{pu}}$ is always less than that required to take the converter into the m.c.m. at that corresponding frequency.

So at

$$\omega_{pu} = 0.65, \quad I_{o_{pu}} = 1.0 \quad (6.7)$$

$$\text{and } I_{o_{pu}} X_{L1_{pu}} \big|_{\omega_{pu}=0.65} = 0.34 \quad (6.8)$$

$$\omega = 0.65 \cdot 2\pi \cdot 10^4 = 4.084 \cdot 10^4 \text{ rad/sec} \quad (6.9)$$

From equation (6.8) the value of inductance can be determined by substituting the values of $I_{o_{pu}}$, ω and Z_{base} from equations (6.7), (6.9) and (6.4) respectively.

$$L = \frac{0.34 \cdot Z_{base}}{I_{o_{pu}} \cdot \omega}$$

$$= \frac{0.34 \cdot 5}{1.0 \cdot 4.084 \cdot 10^4}$$

$$\text{i.e. } L \simeq 41.6 \mu\text{H} \quad (6.10)$$

$$\therefore C = \frac{1}{\omega_{oL}^2} = \frac{1}{(2\pi \cdot 10^4)^2 \cdot 41.6 \cdot 10^{-6}}$$

$$\text{i.e. } C \simeq 6.1 \mu\text{F} \quad (6.11)$$

Figure 6.1 shows the variation of the inductor current i_L and the capacitor voltage v_C with time for the values of L and C chosen when the converter is producing the rated output voltage at $\omega_{pu} = 0.65$ and with $I_{o_{pu}} = 1.0$. These plots have been obtained using the same technique that was used to obtain the plots of Figure 3.4 in Chapter 3.

6.4 DETERMINATION OF COMPONENT RATINGS

The ratings of the various circuit components have been determined by considering only the fundamental components of the circuit currents and voltages. Since the higher harmonics are much smaller in magnitude compared to the fundamental, the error produced by this method is negligible.

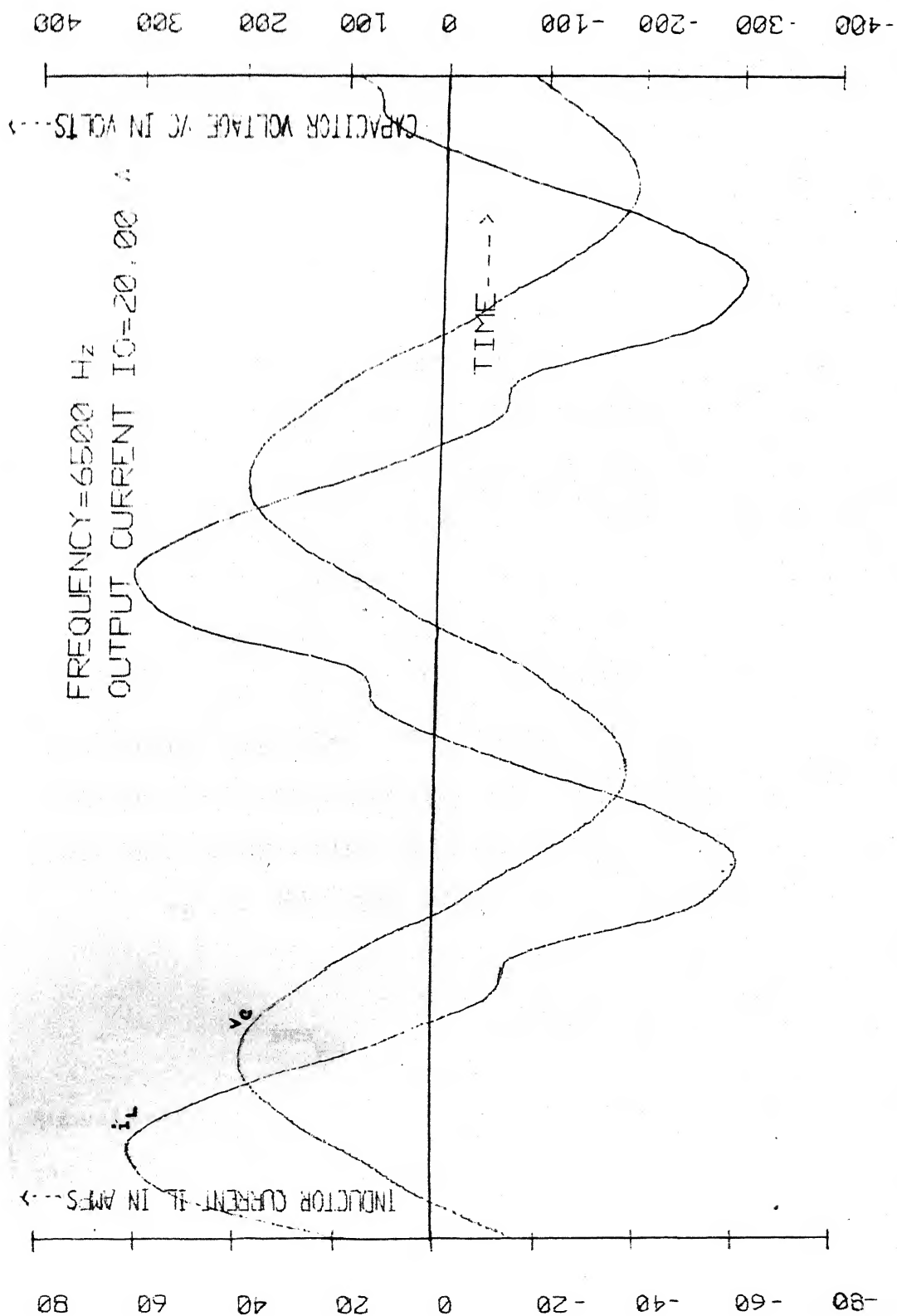
6.4.1 Determination of Ratings of Inductor and Capacitor

From Figure 4.1(b) the value of ϕ corresponding to $I_{o_{pu}} X_{L1_{pu}} = 0.34$ for $\omega_{pu} = 0.65$ can be seen to be

$$\phi = 23.8^\circ$$

$$\text{i.e. } \phi = 0.415 \text{ radians} \quad (6.12)$$

The per unit peak value of the fundamental component of the capacitor voltage, $V_{p1_{pu}}$, has been determined using the same technique that has been used to determine $V_{pn_{pu}}$ in Chapter 5. Substituting $\omega_{pu} = 0.65$, $Q = 10$, $I_{o_{pu}} X_{L1_{pu}} = 0.34$ and $n = 1$ in equations (4.1) through (4.9), the value of $V_{p1_{pu}}$ can be obtained with the help of equations (5.5) and (5.7) through (5.11) using the value of ϕ as given by equation (6.12). This gives



$$V_{p1_{pu}} = 1.895 \quad (6.13)$$

So considering only the fundamental components the per unit peak capacitor voltage is

$$V_{C_{peak_{pu}}} = 1.895 \quad (6.14)$$

The actual value of $V_{C_{peak_{pu}}}$ can be determined from Figure 4.5. From the curve for $\omega_{pu} = 0.65$ the value of per unit peak capacitor voltage corresponding to $I_{o_{pu}} X_{L1_{pu}} = 0.34$ is found to be 1.92. From the close agreement of this value with that given by equation (6.14) it can be concluded that the error produced by neglecting the higher harmonics is negligible. When rms values are calculated, this error is still smaller, since then the amplitudes of the respective harmonic components are squared and added. The effect of higher harmonics, whose amplitudes are much smaller than the fundamental, can then be neglected without producing any serious error.

So per unit rms capacitor voltage is given by

$$V_{C_{rms_{pu}}} = \frac{V_{C_{peak_{pu}}}}{\sqrt{2}} \quad (6.15)$$

Substitution of the value of $V_{C_{peak_{pu}}}$ from (6.14) in (6.15) gives

$$V_{C_{rms_{pu}}} = 1.34 \quad (6.16)$$

To determine $I_{p1_{pu}}$, the peak value of the per unit inductor current, it is necessary to determine the value of $X_{C1_{pu}}$ at the operating frequency

$$X_{C1_{pu}} = \frac{1}{\omega C} \cdot \frac{1}{Z_{base}} \quad (6.17)$$

Substituting the values of ω , C and Z_{base} from equations (6.9), (6.11) and (6.4) respectively one gets

$$X_{C1_{pu}} = 0.80 \quad (6.18)$$

The value of $I_{p1_{pu}}$ has been determined with the help of equations (5.13) and (5.15) through (5.19) using the values of ϕ and $X_{C1_{pu}}$ given by equations (6.12) and (6.18) respectively. The various quantities required for evaluating these expressions have been calculated from equations (4.1) through (4.9) by substituting $\omega_{pu} = 0.65$, $Q = 10$, $I_{o_{pu}} X_{L1_{pu}} = 0.34$ and $n = 1$. Thus one gets

$$I_{p1_{pu}} = 2.738 \quad (6.19)$$

So the per unit peak inductor current

$$i_{L_{peak_{pu}}} = 2.738 \quad (6.20)$$

The per unit rms inductor current is given by

$$I_{L_{rms_{pu}}} = \frac{i_{L_{peak_{pu}}}}{\sqrt{2}}$$

$$\therefore I_{L_{rms_{pu}}} = 1.94 \quad (6.21)$$

From Figures 2.1(a) and 2.1(b) it is seen that the current i_C through the capacitor is the difference of the inductor current i_L and the square wave current i_o whose amplitude

is I_o . So the rms value of the per unit capacitor current is given by

$$I_{C_{rms_{pu}}} = (I_{o_{pu}}^2 + I_{L_{rms_{pu}}}^2)^{1/2} \quad (6.22)$$

Substituting the values of $I_{o_{pu}}$ and $I_{L_{rms_{pu}}}$ from equations (6.7) and (6.21) into equation (6.22) one gets

$$I_{C_{rms_{pu}}} = 2.18 \quad (6.23)$$

Similarly the inductor voltage v_L is given by the difference of the square wave voltage v_i of amplitude v_s and the capacitor voltage v_C . So the rms value of the inductor voltage is

$$V_{L_{rms_{pu}}} = (V_{s_{pu}}^2 + V_{C_{rms_{pu}}}^2)^{1/2} \quad (6.24)$$

The value of $V_{C_{rms_{pu}}}$ is given by (6.16). Since $V_{s_{pu}} = 1.0$,

$$V_{L_{rms_{pu}}} = 1.67 \quad (6.25)$$

Multiplying the per unit voltages and currents by V_{base} and I_{base} respectively the corresponding absolute ratings are obtained. Therefore

$$V_{C_{peak}} = 189.5 \text{ V ,}$$

$$V_{C_{rms}} = 134 \text{ V ,}$$

$$I_{C_{rms}} = 43.6 \text{ A ,}$$

$$V_{L_{rms}} = 167 \text{ V ,}$$

$$i_{L_{peak}} = 54.8 \text{ A}$$

$$\text{and } I_{L_{rms}} = 38.8 \text{ A} \quad (6.26)$$

$$\begin{aligned} \text{Capacitor KVA rating} &= V_{C_{rms}} \cdot I_{C_{rms}} \\ &= 5.84 \text{ KVA} \end{aligned} \quad (6.27)$$

$$\begin{aligned} \text{Inductor KVA rating} &= V_{L_{rms}} \cdot I_{L_{rms}} \\ &= 6.48 \text{ KVA} \end{aligned} \quad (6.28)$$

6.4.2 Determination of Ratings of Power Switches and Diodes

From the circuit diagram of Figure 1.1(b) it is easily observed that the peak voltage appearing across the power switches and the diodes is $2V_s$ i.e. 200 V. So the power switches and the diodes used in the converter should be capable of blocking 200 Volts of forward and reverse voltage drop respectively.

To determine the rms and average current ratings of the respective devices precisely, it is necessary to determine the time t_1 at which the inductor current i_L becomes zero in Figure 1.2(a). However, t_1 takes different values for different values of output load current. Consequently it is not possible to determine uniquely the current ratings of the respective devices for all values of load current. So the current ratings have been determined by considering the worst case conditions. It has been assumed that in the worst case either the power switch or the diode conducts for the entire duration of the half cycle.

$I_{S_{rms}}$ and $I_{D_{rms}}$, the rms current ratings of the power switches and the diodes, therefore, are both given by

$$I_{S_{rms}} = I_{D_{rms}} = \frac{I_{L_{rms}}}{\sqrt{2}} = 27.4 \text{ A} \quad (6.29)$$

Similarly $I_{S_{av}}$ and $I_{D_{av}}$, the average current ratings of the power switches and the diodes respectively are given by

$$I_{S_{av}} = I_{D_{av}} = \frac{I_{L_{av}}}{2} \quad (6.30)$$

where $I_{L_{av}}$ = average value of inductor current i_L over a half cycle

$$= \frac{2}{\pi} \cdot i_{L_{peak}}$$

$$= 34.89 \text{ A.}$$

So from equation (6.30)

$$I_{S_{av}} = I_{D_{av}} = 17.4 \text{ A} \quad (6.31)$$

6.4.2.1 Turn Off Time Available to Power Switches: The turn off time available to the power switches S_1 and S_2 can be determined from the curves of Figure 4.7. It is seen from the curve for $\omega_{pu} = 0.65$ that the per unit turn off time available to the power switches corresponding to $I_{o_{pu}} X_{L1_{pu}} = 0.34$ is given by $t_{q_{pu}} = 0.19$. Since T_{base} is equal to $100 \mu s$ (equation 6.5), this corresponds to a turn off time of $19 \mu s$. This is the turn off time available for the maximum possible value of load current. At lower values of load current the value of $I_{o_{pu}} X_{L1_{pu}}$ is less than 0.34. From Figure 4.7 it is seen that the turn off time available then is greater. So the power switches selected

should be such that the time required to completely turn off the devices is less than 19 μ s.

6.5 COMMENTS ON THE DESIGN PROCEDURE

The design procedure that has been illustrated in this chapter is completely general. Using this technique a parallel resonant converter can be designed to conform to any set of specifications. The following relevant comments can be made about the design procedure adopted.

(1) The frequency of operation has been chosen at $\omega_{pu} = 0.65$ since the efficiency corresponding to $V_{o_{pu}} = 1.2$ at $\omega_{pu} = 0.65$ is 86% which is a reasonably satisfactory value. The values of L and C have been determined from the value of $I_{o_{pu}} X_{L_{pu}}$ corresponding to $V_{o_{pu}} = 1.2$ at $\omega_{pu} = 0.65$. If, however, a specified amount of output power is desired, the frequency of operation should be chosen such that the specified output power is obtained and at the same time the efficiency is also reasonably high. The values of L and C then have to be calculated from the corresponding value of $I_{o_{pu}} X_{L_{pu}}$. However, it must always be ensured that the value of $I_{o_{pu}} X_{L_{pu}}$ is never high enough to take the converter into the multiple conduction mode.

(2) The efficiency of the converter at the rated output voltage and the maximum output current is 86%. This value of efficiency has been determined from the curves of Figure 5.4. These curves have been obtained assuming the value of Q to be 10. If the LC circuit has a higher value of Q, a higher value of efficiency is expected.

(3) It should be noted that the efficiency of the converter has not been optimised. It is possible to operate the converter at frequencies that are slightly below $\omega_{pu} = 0.65$ such that the the value of $I_{o_{pu}} X_{L1_{pu}}$ at which the rated output voltage of $V_{o_{pu}} = 1.2$ is obtained corresponds to a higher value of efficiency. However, from the curves of Figures 4.6 and 5.4 it can be predicted that the increase in efficiency will be marginal in this case.

From Figure 5.4 it is observed that at low values of load current, the efficiency falls rapidly with a decrease in the load current. However, at higher values of the load current the variation of efficiency with the load current is much less. This suggests that it is advantageous to choose the operating frequency such that the rated output voltage is obtained for as high a value of $I_{o_{pu}} X_{L1_{pu}}$ as possible (it must, however, be ensured that the value of $I_{o_{pu}} X_{L1_{pu}}$ is less than that required to take the converter into the m.c.m. at the operating frequency). This ensures that the converter operates with satisfactorily high efficiency for values of load current ranging from $I_{o_{max}}$ down to relatively low values. From Figure 4.6 it can be concluded that to make this possible for the design example chosen, the converter should be operated at frequencies slightly above $0.65 \omega_o$.

(4) The current ratings of the power switches and the feedback diodes have been calculated assuming the worst case conditions. The actual current rating requirements of these devices are less than what have been obtained here. To determine the precise current ratings the time t_1 at which the inductor

current i_L becomes zero in Figure 1.2(a) has to be determined. This can be done by solving equation (4.16). The value of t_1 should be determined for different values of output current. The current ratings of the power switches and the diodes corresponding to each value of t_1 can be determined by integrating the expression for the inductor current i_L (equation (3.23)) from 0 to t_1 and t_1 to $T/2$ respectively. The maximum of these ratings will give the current ratings of the respective devices. This, however, requires considerable computational effort. However, a computer package can be developed for this purpose. The rms and the average current ratings of the power switches and the diodes can then be determined precisely with the help of the package.

CHAPTER 7

CONCLUSIONS

7.1 SUMMARY OF WORK DONE AND IMPORTANT CONCLUSIONS REACHED

A novel frequency domain model for the parallel resonant converters has been proposed and developed. The model is valid for a parallel resonant convertor having an inductor filter at the output. The performance of the parallel resonant converter has been analysed in detail using the proposed model. Expressions for the inductor current and the capacitor voltage have been derived. The waveforms obtained using these expressions have been compared with experimental waveforms reported in literature. The model is validated by the close agreement between the predicted and the experimental waveforms reported in literature. The various expressions and the waveforms have initially been obtained assuming an infinite value of circuit Q . Subsequently all analysis has been carried out assuming a finite value of Q .

A multiple conduction mode (m.c.m.) in which each power switch conducts twice in each half cycle has been identified. The converter has a tendency to enter into the m.c.m. at higher values of the load current. The problems encountered if the converter enters into the m.c.m. have been pointed out.

Several useful and important performance characteristics of the parallel resonant converter have been obtained. While obtaining these characteristics, the quantity $I_{o_{pu}} X_{L1_{pu}}$ has been extensively used as a variable. Thus the effects of the

variations of output current, frequency of operation and component values have all been incorporated in the same variable. The variations of phase difference ϕ with $I_{o_{pu}} X_{L1_{pu}}$ both with ω_{pu} as a parameter and with Q as parameter have been studied. The maximum possible value of $I_{o_{pu}} X_{L1_{pu}}$ at different frequencies have been observed for different values of Q . The variations of peak capacitor voltage, output voltage and turn off time available to the power switches have also been observed as a function of $I_{o_{pu}} X_{L1_{pu}}$. The values of $I_{o_{pu}} X_{L1_{pu}}$ above which the converter enters into the multiple conduction mode at different frequencies have been obtained.

Effects of two common types of control schemes, namely the open-loop frequency control and the closed-loop phase control upon the variations of output power, input power, circuit losses and converter efficiency have been observed. The variations of power and efficiency have been first studied as a function of $I_{o_{pu}} X_{L1_{pu}}$ and then as a function of per unit output current $I_{o_{pu}}$. A comparison of the open-loop and the closed-loop control schemes shows that nearly constant output voltage is obtained with constant frequency operation, while nearly constant output power is obtained with constant phase angle operation, for varying load currents.

The techniques used to obtain each of the performance characteristics have been discussed in detail. Several important conclusions have been drawn from each of the characteristics. These have been given in detail in Chapters 4 and 5. From these it is concluded that when the converter is operated

in the normal frequency range of $0.5 < \frac{f}{f_0} < 1.0$, there are several advantages if the frequency of operation is as low as possible. These include better regulation of output voltage, higher efficiency and greater turn off time for the power switches.

Finally an example of the design of the parallel resonant converter for a typical set of input and output parameters has been given. The design procedure developed is completely general and can be used to design a parallel resonant converter to match any specified set of parameters. Modifications of the design procedure necessary to meet different requirements have also been discussed.

7.2 ADVANTAGES AND LIMITATIONS OF THE PROPOSED MODEL

As pointed out earlier in Chapter 1, all methods of analysis of the resonant converters have till now used a time domain approach. However, as shown in this work, the parallel resonant converter can be analysed from a frequency domain standpoint as well using the proposed model. There are several advantages in adopting this approach instead of the conventional time domain approach.

In the time domain analysis the operation of the circuit is described in terms of differential equations. The different circuit variables are obtained by solving these differential equations by numerical integration. If the steady state performance of the converter has to be analysed, the integration is started from $t = 0$ and is continued for successive half cycles

till the values obtained at the end of two successive cycles agree within a specified tolerance [1]. The value of the variable at that point is the corresponding steady state value. This method, however, is extremely uneconomical in terms of computer time. With the help of the frequency domain model, however, steady state analysis becomes much simpler. Steady state expressions for circuit currents, voltages and powers can be obtained straightaway from the model using simple methods of circuit analysis. Compared to the time domain approach, steady state analysis using the frequency domain approach requires considerably less computational effort.

Although the proposed frequency domain model is useful in many ways, it has got some limitations as well. Some of these are discussed below.

(1) Although the model is extremely useful for steady state analysis, the transient behaviour of the converter cannot be analysed with the help of this model.

(2) The model is valid for a parallel resonant converter having an inductor filter at the output. Under such conditions the output current can be considered to be constant. Looking from the capacitor terminals this current can then be modelled as a square wave current source. If, however, the inductor filter is not present and only the capacitor filter is present at the output, the output current can no longer be assumed to be constant. The proposed model will fail in such a situation. However, it should be noted that the inductor filter at the output is almost always present in all parallel resonant

converters. A time domain analysis of the parallel resonant converter for the case when the inductor filter at the output is absent is given in [13].

(3) The model will fail in all cases of discontinuous conduction, since discontinuous conduction violates the basic assumption on which the model is based. When conduction is discontinuous, the exact nature of circuit currents and voltages cannot be predicted by the model. The assumption that the output current is constant is not likely to be valid in such cases.

7.3 SUGGESTIONS FOR FUTURE WORK

Some of the areas in which future work can concentrate are now discussed.

(1) The series resonant converter of Figure 1.1(a) can be analysed using a similar frequency domain model. For this the square wave current source i_o in parallel with the resonant capacitor in the equivalent circuit of Figure 3.1 has to be replaced by a square wave voltage source of amplitude V_o in series with the LC resonant circuit. The polarity of this current source reverses as soon as the inductor current i_L changes direction.

Using this model the behaviour of the series resonant converter can be analysed using the same techniques that have been used to analyse the parallel resonant converter.

(2) The variations of power and efficiency have been observed for two most popular control schemes. Similar

relationships may be obtained for other types of control schemes also.

(3) A computer package can be developed with the help of which a converter may be designed to match a given set of specifications while simultaneously optimising the various quantities like efficiency, regulation, turn off time etc. The package can also be used to calculate the exact current rating requirements of the power switches and the feedback diodes (Section 6.5).

REFERENCES

- 1 R.L. Steigerwald, 'High Frequency Resonant Transistor DC-DC Converters', IEEE Transactions on Industrial Electronics, Vol. IE-31, No. 2, pp. 181-191, May 1984.
- 2 V. Vorperian and S. Cuk, 'A Complete DC Analysis of the Series Resonant Converter', Conf. Rec. IEEE Power Electronics Specialists Conference, June 1982, pp. 85-100.
- 3 V. Vorperian and S. Cuk, 'Small Signal Analysis of Resonant Converters', Conf. Rec. IEEE Power Electronics Specialists Conference, June 1983, pp. 269-282.
- 4 F.C. Schwarz, 'An Improved Method of Resonant Current Pulse Modulation for Power Converters', IEEE Transactions on Industrial Electronics and Control Instrumentation, Vol. IECI-23, No. 2, pp. 133-141, May 1976.
- 5 R.J. King and T.A. Stuart, 'A Normalized Model for the Half-Bridge Series Resonant Converter', IEEE Transactions on Aerospace and Electronic Systems, Vol. AES-17, No. 2, pp. 190-198, March 1981.
- 6 R.J. King and T.A. Stuart, 'Modeling the Full-Bridge Series Resonant Power Converter', IEEE Transactions on Aerospace and Electronic Systems, Vol. AES-18, No. 4, pp. 449-459, July 1982.
- 7 R.J. King and T.A. Stuart, 'A Large-Signal Dynamic Simulation for the Series Resonant Converter', IEEE Transactions on Aerospace and Electronic Systems, Vol. AES-19, No. 6, pp. 859-870, November 1983.
- 8 R.J. King and T.A. Stuart, 'Small Signal Model for the Series Resonant Converter', IEEE Transactions on Aerospace and Electronic Systems, Vol. AES-21, No. 3, pp. 301-319, May 1985.
- 9 R. Oruganti and F.C. Lee, 'Resonant Power Processors, Part I - State Plane Analysis', IEEE Transactions on Industry Applications, Vol. IA-21, No. 6, pp. 1453-1460, November/December 1985.
- 10 R. Oruganti and F.C. Lee, 'Resonant Power Processors, Part II - Methods of Control', IEEE Transactions on Industry Applications, Vol. IA-21, No. 6, pp. 1461-1471, November/December 1985.
- 11 V.T. Ranganathan, P.D. Ziogas and V.R. Stefanovic, 'A Regulated DC-DC Voltage Source Converter Using a High Frequency Link', IEEE Transactions on Industry Applications, Vol. IA-18, No. 3, pp. 279-287, May/June 1982.

- 12 R.L. Avant and F.C. Lee, 'The J3SCR Model Applied to Resonant Converter Simulation', IEEE Transactions on Industrial Electronics, Vol. IE-32, No. 1, pp. 1-12, February 1985.
- 13 R.L. Steigerwald, 'Analysis of a Resonant Transistor DC-DC Converter with Capacitive Output Filter', IEEE Transactions on Industrial Electronics, Vol. IE-32, No. 4, pp. 439-444, November 1985.

Some other publications related to the present topic are listed below:

- 14 F.C. Schwarz, 'A Method of Resonant Current Pulse Modulation for Power Converters', IEEE Transactions on Industrial Electronics and Control Instrumentation, Vol. IECI-17, No. 3, pp. 209-221, May 1970.
- 15 J. Beiss, L. Inouye and J.H. Shank, 'High Voltage Series Resonant Inverter Ion Engine Screen Supply', Conf. Rec. IEEE Power Electronics Specialists Conference, June 1974, pp. 97-105.
- 16 F.C. Schwarz and J.B. Klaassens, 'A Controllable Secondary Multikilowatt DC Current Source with Constant Maximum Power Factor in Its Three-Phase Supply Line', IEEE Transactions on Industrial Electronics and Control Instrumentation, Vol. IECI-23, No. 2, May 1976.
- 17 P.M. Espelage and B.K. Bose, 'High Frequency Link Power Conversion', IEEE Transactions on Industry Applications, Vol. IA-13, No. 5, pp. 388-394, September/October 1977.
- 18 F.C. Schwarz and J.B. Klaassens, 'A 95-percent Efficient 1-KW Converter with an Internal Frequency of 50 KHz', IEEE Transactions on Industrial Electronics and Control Instrumentation, Vol. IECI-25, No. 4, pp. 326-333, November 1978.
- 19 M.P. Dougherty, 'A Series Resonant Inverter Simulation Using Super-Sceptre', Conf. Rec. National Aerospace and Electronics Conference, May 1979, pp. 517-524.
- 20 R.R. Robson, 'Advancement in Series Resonant Inverter Technology and Its Effect on Spacecraft Employing Electric Propulsion', Conf. Rec. AIAA/JSASS/DGLR 16th International Electric Propulsion Conference, November 1982.
- 21 R.J. King and T.A. Stuart, 'Transformer Induced Instability of the Series Resonant Converter', IEEE Transactions on Aerospace and Electronic Systems, Vol. AES-19, No. 3, May 1983.

- 22 R.J. King and T.A. Stuart, 'Inherent Overload Protection for the Series Resonant Converter', IEEE Transactions on Aerospace and Electronic Systems, Vol. AES-19, No. 6, pp. 820-830, November 1983.
- 23 J.B. Klaassens, 'DC to AC Series-Resonant Converter System with High Internal Frequency Generating Synthesized Waveforms for Multikilowatt Power Levels', Conf. Rec. IEEE Power Electronics Specialists Conference, June 1984.
- 24 S.W.H. de Haan, 'A New Integral Pulse Module for the Series Resonant Converter', IEEE Transactions on Industrial Electronics, Vol. IE-31, No. 3, pp. 255-262, August 1984.
- 25 H. Huisman and S.W.H. de Haan, 'A DC to 3-Phase Series-Resonant Converter with Low Harmonic Distortion', IEEE Transactions on Industrial Electronics, Vol. IE-32, No. 2, pp. 142-149, May 1985.
- 26 S.W.H. de Haan and H. Huisman, 'Novel Operation and Control Modes for Series-Resonant Converter', IEEE Transactions on Industrial Electronics, Vol. IE-32, No. 2, pp. 150-157, May 1985.
- 27 R. Oruganti and F.C. Lee, 'State Plane Analysis of Parallel Load-Capacitor Link Resonant Converter', Conf. Rec. IEEE Power Electronics Specialists Conference, June 1985.
- 28 K.H. Liu, R. Oruganti and F.C. Lee, 'Resonant Switches - Topologies and Characteristics', Conf. Rec. IEEE Power Electronics Specialists Conference, June 1985.
- 29 V. Vorperian, 'High-Q Approximations in the Small Signal Analysis of Resonant Converters', Conf. Rec. IEEE Power Electronics Specialists Conference, June 1985.
- 30 F.S. Tsai, R. Oruganti and F.C. Lee, 'A Novel Control Method for Achieving Bidirectional Power Flow of a Parallel Resonant Converter', Conf. Rec. IEEE-IAS Annual Meeting, October 1985.
- 31 P.R.K. Chetty, 'A New Resonant Mode Amplifier Produces Clean AC Power', IEEE Transactions on Aerospace and Electronic Systems, Vol. AES-21, No. 6, pp. 800-803, November 1985.